

Inhibition of LSD1 as a Therapeutic Strategy for Acute Myeloid Leukemia

By

Gretchen Johnston

Dissertation

Submitted to the Faculty of the
Graduate School of Vanderbilt University
in partial fulfillment of the requirements

for the degree of

DOCTOR OF PHILOSOPHY

in

Biochemistry

August 7, 2020

Nashville, Tennessee

Approved:

Scott Hiebert, Ph.D.

Kevin Schey, Ph.D.

Bruce Carter, Ph.D.

Emily Hodges, Ph.D.

William Tansey, Ph.D.

To my wonderful parents and grandparents

ACKNOWLEDGEMENTS

I would not have been able to complete graduate school without the help of many amazing people I have met during my time at Vanderbilt. First, I want to thank Scott for being a great mentor and encouraging me through experiment failures and negative data. I am grateful for all of the advice and desserts he provided. I also owe many thanks to all the current and former members of the Hiebert lab. A special thanks goes to Kristy Stengel for letting me work with her during my rotation and for being the lab's protocol troubleshooting expert. Former postdocs Yue Zhao, Pankaj Acharya, Shilpa Sampathi, and Suneethi Sivakumaran were very kind and willing to teach me new skills. I also want to thank Steven Pierce for helping me track down random reagents and assisting with experiments. Additional thanks go to Brenda Starks for keeping the lab tidy and making us all laugh. To my fellow students Monica Bomber, Susu Zhang, Hillary Layden, and Clare Spielman – I really appreciate all of your encouragement, coffee breaks, proofreading skills, and commiseration during rough days.

I would also like to thank my committee members for their advice and guidance throughout my project. I owe many thanks to the lab's bioinformatics collaborators Qi Liu and Jing Wang for patiently assisting me with the details of data analysis. I am also grateful to Michael Savona and his lab for their collaboration on the mouse and human bone marrow experiments. Haley Ramsey has been especially helpful with the platelet-related experiments.

Finally, I want to thank my family for their continued love and support. I am especially thankful to Trevor for chauffeuring me to the lab at weird hours and for making an effort to learn about histones.

TABLE OF CONTENTS

	Page
DEDICATION.....	ii
ACKNOWLEDGEMENTS	iii
LIST OF TABLES.....	viii
LIST OF FIGURES	ix
LIST OF ABBREVIATIONS.....	xi
Chapter	
I. INTRODUCTION	1
Overview of Histone Modifications.....	2
Acetylation.....	2
Methylation.....	4
Characterization of LSD1	7
Discovery of LSD1 in corepressor complexes.....	7
Enzymatic activity of LSD1.....	9
Protein structure.....	10
LSD1 as a Therapeutic Target.....	12
Overview of AML.....	13
LSD1 in AML.....	16
LSD1 in hematopoiesis	17
Inhibitors of LSD1.....	18
Roles of GF11 and GF11B.....	21
Discovery as transcriptional repressors.....	21
Structure.....	22
Roles in hematopoiesis	23
GF11.....	23
GF11B	25
Scope of the Dissertation	27
II. MATERIALS AND METHODS	28
Cell Culture and <i>in vitro</i> Experiments	28
Cell lines and culture conditions.....	28
Patient bone marrow and culture conditions	28
Drugs.....	29
Plasmids.....	29
Transfection	30

Retroviral expression of shRNA	30
Immunoprecipitation	30
Protein harvest and western blotting	31
MNase assay	32
Wright-Giemsa staining	33
Flow cytometry analysis	33
RT-PCR.....	33
RNA-seq and analysis.....	34
PRO-seq and analysis.....	35
H3K4me1/2 ChIP-seq and analysis	39
H3K27ac ChIP-seq and analysis.....	41
Single-cell RNA-seq and analysis	43
Mouse Experiments.....	43
Mice	43
Platelet counts.....	43
Flow cytometry analysis	44
Single-cell RNA-seq and analysis	45
RNA-seq and analysis.....	46
III. INHIBITION OF LSD1 INDUCES DIFFERENTIATION OF ACUTE MYELOID LEUKEMIA CELLS	47
Background and Significance	47
Results	48
AML cell lines are sensitive to INCB059872.....	48
Reduced expression of CoREST components mimics INCB059872 treatment.....	50
RNA-seq identifies differentiation signature associated with INCB059872 treatment.....	51
PRO-seq of INCB059872-treated cells reveals increased transcription at myeloid differentiation genes	56
PRO-seq of THP-1 cells treated with INCB059872 reveals increased transcription at GFI1-regulated enhancers	58
Transcriptional changes caused by INCB059872 are consistent with loss of LSD1:CoREST activity at GFI1 binding sites.....	61
Single-cell RNA-seq analysis of AML patient bone marrow reveals gene expression changes caused by INCB059872	65
Discussion	71
IV. INHIBITION OF LSD1 IMPAIRS MATURATION OF MEGAKARYOCYTE PROGENITORS	73
Background and Significance	73
Results	74
Single-cell RNA-seq reveals changes in bone marrow progenitor populations following INCB059882 treatment	74

Flow cytometry analysis of bone marrow from INCB059872- treated mice confirms lineage defects.....	79
RNA-seq analysis of MkP suggests that INCB059872 impairs platelet production.....	83
Discussion	83
V. CONCLUSIONS AND FUTURE DIRECTIONS.....	88
Appendix.....	98
REFERENCES	101

LIST OF TABLES

Table	Page
1. Therapies for AML recently approved by FDA	16
2. Ongoing clinical trials involving LSD1 inhibitors	20
3. shRNA sequences.....	29
4. Primary antibodies for western blotting	32
5. Primer sequences for RT-PCR.....	34
6. Antibodies for mouse immunophenotyping	45

LIST OF FIGURES

Figure	Page
1. Diagram of methylation sites on histones H3 and H4	5
2. Schematic of CoREST complex recruited to a GF11 binding site.....	8
3. Schematic representation of human LSD1 domains	11
4. LSD1 expression in normal versus malignant tissues.....	12
5. Schematic representation of protein domains of human GF11 and GF11B	23
6. INCB059872 impairs proliferation and induces differentiation of AML cell lines	49
7. INCB059872 is an irreversible LSD1 inhibitor	50
8. Reduced expression of CoREST components mimics LSD1 inhibition...	51
9. RNA-seq analysis: Volcano plots show gene expression changes caused by 3hr or 24hr INCB059872 treatment in AML cell lines.....	52
10. Gene set enrichment analysis of RNA-seq data shows differential response to INCB059872 between THP-1 and MV-4-11 cell lines.....	53
11. RNA-seq analysis of LSD1i in AML cell lines shows commonly upregulated genes are associated with myeloid differentiation.....	55
12. PRO-seq analysis of gene expression changes in THP-1 cells in response to LSD1i	57
13. PRO-seq analysis of transcriptional changes in MV-4-11 cells after 24hr INCB059872 treatment.....	59
14. PRO-seq analysis of transcriptional changes at enhancers in THP-1 cells in response to INCB059872.....	60
15. INCB059872 induces expression of GF11B in MV-4-11 cells.....	62
16. INCB059872 treatment does not change global levels of H3K4 methylation or nucleosome structure	63

17. ChIP-seq analysis shows INCB059872 causes more dramatic changes in histone acetylation than methylation	64
18. Histone modification changes caused by INCB059872 are consistent with loss of LSD1:CoREST activity at GFI1 binding sites	66
19. INCB059872 disrupts the LSD1:GFI1 interaction.....	67
20. Single-cell RNA-seq analysis of AML patient bone marrow	68
21. Single-cell RNA-seq analysis of AML patient bone marrow reveals gene expression changes caused by INCB059872	70
22. Single-cell RNA-seq defines distinct subpopulations within murine Lin-bone marrow	75
23. Single-cell RNA-seq reveals changes in bone marrow progenitor populations following INCB059872 treatment in mice.....	77
24. Single-cell RNA-seq reveals gene expression changes in murine bone marrow caused by INCB059872 treatment.....	78
25. INCB059872 has little effect on most murine bone marrow populations.	80
26. INCB059872 treatment expands megakaryocyte progenitor population and decreases plasmacytoid dendritic cell progenitor and monocyte progenitor populations	82
27. RNA-seq analysis of megakaryocyte progenitors shows that INCB059872 impairs platelet production.....	84
28. Model of INCB059872 disrupting the LSD1:GFI1 interaction to prevent CoREST activity at GFI1 binding sites	90

LIST OF ABBREVIATIONS

ac – acetylation

AML – acute myeloid leukemia

AOL – amine oxidase-like

APL – acute promyelocytic leukemia

AR – androgen receptor

ATRA – all-trans retinoic acid

AZA – azacitidine

BCL11B – B-cell Lymphoma/Leukemia 11B

BET – bromodomain and extra-terminal domain

BrdU – bromodeoxyuridine

CARM1 – Coactivator Associated Arginine Methyltransferase 1

cDC – conventional dendritic cell

CHD – chromodomain helicase

CLP – common lymphoid progenitor

CMP – common myeloid progenitor

CSF1R – Colony Stimulating Factor 1 Receptor

CtBP1 – C-terminal Binding Protein 1

CYBB – Cytochrome B-245 Beta Chain

DAC – decitabine

DNMT – DNA methyltransferase

DOT1L – Disruptor of Telomeric Silencing 1 Like

ESC – embryonic stem cell

ETO – Eight Twenty-One

EZH2 – Enhancer of Zeste Homolog 2

FAD – flavin adenine dinucleotide

FLT3 – Fms Related Receptor Tyrosine Kinase 3

FOG1 – Friend of GATA 1

GFI – Growth Factor Independent

GFP – green fluorescent protein

GH – growth hormone

GLIPR1 – GLI Pathogenesis Related 1

GMP – granulocyte/monocyte progenitor

Gp1ba – glycoprotein 1b, alpha polypeptide

HAT – histone acetyltransferase

HCT – hematopoietic cell transplantation

HDAC – histone deacetylase

HLA-DMB – Major Histocompatibility Complex, Class II, DM Beta

HMG20B – High Mobility Group 20B

HOXA9 – Homeobox A9

HP1 – Heterochromatin Protein 1

HSC – hematopoietic stem cell

HSPC – hematopoietic stem and progenitor cell

ID2 – Inhibitor of DNA Binding 2

IDH1/2 – Isocitrate Dehydrogenase 1/2

ITGAM – Integrin Alpha Subunit M

JmjC – Jumonji C

KANSL1 – KAT8 Regulatory NSL Complex Subunit 1

Klf1 – Kruppel-like factor 1

KMT – lysine methyltransferase

LMPP – lymphoid-primed multipotent progenitor

LSD1 – Lysine Specific Demethylase 1

LSK – Lineage- Sca1+ cKit+

Ly6d – lymphocyte antigen 6 complex, locus D

MAO – monoamine oxidase

MDS – myelodysplastic syndrome

me – methylation

MEP – megakaryocyte/erythroid progenitor

MkP – megakaryocyte progenitor

MLL1 – Mixed Lineage Leukemia 1

MNase – micrococcal nuclease

Mpl – myeloproliferative leukemia virus oncogene

MPN – myeloproliferative neoplasm

MTA1 – Metastasis Associated 1

NuRD – nucleosome remodeling and deacetylase

P2ry12 – purinergic receptor P2Y, G-protein coupled 12

Pbx1 – pre B cell leukemia homeobox 1

pDC – plasmacytoid dendritic cell

Pf4 – platelet factor 4

PHF21A – PHD Finger Protein 21A

PRC2 – Polycomb Repressive Complex 2

PRMT – protein arginine methyltransferase

PRO-seq – precision nuclear run-on transcription and sequencing

Prss34 – serine protease 34

RCOR1 – REST Corepressor 1

SANT – SWI3, ADA2, NCoR, and TFIIB

SCD – sickle cell disease

scRNA-seq – single-cell RNA sequencing

Siglech – sialic acid binding Ig-like lectin H

SMYD2 – SET and MYND Domain Containing 2

SNAG – SNAIL/GFI1

SWIRM – SWI3, RSC8, and Moira

SUMO – small ubiquitin-like modifier

SUV39H1 – Suppressor of Variegation 3-9 Homolog 1

t-AML – treatment-related acute myeloid leukemia

TCP – tranlycypromine

Thbs1 – thrombospondin 1

UMAP – uniform manifold approximation and projection

Vwf – von Willebrand factor

ZNF217 – Zinc Finger Protein 217

CHAPTER ONE

INTRODUCTION

Over 6 billion nucleotides of DNA are compacted into the nucleus of a cell by wrapping around nucleosomes composed of a histone octamer. These nucleosomes are organized into chromatin through the linker histone (H1) and modifications of the N-terminal tails of histones H2A, H2B, H3 and H4. The enzymes that control the phosphorylation, acetylation and methylation of the histone tails can drive the development of cancer when their normal functions are altered via activating or inactivating mutations, such as mutations in the H3K27 methyltransferase EZH2. Chromosomal translocations and/or mutations within genes encoding regulators of chromatin structure are found in many cases of acute myeloid leukemia (AML), and in other cases these enzymes are recruited to the wrong genomic loci to alter gene expression by changing the local chromatin structure. The histone demethylase Lysine Specific Demethylase 1 (LSD1, also known as KDM1A) is crucial for the maintenance of certain AML subtypes, making it a potential therapeutic target. Drugs targeting LSD1 have entered clinical trials but with limited success, in part due to dose-limiting toxicities. Though LSD1 inhibitors have been shown to induce differentiation of certain leukemia subtypes, further studies are needed to inform therapeutic uses for this type of drug.

Overview of Histone Modifications

Post-translational modifications of histones regulate gene expression, presumably by altering local chromatin structures. Residues on histone tails can be marked by phosphorylation, acetylation, methylation, or small proteins such as ubiquitin or SUMOs (small ubiquitin-like modifiers). Chromatin-associated proteins can be divided into three categories: readers, writers, or erasers (Strahl and Allis, 2000). Reader proteins contain domains that bind to specific chromatin marks, e.g. bromodomains that recognize acetylated lysine residues (Jain and Barton, 2017). Writers are enzymes, such as acetyltransferases or methyltransferases, that place modifications on histone residues. Eraser proteins, such as deacetylases or demethylases, catalyze the removal of covalent modifications.

Acetylation

Evidence of post-translational acetylation of histones was first described in 1964 (Allfrey et al., 1964), but the first-discovered histone acetyltransferase (HAT) was not purified until three decades later (Brownell and Allis, 1995). HATs can be categorized into five main subfamilies: Hat1, Gcn5/PCAF, MYST, p300, CBP, and Rtt109. Each subfamily uses a distinct mechanism to transfer the acetyl group from acetyl-CoA to the ϵ -amino group of a histone tail lysine residue (Marmorstein and Zhou, 2014). Residues that are acetylated include H3 lysines 9, 14, 18, 27, 56 and H4 lysines 5, 8, 13, 16. Acetylation of a histone tail reduces its overall positive charge, which weakens the interaction of the histone with negatively-charged DNA and presumably facilitates

binding of transcription factors. Thus, HATs and histone deacetylases (HDACs) are associated with transcriptional activation and repression, respectively (Mizzen and Allis, 1998). H3K27ac is prominent at active promoters and can be used to distinguish active enhancers from inactive “poised” enhancers (Creighton et al., 2010).

The first mammalian HDAC was discovered shortly after HATs were identified (Taunton et al., 1996). There are four classes of mammalian HDACs: class I (HDACs 1, 2, 3, and 8), class II (HDACs 4, 5, 6, 7, 9, and 10), class III (SIRT1-7), and class IV (HDAC11). Class I enzymes are ubiquitously expressed, while the others exhibit tissue-specific expression (Zhao and Shilatifard, 2019). Class I, II, and IV HDACs use a zinc-dependent mechanism, while class III sirtuins depend on NAD⁺ as an enzymatic cofactor (McClure et al., 2018). Though all HDACs were initially thought to deacetylate lysine residues, catalytic studies found that HDACs 1, 2, 3, and 6 were the only metal-containing family members to have robust deacetylase activity (Bradner et al., 2010; McClure et al., 2018).

As HDACs are overexpressed in various types of cancer, targeting their enzymatic activity is a potential therapeutic strategy (West and Johnstone, 2014). Vorinostat and romidepsin were the first pan-HDAC inhibitors to reach FDA approval for the treatment of refractory cutaneous T-cell lymphoma (West and Johnstone, 2014). More recently, the pan-HDAC inhibitor panobinostat was the first of its kind to be approved for treatment of relapsed/refractory multiple myeloma (McClure et al., 2018). Though class I-selective compounds have been developed (Ryan et al., 2005), clinical trial results have not demonstrated these to be more effective than pan inhibitors. HDAC inhibitors are likely to be more beneficial when used in combination with other therapies,

as suggested by the synergy between HDAC inhibitors and DNA methyltransferase inhibitors (Marchi et al., 2015).

Alternatively, aberrant histone acetylation can be addressed by targeting the bromodomain and extra-terminal (BET) family of proteins, which consists of BRD2, BRD3, BRD4, and BRDT. The deep acetyl-lysine binding pocket within the BET proteins can be targeted by small molecules to disrupt the interaction with acetylated histone tails (Filippakopoulos et al., 2010). As BRD4 regulates expression of MYC (Delmore et al., 2011), BET inhibition can be used to combat the proliferative and metabolic effects caused by elevated MYC activity. BET inhibitors have reached clinical trials and have shown antiproliferative effects in various tumor models, including breast cancer, hepatocellular carcinoma, and lymphomas (Pervaiz et al., 2018).

Methylation

Methylation of mammalian histone residues was first reported in 1964 (Murray). Coincident with the discovery of post-translational histone acetylation, Allfrey et al. showed that methylation of histones occurred after histone synthesis was completed (Allfrey et al., 1964). The first methyltransferase enzyme to be discovered was the arginine-specific methyltransferase Coactivator Associated Arginine Methyltransferase 1 (CARM1) (Chen et al., 1999), and the lysine-specific methyltransferase Suppressor of Variegation 3-9 Homolog 1 (SUV39H1) was discovered shortly after (Rea et al., 2000). Protein arginine methyltransferases (PRMTs) and protein lysine methyltransferases (KMTs) include more than 60 proteins, all of which transfer a methyl group from the cofactor S-adenosylmethionine to the target residue (Helin and Dhanak, 2013).

Transcriptional effects of histone methylation are dependent on the specific residue being methylated and the number of methyl moieties placed (i.e. mono-, di-, or tri-methylation). For example, methylation of histone H3 lysine 4 (H3K4) is associated with active transcription, while methylation of lysine 9 (H3K9) is associated with a transcriptionally repressed state (Helin and Dhanak, 2013). Methylation sites and their relation to gene expression are summarized in Fig. 1. Transcriptional outputs of histone methylation are mediated through the binding of reader proteins, such as heterochromatin protein HP1, which contains a chromo domain that binds H3K9 methylation to compact chromatin and silence transcription (Bannister et al., 2001).

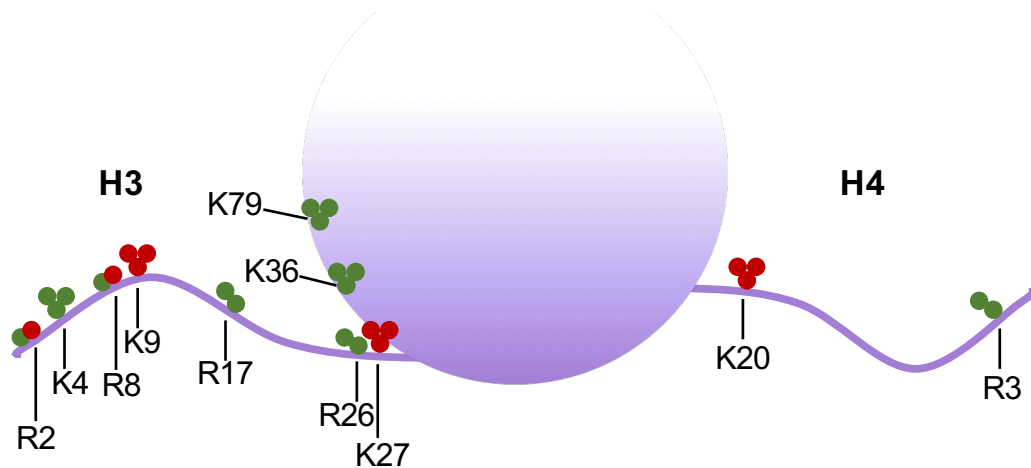


Figure 1. Diagram of methylation sites on histones H3 and H4. Methylated residues associated with active transcription are indicated in green, and those associated with repressed transcription are indicated in red. In the cases of H3R2 and H3R8, both activation and repression have been reported.

The turnover of histone methylation is much slower than the turnover of other post-translational modifications (Barth and Imhof, 2010). Active demethylation of histones was not reported until 2004 with the discovery of the enzymatic activity of

LSD1 (discussed in the following section). Histone demethylases can be categorized into two major families: KDM1 or JmjC-domain (Jumonji C). The KDM1 family consists of LSD1 and LSD2, while the JmjC-domain family contains at least 17 members (Zhao and Shilatifard, 2019). JmjC demethylases use an oxidative mechanism that requires iron and α -ketoglutarate as cofactors to remove mono-, di-, or tri-methylation (Helin and Dhanak, 2013).

Aberrant histone methylation is associated with multiple malignancies. The H3K27 methyltransferase Enhancer of Zeste Homolog 2 (EZH2), the catalytic component of Polycomb Repressive Complex 2 (PRC2), is a therapeutic target due to its overexpression and mutation in various cancer types (Helin and Dhanak, 2013). The H3K4 methyltransferase Mixed Lineage Leukemia 1 (MLL1) is also a therapeutic target. Chromosomal translocations involving MLL1 are associated with development of acute leukemia and represent approximately 10 percent of detectable translocations. The resulting MLL fusion proteins drive leukemogenesis by activating transcription of developmentally regulated genes (Mohan et al., 2010). Interestingly, deletion of the *Mll1* paralog *Mll2* reduced viability of MLL-AF9-transformed cells (Chen et al., 2017), suggesting histone methylation has an important role in disease pathology. The H3K79 methyltransferase Disruptor of Telomeric Silencing-Like (DOT1L) is recruited by MLL fusion partners, and DOT1L inhibition was lethal in cells with MLL translocation (Daigle et al., 2011).

Characterization of LSD1

Discovery of LSD1 in corepressor complexes

Prior to the discovery of enzymatic histone demethylation, LSD1 protein was first identified in an immunoprecipitation of the histone-modifying NuRD (nucleosome remodeling and deacetylase) complex (Tong et al., 1998b). This complex has deacetylase activity mediated by HDAC1/2 and also contains ATP-dependent helicases Chromodomain Helicase DNA Binding Protein 3 and 4 (CHD3/4), which remodel nucleosomes (Wang et al., 2009). The NuRD complex decommissions enhancers during the differentiation process of embryonic stem cells and can promote or repress tumorigenesis depending on cellular context (Lai and Wade, 2011; Whyte et al., 2012). Conditional deletion of *Chd4* (also known as *Mi-2b*) in adult mouse bone marrow demonstrated that the NuRD complex is critical for maintaining appropriate ratios of myeloid and lymphoid progenitors to erythroid progenitors (Yoshida et al., 2008). Hematopoietic lineage-specific transcription factors associated with this complex include Friend of GATA 1 (FOG1, also known as ZFPM1) and B-cell Lymphoma/Leukemia 11B (BCL11B) (Hong et al., 2005; Cismasiu et al., 2005).

LSD1 was later discovered in another histone deacetylase complex, termed the CoREST complex (You et al., 2001; Humphrey et al., 2001). This transcriptional repressor complex contains HDAC1/2, REST Corepressor 1 (RCOR1), Zinc Finger Protein (ZNF217), PHD Finger Protein 21A (PHF21A, also known as BHC80), High Mobility Group 20B (HMG20B, also known as BRAF35) and other components that vary among cell types (Lee et al., 2005; Macinkovic et al., 2019). Initially, the CoREST

complex was found to be required to repress transcription of neuron-specific genes in non-neural cells (Andres et al., 1999; Qureshi et al., 2010). In a human lung fibroblast cell line, a variant of the CoREST complex containing the histone deacetylase SIRT1 was required to repress Notch target genes (Mulligan et al., 2011). In mouse pituitary cells, a CoREST complex containing C-terminal Binding Protein 1 (CtBP1) regulated growth hormone (GH) gene repression (Wang et al., 2007). In hematopoietic cells, Growth Factor Independent family members GFI1 and GFI1B recruit the CoREST complex to lineage-specific genes (Saleque et al., 2007; Fig. 2).

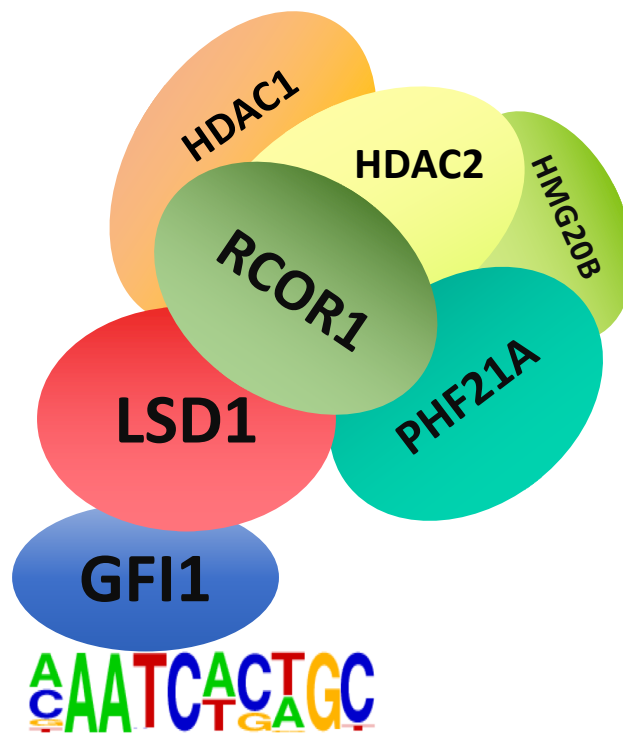


Figure 2. Schematic of CoREST complex recruited to a GFI1 binding site.

Enzymatic activity of LSD1

Histone demethylase enzymatic activity was initially observed and partially purified from rat kidney homogenate (Paik and Kim, 1973). Previously, histone methylation had been assumed to be removed via passive mechanisms, such as a modified histone being replaced by an unmodified histone during replication (Bannister et al., 2002). LSD1 (formerly known as KIAA0601) was suspected to have histone demethylase activity because of its homology to amine oxidases (Humphrey et al., 2001). Indeed, LSD1 catalyzed the removal of mono- or di-methylation from histone H3 lysine 4 (H3K4me1/2) via an oxidation reaction that generated formaldehyde (Shi et al., 2004). The *N*-methyl group of the lysine was oxidized by the cofactor FAD (flavin adenine dinucleotide) to an imine intermediate that was hydrolyzed (Forneris et al., 2006). This mechanism relies on a lone electron pair on the lysine nitrogen atom, which means that it cannot use trimethylated lysine as a substrate (Forneris et al., 2005; Hodjfeldt et al., 2013).

Although Shi et al. did not detect any enzymatic activity of LSD1 on histone H3 lysine 9 methylation, other groups (Metzger et al., 2005; Ray et al., 2014; Laurent et al., 2015; Carnessechi et al., 2017) have reported that LSD1 demethylated this residue, suggesting a context-dependent role for the enzyme. Of note, LSD1-mediated demethylation of H3K9 was discovered in a study of the interaction of LSD1 with androgen receptor (AR), in which case removal of the repressive H3K9me2 mark is consistent with the function of AR to induce transcription of its target genes (Metzger et al., 2005). LSD1 has also been shown to demethylate lysine residues of non-histone

proteins including p53, DNA Methyltransferase 1 (DNMT1), and E2F1 (Huang et al., 2007; Wang et al., 2009; Kontaki et al., 2010).

Protein structure

The enzymatic amine oxidase-like (AOL) domain of LSD1 folds into two parts: a substrate-binding subdomain and an FAD-binding subdomain. These two subdomains form a large catalytic cavity with highly negative electrostatic potential (Chen et al., 2006). A conserved lysine residue (K661) within the catalytic pocket is essential for demethylase activity (Lee et al., 2005). The crystal structure of LSD1 confirmed hydrogen-bonding interactions mediated by a water molecule between this residue and FAD (Chen et al., 2006). Interestingly, a splice variant of LSD1 containing 4 additional amino acids within the AOL domain exists only in neurons and has been independently reported to have demethylase activity on H3K9 (Laurent et al., 2015) and H4K20 (Wang et al., 2015).

In addition to the AOL domain, LSD1 contains two additional conserved domains: the SWIRM (SWI3, RSC8, and Moira) domain and the Tower domain (Fig. 3). The N-terminal 171 residues are unstructured and dispensable for demethylase activity (Chen et al., 2006). The SWIRM domain is an evolutionarily conserved domain that is specific to chromatin-associated proteins (Tochio et al., 2006). SWIRM domains from *S. cerevisiae* Rsc8 and Swi3 bind mononucleosomes and are essential for assembly of chromatin-modifying complexes (Da et al., 2006). Thus, the SWIRM domain of LSD1 is presumed to mediate protein-protein interactions with components of transcriptional repressor complexes.

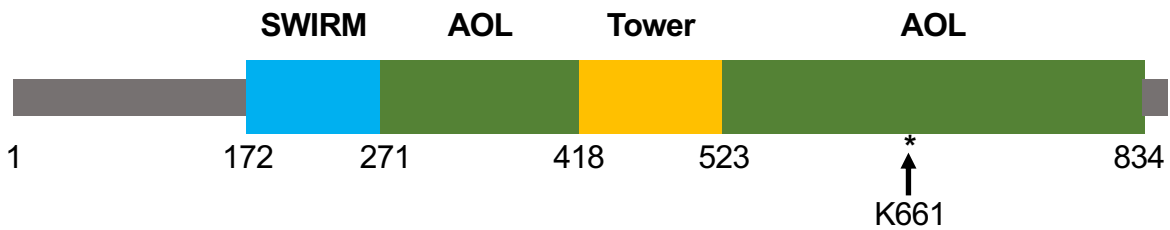


Figure 3. Schematic representation of human LSD1 domains. Diagram highlights conserved domains: SWIRM (SWI3, RSC8, and Moira) in blue, AOL (amine oxidase-like) in green, Tower in yellow. Asterisk indicates lysine residue essential for enzymatic activity. Unstructured regions are shown in grey.

The Tower domain of LSD1 consists of a pair of long helices inserted within the AOL domain (Chen et al., 2006). The presence of this domain distinguishes LSD1 from its most similar homolog LSD2 (KDM1B). The Tower domain makes extensive interactions with the SANT2 (SWI3, ADA2, NCoR, and TFIIB) domain of RCOR1 of the CoREST complex (Yang et al., 2006). Though LSD1 alone can demethylate histone H3K4 peptides *in vitro*, its association with CoREST is necessary for it to demethylate nucleosomes (Lee et al., 2005). Mutations within the RCOR1 SANT2 domain limited the enzymatic activity of LSD1 (Yang et al., 2006). As part of the NuRD complex, the Tower domain of LSD1 interacts with the SANT domains of Metastasis Associated 1/2/3 (MTA1/2/3) (Wang et al., 2009).

LSD1 as a Therapeutic Target

LSD1 plays a role in determining cell identity, and its dysregulation can drive human disease. Though mutations within *KDM1A* are uncommon, LSD1 is overexpressed in several types of malignancies, including breast, lung, kidney, and colorectal tumors (Hayami et al., 2011; Fig. 4). In many cases, high LSD1 expression marks poorly differentiated tumors and is correlated to poor prognosis (Karakaidos et al., 2019). Within the hematopoietic system, LSD1 acts as a key regulator of lineage-defining genes, making it an interesting target for the treatment of AML.

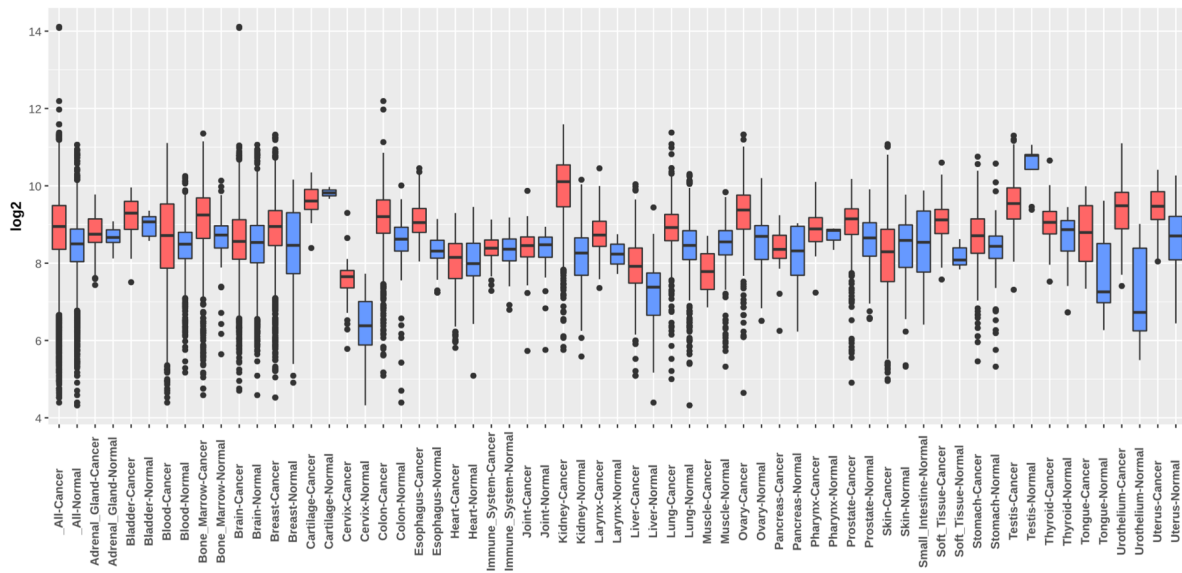


Figure 4. LSD1 expression in normal vs malignant tissues. Boxplots show log₂ expression values of LSD1 expression in types of cancer (red) or normal tissue (blue) as measured by Affymetrix U133A microarray platform in the GENT2 database.

Overview of AML

AML is a heterogeneous disease characterized by accumulation of incompletely differentiated hematopoietic progenitor cells in the bone marrow. These cells (known as blasts) crowd out normal hematopoietic progenitor cells in the marrow and can enter the circulation and cause anemia and impair immunity to increase the propensity to infection. Around a quarter of AML cases evolve from myelodysplastic syndrome (MDS) or myeloproliferative neoplasms (MPN). Therapy-related AMLs, found in patients treated with radiation or cytotoxic therapy for solid tumors, make up 5-10 percent of cases (Ossenkoppele and Montesinos, 2019). AMLs can be classified into subtypes based on the stage of differentiation at which they have been blocked. Around half of new AML diagnoses have readily detectable cytogenetic abnormalities, and karyotype is the most prominent prognostic factor (Mould et al., 2015). In general, AML has a lower mutational burden than most other malignancies. Recurrent point mutations and chromosomal translocations often affect genes encoding proteins that regulate the conformation of chromatin or are involved in DNA methylation or modification of histone tails (Gambacorta et al., 2019).

Overall survival rates for AML are largely dependent on age; patients under 60 have a 30-40 percent survival rate at 5 years post-diagnosis, but for patients over 60, this rate is under 20 percent (Mould et al., 2015). For decades, the standard treatment for newly diagnosed AML has been 1-2 cycles of “induction” chemotherapy using an anthracycline (e.g. daunorubicin) combined with cytarabine (Mould et al., 2015). For most patients, this is followed by further rounds of “consolidation” chemotherapy. In cases deemed to have high risk of relapse, allogeneic hematopoietic cell transplantation

(HCT) can be used after achieving remission with chemotherapy (Kassim and Savani, 2017). Though HCT can be curative, it is unsuitable for many patients due to their comorbidities and the risks associated with transplant.

The pyrimidine analogs decitabine (DAC) and azacitidine (AZA) are now being used to treat elderly patients who are unfit for standard chemotherapy. These drugs were developed in the 1960s as cytostatic agents but were discovered to inhibit DNA methylation in 1980 (Jones and Taylor). At low concentrations, the incorporation of DAC or AZA into DNA inhibits DNA methyltransferases (DNMTs), but high concentrations of these compounds are cytotoxic without affecting DNMT activity (Pleyer and Greil, 2015). DAC is incorporated only into DNA, while AZA is mostly incorporated into RNA (~85%) instead of DNA (~15%). Thus, both drugs can de-repress genes that have been aberrantly silenced by DNA methylation, but AZA can also inhibit protein synthesis (Pleyer and Greil, 2015). Despite this difference, meta-analyses of clinical data have shown similar outcomes for patients treated with either drug, with median overall survival comparable to that achieved by more intensive therapies (Gardin and Dombret, 2017).

More recent advancements for treating AML include other therapies targeted toward epigenetic deregulation. HDAC genes are not mutated in AML, but HDAC proteins are recruited by oncogenic fusion proteins, such as AML1-ETO (Amann et al., 2001), to repress target genes. Preclinical studies have shown accumulation of acetylated histones and apoptosis in AML cells treated with HDAC inhibitors (San Jose-Eneriz et al., 2019). Pan-HDAC inhibitors, such as vorinostat and panobinostat, have shown little efficacy as monotherapies but are potentially useful in combination with

other drugs. Targeting the readers of histone acetylation is also a promising therapeutic strategy. BET inhibition reduced the proportion of stem-like cells in AML patient-derived xenografts, though the effect varied among samples with different mutational backgrounds (Masse et al., 2019).

Other recent therapeutic developments include inhibitors of histone methyltransferases. The DOT1L inhibitors pinometostat and EPZ-5676 have entered clinical trials. Pinometostat showed modest efficacy as a single agent and is now being tested in combination with AZA or standard chemotherapy (Stein et al., 2018). Other compounds in preclinical studies include PRMT inhibitor MS023 (He et al., 2019), EZH1/2 dual inhibitor OR-S1 (Fujita et al., 2017), and Menin:MLL interaction inhibitor VTP50469 (Krivtsov et al., 2019).

Personalized medicine is also becoming incorporated into AML treatment strategies, as several common mutations can be targeted by small molecules. Inhibitors specific to mutant forms of Isocitrate Dehydrogenase 1 and 2 (IDH1 and IDH2), which play a role in the DNA demethylation process, are now available (Stein et al., 2017; DiNardo et al., 2018). Leukemias with mutations in Fms Related Receptor Tyrosine Kinase 3 (FLT3) can be treated with FLT3 inhibitors midostaurin or gilteritinib (Stone et al., 2017). Drugs recently approved by the FDA for treatment of AML are summarized in Table 1.

Drug	Mechanism	Indication	Clinical Trial Ref #
Enasidenib	Inhibitor of mutant IDH2	Relapsed/ refractory AML with IDH2 mutation	NCT01915498
Gemtuzumab ozogamicin	Anti-CD33 antibody conjugated to the toxin calicheamicin	Newly diagnosed or relapsed/ refractory CD33-positive AML; in combination with chemotherapy	NCT00927498
Gilteritinib	Inhibitor of FLT3	Relapsed/ refractory AML with FLT3 mutation	NCT02421939
Glasdegib	Inhibitor of SMO (Hedgehog pathway)	Newly diagnosed AML; in combination with low-dose cytarabine	NCT01546038
Ivosidenib	Inhibitor of mutant IDH1	Newly diagnosed AML with IDH1 mutation	NCT02074839
Midostaurin	Inhibitor of FLT3	Newly diagnosed AML with FLT3 mutation; in combination with chemotherapy	NCT00651261
Venetoclax	Inhibitor of BCL-2	Newly diagnosed AML; in combination with chemotherapy	NCT02203773 NCT02287233

Table 1. Therapies for AML recently approved by FDA.

LSD1 in AML

LSD1 gained interest as a potential therapeutic target in AML due to the frequent deregulation of histone methylation and high expression of LSD1 in AML cells. Adamo et al. (2011) showed that LSD1 is highly expressed in human embryonic stem cells (ESCs) and downregulated during differentiation, suggesting it could be involved in maintaining pluripotency. Whyte et al. (2012) described a role for LSD1 within the differentiation process of mouse ESCs; as part of the NuRD complex, it removed H3K4me1 to silence enhancers that control expression of key ESC genes. Consistent

with these findings, expression of LSD1 within MLL-rearranged murine leukemias was highly correlated to the colony-forming cell frequency (a proxy for leukemia stem cell potential) of the leukemia. Inhibition or knockdown of LSD1 reduced the clonogenic potential and expression of MLL-AF9 target genes in this leukemia model (Harris et al., 2012).

LSD1 is especially appealing as a therapeutic target due to its potential to induce differentiation of leukemia cells. Currently, all-trans retinoic acid (ATRA) is used to treat acute promyelocytic leukemia (APL), a subtype of AML driven by the PML-RARA fusion protein, by causing leukemic blasts to differentiate. In non-APL cell lines that were insensitive to ATRA alone, knockdown or inhibition of LSD1 in combination with ATRA treatment induced differentiation (Schenk et al., 2012). LSD1 inhibition limited proliferation and increased cell surface expression of myeloid lineage markers CD11b and CD86 in MLL-rearranged AML cell lines (Fang et al., 2017; Feng et al., 2016).

LSD1 in hematopoiesis

LSD1 is a critical regulator of embryonic and adult hematopoiesis. In mice, deletion of *Kdm1a* is lethal at embryonic day 7.5 (Wang et al., 2007). Kerényi et al. (2013) created a hematopoietic-specific *Kdm1a* knockout mouse model using a *Vav-Cre* system to delete the gene by embryonic day 9. *Kdm1a^{fl/fl}-VavCre* mice had a 30-fold reduction in the frequency of Lineage- Sca1+ cKit+ (LSK) cells in their bone marrow and died neonatally of severe anemia. *Mx1-Cre*-mediated conditional deletion of *Kdm1a* in adult mice caused fatal anemia within 10 days. These mice had accumulated a population of immature granulocytes but had almost no mature granulocytes within their

bone marrow (Kerenyi et al., 2013). Additionally, Kerenyi et al. showed that LSD1 is essential for HSC self-renewal, as *Kdm1a^{fl/fl} Mx1Cre* hematopoietic stem and progenitor cells (HSPCs) were undetectable 12 weeks post-deletion after a competitive bone marrow transplant.

LSD1 has unique roles at different stages of hematopoietic differentiation. In zebrafish hemangioblasts, which have the capacity to differentiate toward endothelial or hematopoietic lineages, LSD1 suppresses expression of the endothelial factor ETS variant transcription factor 2 (*Etv2*) to shift the cells toward hematopoietic differentiation (Takeuchi et al., 2015). In undifferentiated progenitor cells, LSD1 was in complex with GATA2 to repress transcription of GATA1, but in cells differentiating toward the erythroid lineage it forms a complex with TAL1 to repress transcription of GATA2 (Hu et al., 2009; Guo et al., 2016). The transcription factor GFI1B recruits LSD1 to repress its target genes in megakaryocyte progenitors (Saleque et al., 2007). Inducible knockdown of LSD1 within mouse bone marrow caused enhanced monopoiesis and reduced granulopoiesis, suggesting LSD1 was required to regulate cell fate decisions between the granulocytic and monocytic lineages (Sprussel et al., 2012).

Inhibitors of LSD1

Within the past decade, several small molecule inhibitors of LSD1 have been developed, though clinical trials utilizing these compounds have had mixed success (Magliulo et al., 2018). The majority of LSD1 inhibitors described thus far are based on the structure of tranylcyproamine (TCP), a nonselective monoamine oxidase inhibitor used to treat depression. Based on the sequence homology between LSD1 and the

monoamine oxidases MAOA/B, inhibitors of MAO enzymatic activity were tested against LSD1 demethylase activity, and TCP was found to be the most potent with an IC_{50} of $<2 \mu\text{M}$ (Lee et al., 2006). In vitro assays with purified nucleosomes confirmed that TCP inhibited the demethylase activity, but not the deacetylase activity of immunoprecipitated CoREST complex (Lee et al., 2006). Yang et al. (2007) determined the crystal structure of LSD1:CoREST with TCP and found that TCP forms a covalent FAD adduct that is distinct from the adduct formed with TCP and MAOB. The adduct does not have extensive interactions with active site residues of LSD1, implying that it could be used as a scaffold to design more potent inhibitors (Yang et al., 2007).

ORY-1001 is a potent and selective LSD1 inhibitor that was developed using TCP as a chemical starting point. It is highly selective for LSD1 over MAOA/B and has an IC_{50} of 18 nM (Maes et al., 2018). In a phase I clinical trial, ORY-1001 promoted blast differentiation in blood or bone marrow of patients with acute erythroleukemia or MLL-rearranged AML (Pandey and Wang, 2019). GSK2879552, another TCP-based compound, showed synergy with ATRA to slow growth and increase markers of differentiation in multiple AML cell lines (Smitheman et al., 2019). However, clinical trials studying GSK2879552 in the context of MDS, AML, and small cell lung carcinoma (SCLC) were terminated due to unfavorable risk-benefit ratio.

LSD1 inhibitors have also been tested in other blood disorders, such as MPN or sickle cell disease (SCD), as well as solid tumors. Table 2 lists current clinical trials involving LSD1 inhibitors. In a mouse model of SCD, the LSD1 inhibitor RN-1 increased fetal hemoglobin levels and reduced disease symptoms (Cui et al., 2015). Another LSD1 inhibitor, IMG-7289, is in early phase clinical trials for MPN. In a mouse model,

IMG-7289 improved several key features of the disease, such as erythrocytosis and hepatosplenomegaly (Jutzi et al., 2018). Thus far only one non-TCP-derived LSD1 inhibitor, SP-2577, has reached clinical development. SP-2577 is a reversible and noncompetitive inhibitor that impaired tumor growth in a xenograft model of Ewing sarcoma (Reed et al., 2019).

Drug	Condition(s)	Phase	Clinical Trial Ref #
TCP (with ATRA)	AML/MDS	1	NCT02273102
TCP (with ATRA)	AML excluding APL	1/2	NCT02717884
IMG-7289	Essential Thrombocythemia	2	NCT04081220
IMG-7289	Myelofibrosis	2b	NCT03136185
SP-2577	Ewing Sarcoma	1	NCT03600649
SP-2577	Advanced solid tumors	1	NCT03895684
INCB059872	Ewing Sarcoma	1	NCT03514407
INCB059872 (with pembrolizumab & epacadostat)	Advanced solid tumors	1/2	NCT02959437
INCB059872 (with AZA & ATRA in AML; with nivolumab in SCLC)	Advanced malignances	1/2	NCT02712905

Table 2. Ongoing clinical trials involving LSD1 inhibitors.

Aside from inhibiting the catalytic activity of the enzyme, compounds that target LSD1 can disrupt its interaction with the transcription factors GFI1/1B. T-3775440 is a TCP derivative that disrupted the interaction of LSD1 with GFI1B and induced transdifferentiation of erythroid and megakaryocytic cells toward a granulomonocytic-

like lineage (Ishikawa et al., 2017). Likewise, the LSD1 inhibitor NCD38, which activated enhancers involved in myeloid differentiation (Sugino et al., 2017), was later shown to disrupt the LSD1:GFI1B interaction in erythroleukemia cells (Yamamoto et al., 2018). The LSD1 inhibitor OG86 disrupted the interaction of LSD1 with GFI1 in AML cells and induced differentiation by de-repressing GFI1:CoREST targets (Maiques-Diaz et al., 2018).

Roles of GFI1 and GFI1B

Discovery as transcriptional repressors

Gfi1 was discovered in a screen of provirus insertions that mediated IL-2-independent growth of Moloney murine leukemia virus-induced rat T cell lymphomas (Gilks et al., 1993). Zweidler-Mckay et al. (1996) showed that GFI1 functioned as a transcriptional repressor in chloramphenicol acetyltransferase reporter assays. *Gfi1b* was discovered based on its homology to *Gfi1*. Interestingly, *Gfi1b* was also found to be a target of provirus integration by Moloney murine leukemia virus (Tong et al., 1998a). GFI1 and GFI1B autoregulate and trans-regulate the expression of one another (Doan et al., 2004). The GFI proteins repress transcription by recruiting chromatin modifying complexes to target genes. Both proteins interact with histone methyltransferases G9A and SUV39H1 as well as histone deacetylases HDACs 1-3 and the corepressor Eighty-One (ETO, also known as RUNX1T1) (McGhee et al., 2003; Moroy et al., 2015). Saleque et al. (2007) found that GFI1 and GFI1B recruit the CoREST complex via a direct interaction with LSD1.

Structure

GFI1 and GFI1B are zinc finger transcription factors that have nearly identical N- and C-termini, but their central domains differ and are not well conserved between species (Moroy et al., 2015). The C-terminal domains contain six C₂H₂-type zinc fingers (Fig. 5). Only zinc fingers 3-5 are necessary for sequence-specific DNA binding (Zweidler-Mckay et al., 1996). The two proteins share a consensus DNA-binding motif that includes a core sequence of AATC (Zweidler-Mckay et al., 1996).

GFI1 and GFI1B also contain a conserved 20-residue N-terminal domain, the SNAIL/GFI1 (SNAG) domain, which contains a nuclear localization signal (Grimes et al., 1996; Fig. 5). The SNAG domain is essential for the interaction of GFI1/1B with LSD1 (Saleque et al., 2007). The SNAG domain of the transcription factor SNAIL also binds to LSD1 (Lin et al., 2010). SNAG domains interact with LSD1 in a manner that mimics interaction with a histone tail (Baron et al., 2011). Lysine-8 within the SNAG domain is methylated by SET and MYND Domain Containing 2 (SMYD2), and this methylation is critical for recruitment of LSD1 (Velinder et al., 2016). Mutations within the SNAG domain of *Gfi1* mimic genetic deletion of *Gfi1* (Fiolka et al., 2006). Apart from LSD1, there is no other known protein that associates with the SNAG domain of GFI1/1B (Moroy et al., 2015), suggesting that LSD1 is essential for GFI1 and GFI1B to repress transcription.

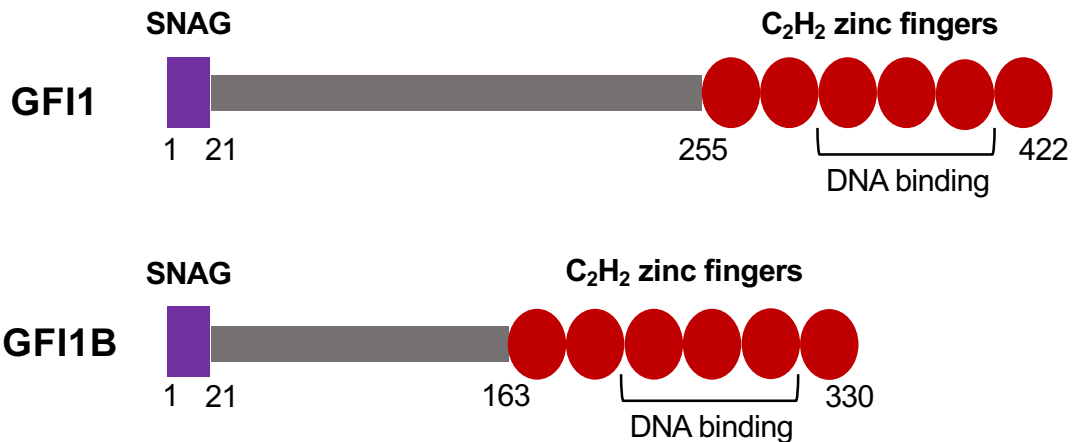


Figure 5. Schematic representation of protein domains of human GF1 and GF11B. Diagram highlights conserved domains of each protein: SNAG (SNAIL/GF11) domain in purple, C₂H₂-type zinc fingers in red. Zinc fingers 3-5, which mediate DNA binding, are indicated by brackets. Middle regions shown in grey differ between the two proteins and are not well-characterized.

Roles in hematopoiesis

GF1 and GF11B are both crucial factors in embryonic and adult hematopoiesis. Given the sequence similarity between the functional domains of the two proteins, overlapping roles were expected. Though both are expressed in hematopoietic progenitor cells, GF1 and GF11B have unique expression patterns in more differentiated cells. Replacement of the *Gfi1* gene with the coding sequence of *Gfi1b* only partially rescued hematopoiesis, suggesting the non-conserved domains may have separate functions (Fiolka et al., 2006).

GF1

GF1 regulates development of various hematopoietic lineages. Like LSD1, GF1 was also suggested to be a determinant of the neutrophil vs macrophage cell fate

decision. *Gfi1*-knockout mice had severe neutropenia and accumulation of immature monocytic cells in their bone marrow (Karsunky et al., 2002). Myeloid precursor cells from these mice could be stimulated to differentiate into macrophages but not granulocytes in vitro. Later studies showed that GFI1 counteracted the transcriptional program mediated by Early Growth Response 1/2 (EGR1/2), which regulate macrophage cell fate (Laslo et al., 2006). *Gfi1* knockout also caused defective maturation of dendritic cells and increased their cytokine production (Rathinam et al., 2005).

An early study of GFI1 expression, in which the *Gfi1* coding region was replaced by a gene encoding green fluorescent protein (GFP), found that it was highly expressed in early B cells and differentially expressed at various stages of T cell development (Yucel et al., 2004). Later studies showed that GFI1-mediated repression of Inhibitor of DNA Binding 2 (ID2) expression was necessary for B cell and myeloid development (Li et al., 2010). T cell-specific deletion of *Gfi1* expanded the population of regulatory T cells, implying that GFI1 is needed to negatively regulate factors that promote development of this T cell subset (Shi et al., 2013). In addition, GFI1 modulated the immune response by repressing the T helper type I transcriptional program, favoring development of other T helper subsets (Suzuki et al., 2016).

GFI1 expression is also required within the hematopoietic stem cell (HSC) compartment. Flow cytometry analysis of bone marrow from *Gfi1*^{GFP/+} mice showed that GFI1 was highly expressed in the LSK (Lin⁻ Sca-1⁺ c-Kit⁺) population, which contains HSCs and multipotent progenitor cells (Zeng et al., 2004). It was also detected in common lymphoid progenitors (CLP) and granulocyte/monocyte progenitors (GMP) but

not in common myeloid progenitor cells (CMP) or megakaryocyte/erythroid progenitor cells (MEP). Two independent studies (Hock et al., 2004; Zeng et al., 2004) discovered that LSKs from *Gfi1*^{-/-} mice were extremely impaired in their ability to reconstitute hematopoiesis in competitive bone marrow transplants. Additionally, bromodeoxyuridine (BrdU) incorporation experiments demonstrated that *Gfi1*^{-/-} LSKs were more proliferative than wild-type cells, implying the HSC defect was due to excessive cycling.

Mutations in the C-terminal domain of *GFI1* cause severe congenital neutropenia in humans (Person et al., 2003). Among AML patients with normal karyotype, high GFI1 expression is associated with poor prognosis and is often accompanied by high FLT3 expression (Volpe et al., 2017). A variant allele of *GFI1* (found in less than 5 percent of the population) confers a 1.6-fold increased risk to develop AML (Khandanpour et al., 2010b). This variation, which places an asparagine in place of the more common serine at position 36, accelerated development of KRAS-driven myeloproliferative disorder (Khandanpour et al., 2012). In a study of MDS patients treated with hypomethylating agents, GFI1^{36N} was an adverse prognostic factor for overall survival (Botezatu et al., 2016).

GFI1B

Analysis of a mouse strain with GFP inserted into the *Gfi1b* locus showed that the expression pattern of GFI1B mostly differs from that of GFI1 (Vassen et al., 2007). GFI1B is expressed in MEPs, megakaryocytes, erythrocytes, and early stage lymphocytes. Heterozygous *Gfi1b*^{+/-} mice had no obvious defects, but knockout of *Gfi1b* was lethal by embryonic day 15 due to defective erythropoiesis (Saleque et al., 2002). Megakaryocyte development in *Gfi1b*^{-/-} embryos appeared to be defective as well, given

the lack of mature megakaryocytes in fetal livers (Saleque et al., 2002). Conditional deletion of *Gfi1b* in bone marrow of adult mice caused severe decreases in hemoglobin levels and platelet counts and was lethal within 3 weeks. Interestingly, the deletion disrupted erythropoiesis at a very early stage, while megakaryopoiesis was not arrested until after polyploidization at the promegakaryocyte stage (Foudi et al., 2014).

In contrast to *Gfi1* expression, *Gfi1b* is most highly expressed in the HSC subset (LSK CD150+ CD48-) and downregulated upon differentiation to MPP subsets (LSK CD48+). Conditional deletion of *Gfi1b* in murine hematopoietic cells caused over 30-fold expansion of HSCs in bone marrow and peripheral blood (Khandanpour et al., 2010a). These *Gfi1b*^{-/-} HSCs showed increased proliferation, but their pluripotency and self-renewal capacity were comparable to wild-type cells. After additional deletion of *Gfi1* within *Gfi1b*^{-/-} murine hematopoietic system, HSCs could not be detected, indicating that at least one GFI family member is essential for generation of HSCs (Khandanpour et al., 2010a).

Mutations within *GFI1B* have been reported in patients with platelet disorders (Moroy et al., 2015). As is the case with *GFI1* mutations, most of these disease-associated variants are within the zinc finger domain. Stevenson et al. (2013) discovered a frameshift mutation within the DNA-binding domain of *GFI1B* in family members with an autosomal dominant bleeding disorder. Similarly, Monteferrario et al. (2014) found a nonsense mutation within the gene that caused autosomal dominant gray platelet syndrome. Only one case of AML with a somatic mutation in *GFI1B* has been reported (Anguita et al., 2016). In functional assays, the mutant protein *GFI1B*^{D262N} antagonized the transcriptional repression mediated by wild-type *GFI1B*.

Scope of the Dissertation

Given the prevalence of epigenetic dysregulation in cancer, drugs that target chromatin-modifying enzymes are now being developed as therapeutic agents. One example of this is the inhibition of histone demethylase LSD1 for the treatment of hematological malignancies. In my dissertation work, I focused on understanding the molecular mechanism of action by which inhibition of LSD1 controls gene expression to trigger the differentiation of AML cells and normal myeloid progenitor cells *in vivo*. This dissertation will describe the action of INCB059872, a potent and selective inhibitor that also disrupts the LSD1:GFI1 interaction. The majority of data in Chapters III and IV has been published in *Gene* (Johnston et al., 2020). Chapter III provides genomic analyses of the differentiation-related effects of INCB059872 in AML cells. Chapter IV examines the *in vivo* effects of INCB059872 on hematopoietic progenitor populations. Chapter V provides an overview of the results and consideration of future clinical uses of LSD1 inhibitors.

CHAPTER TWO

MATERIALS AND METHODS

Cell Culture and *in vitro* Experiments

Cell lines and culture conditions

MV-4-11 cells (ATCC, CRL-9591) were cultured in IMDM (Gibco, cat# 12440046) containing 10% FetalPlex (Gemini, cat# 100-602), 100 U/mL penicillin and 100 µg/mL streptomycin (Corning, cat# 30002CI). THP-1 cells (ATCC, TIB-202) were cultured in RPMI (Corning, cat# 15040CV) containing 10% FetalPlex, 2 mM L-glutamine (Corning, cat# 25005CI), 100 U/mL penicillin, 100 µg/mL streptomycin, and 50 µM 2-mercaptoethanol (Gibco, cat# 31350010). 293T cells (ATCC, CRL-3216) were cultured in DMEM (Corning, cat# 10013CM) containing 10% FetalPlex, 100 U/mL penicillin, and 100 µg/mL streptomycin. S2 cells (provided by Dr. Emily Hodges's lab) were cultured in Schneider's Drosophila Medium (Gibco, cat# 21720024) containing 10% FetalPlex.

Patient bone marrow and culture conditions

A primary patient sample was provided by the Vanderbilt-Ingram Cancer Center Hematopoietic Malignancies Repository and in accordance with the tenets of the Declaration of Helsinki and approved by the Vanderbilt University Medical Center Institutional Review Board. Cells were cultured in IMDM containing 10% Stasis Stem Cell Qualified Fetal Bovine Serum (Gemini, cat# 100-125), 2 mM L-glutamine, 10 ng/mL

IL-3, 10 ng/mL Flt3, 10 ng/mL SCF, 10 ng/mL TPO, 5 ng/mL IL-6, 10 μ M 2-mercaptoethanol, and 4 μ g/mL LDL.

Drugs

INCB059872 was supplied under a material transfer agreement through Incyte Corporation. INCB059872 was dissolved in DMSO and stored as a 5 mg/mL stock solution at room temperature. Azacitidine (AZA) was provided by Dr. Michael Savona's lab. AZA was dissolved in DMSO immediately before use.

Plasmids

pCMV3-GFI1 was purchased from Sino Biological (cat# HG13131-UT). pCMV-VSV-G (cat# 8454) and psPax2 (cat# 12260) were purchased from Addgene. Lentiviral vectors (PLKO.1) containing shRNA sequences (listed in Table 3) were obtained from MISSION[®] shRNA library (Sigma), and puromycin selectable marker was replaced by YFP sequence using Gibson cloning.

Target	Sequence
shCHD3	CCGGCGCAAGCAAGTAACTACAATCTCGAGATTGTAGTAACTTGCTTGCGTTTTTG
shCHD4	CCGGGCTGCTGACATCCTATGAATTCTCGAGAATTCATAGGATGTCAGCAGCTTTTTG
shKANSL1	CCGGACTCACTAACTATTGGCATTACTCGAGTAATGCCAATAGTTAGTGAGTTTTTG
shLSD1	CCGGCCACGAGTCAAACCTTTATTTCTCGAGAAATAAAGGTTTGACTCGTGTTTTTG
shRCOR1	CCGGGATGGTGGAATAGAACCATATCTCGAGATATGGTTCTATTCCACCATCTTTTTTG

Table 3. shRNA sequences.

Transfection

Plasmids were mixed with 250 μ l serum-free DMEM and 24 μ l PEI (polyethylenimine; Polysciences, cat# 23966) and incubated for 15 min at room temperature before mixture was added dropwise to 10 cm dishes containing 293T cells.

Retroviral expression of shRNA

Each 10cm plate of 293T cells was transfected with 0.5 μ g VSVG, 1.5 μ g psPax2, and 3 μ g PLKO.1 plasmids. Lentivirus-containing media was harvested 48 hours after transfection and passed through Nalgene 0.45 μ m PES syringe filters (Thermo, cat# 725-2545). In 6-well plates, 2 mL viral media was added to 1.25×10^6 THP-1 cells with final concentration of 8 μ g/mL polybrene (Sigma, cat# H9268). Plates were centrifuged at room temperature at 1500 rpm for 90 minutes. Cells were washed with PBS before resuspending in fresh media. Infection efficiency was measured by flow cytometry at 3 days post-infection.

Immunoprecipitation

293T cells were transfected with CMV-GFI1 or empty CMV vector then treated with DMSO or 250 nM INCB059872. After 48 hours, cells were lysed in NETN buffer (100 mM NaCl, 2 mM Tris pH 8.0, 0.5 mM EDTA, 0.5% NP-40, 25 mM NaF, 2 mM PMSF, 0.1% aprotinin). After removing an aliquot to serve as an "input" sample, each lysate was divided into two IP samples. For IgG control IPs, 3 μ g rabbit IgG (Invitrogen cat# 02-6102) was added to each sample. For LSD1 IPs, 3 μ g anti-LSD1 (Abcam, ab17721) was added to each sample. Lysates were incubated with antibody for 3 hours

while rotating at 4°C. Protein A (Invitrogen cat# 10001D) and Protein G (Invitrogen cat# 10003D) Dynabeads (15 µl of each) were added to each IP sample, and tubes were rotated at 4°C for 1 hour. Beads were washed three times with 0.5X NETN buffer by rotating 4°C for 5 min. Beads were resuspended in SDS loading buffer (40% glycerol, 240 mM Tris pH 6.8, 8% SDS, 0.4 mg/mL bromophenol blue, 5% beta-mercaptoethanol) and boiled for 10 min.

Protein harvest and western blotting

Cells were washed with cold PBS, and pellets were resuspended in RIPA buffer (150 mM NaCl, 50 mM Tris pH 8.0, 1% NP-40, 0.5% Na-deoxycholate, 0.1% SDS, 25 mM NaF, 2 mM PMSF, 0.1% aprotinin). Samples were vortexed and incubated for 15 min on ice before sonicating 5 short pulses using setting 5 on Virtis Virsonic homogenizer. Lysates were centrifuged at top speed for 15 min, and supernatants were transferred to new tubes. Protein samples were mixed with SDS loading buffer (final concentration 10% glycerol, 60 mM Tris pH 6.8, 2% SDS, 0.1 mg/mL bromophenol blue, 1.25% beta-mercaptoethanol) and boiled for 10 min. For histone blots, samples were run on 15% SDS-PA gel and transferred onto 0.22 µm nitrocellulose membrane (Licor Odyssey, cat# 926-31092). For other blots, samples were run on 8% SDS-PAGE gel and transferred onto 0.45 µm Immobilon FL PVDF membrane (Millipore, cat # IPFL00010). Primary antibodies used for Western blots are listed in Table 4.

Protein target	Company	Catalog #	Species	Dilution
LSD1	Abcam	ab17721	rabbit	1:1000
GFI1	Santa Cruz Biotechnology	sc-376949	mouse	1:200
Histone H3	Cell Signaling Technology	96C10	mouse	1:2500
H3K4me2	Abcam	ab7766	rabbit	1:2500
H3K4me1	Abcam	ab8895	rabbit	1:2500
RCOR1	Santa Cruz Biotechnology	sc-376567	mouse	1:500
Lamin B	Santa Cruz Biotechnology	sc-6217	goat	1:1000

Table 4. Primary antibodies for Western blotting.

MNase assay

Cells were pelleted and resuspended in 1 mL of lysis buffer (10 mM Tris pH 7.4, 300 mM sucrose, 3 mM CaCl₂, 2 mM MgCl₂, 1% Triton X-100, 5 mM DTT, 2 mM PMSF, 0.1% aprotinin). Samples were incubated on ice for 5 min. Nuclei were pelleted by centrifuging at 3500 rpm for 5 min. Pellets were resuspended in 250 µl reaction buffer (50 mM Tris pH 8.0, 5 mM CaCl₂). DNA concentration was measured by NanoDrop, and chromatin was aliquotted into 40 µg samples, 4 aliquots per condition, and reaction buffer was added to reach volume of 50 µl. Micrococcal nuclease (Thermo Scientific, cat# 88216) was diluted to 1 U/µl in 50% glycerol. Samples were equilibrated to room temp, then 1.25 µl diluted MNase was added to samples for 3, 6, or 9 min. At end of incubation, 75 µl cold reaction buffer and 12.5 µl 10X stop solution (250 mM EDTA pH 8.0, 5% SDS) were added. Samples were briefly vortexed then incubated on ice for 15

min. 1 μ l RNase A (10 μ g/ μ l) and 10 μ l 10% SDS were added to each tube, and samples were incubated at 37°C for 30 min. 1.5 μ l Proteinase K was added to each tube, and samples were incubated at 42°C overnight. DNA was phenol:chloroform extracted and ethanol precipitated twice. Samples were run on 1.5% agarose gel with ethidium bromide.

Wright-Giemsa staining

50,000 cells in 300 μ l volume of PBS were loaded into EZ Single Cytofunnels (Thermo, cat# A78710003). Funnels were spun in Cytospin centrifuge at 800 rpm for 3 min to transfer cells onto glass slides. For Wright-Giemsa staining, Fischer Hema 3 Stat Pack (cat# 123-869) was used according to manufacturer's instructions.

Flow cytometry analysis

Cells were washed with PBS containing 0.5% BSA and stained with BD Pharmingen anti-CD11b (clone ICRF44) conjugated to PE (cat# 301306) or APC (cat# 301310) using 18 μ l antibody per 10^6 cells, following manufacturer's staining protocol. Data were analyzed using FlowJo software (Becton, Dickinson and Company).

RT-PCR

RNA was isolated from cell lines by following manufacturer's instructions for TRIzol (Ambion, cat # 15596018) extraction. Aliquots of RNA were DNase-treated using Invitrogen Amplification Grade DNase I (cat# 18068015). Reverse transcription was performed with Applied Biosystems High-Capacity cDNA Reverse Transcription Kit

(cat# 4368814). PCR was performed using Bio-Rad iProof High-Fidelity DNA Polymerase (cat# 1725301) according to manufacturer's instructions. Primer sequences are listed in Table 5. Half of each PCR reaction was run on 1.5% agarose gel containing ethidium bromide.

Gene	Sequence	
GFI1B	forward	AGAAGGCTCACACCTACCAC
	reverse	GCTAGGCTTGTAGAATGGGGG
SDHA	forward	GGGTCCATCCATCGCATAAGA
	reverse	CTCCACGACATCCTTCCGTA

Table 5. Primer sequences for RT-PCR.

RNA-seq and analysis

For each sample, 0.75 million cells were resuspended in 1 mL TRIzol (Ambion, cat# 15596018), and RNA was isolated according to manufacturer's instructions. Samples were submitted to Vanderbilt Technologies for Advanced Genomics (VANTAGE) for polyA-enriched library preparation and sequencing on Illumina NextSeq500. Reads were aligned to hg19 genome using TopHat. Cuffdiff (Cufflinks software suite; Trapnell et al., 2010) was used to calculate differential gene expression. Heatmaps were generated using ClustVis web tool (Metsalu and Vilo, 2015). Gene Set Enrichment Analysis software v3.0 (Subramanian et al., 2005) was used to identify gene signatures associated with expression changes.

PRO-seq and analysis

Cells (~30 million per sample) were pelleted and resuspended in lysis buffer (10 mM Tris pH 7.4, 300 mM sucrose, 3 mM CaCl₂, 2 mM MgCl₂, 10% glycerol, 0.1% Triton X-100, 0.1% aprotinin) and incubated on ice for 5 min. Samples were dounce-homogenized 20 times and transferred to 15mL conical tubes. Nuclei were pelleted by spinning at 1500 rpm for 5 min. Nuclei were washed once with 3 mL cell lysis buffer and once with 1 mL glycerol storage buffer (50 mM Tris pH 8.3, 40% glycerol, 0.1 mM EDTA, 5 mM MgCl₂, 0.1% aprotinin). Nuclei were resuspended in 100 µl glycerol storage buffer, transferred to 1.5mL tubes, and stored at -80°C.

Buffers for PRO-seq were prepared using DEPC-treated H₂O. 2X reaction mix (10 mM Tris pH 8.0, 5 mM MgCl₂, 1 mM DTT, 300 mM KCl, 375 µM ATP, 375 µM GTP, 375 µM UTP, 500 µM biotin-11-CTP (Perkin-Elmer, cat# NEL542001), 0.8 U/µl SUPERase-In RNase inhibitor (Thermo, cat# AM2694), 1% sarkosyl) was equilibrated by incubating at 30°C. Nuclei were thawed on ice. Each nuclei sample was mixed with 100 µl 2X reaction mix and pipetted slowly 20X to mix. Reactions were incubated at 30°C for 3 min then stopped by adding 600 µl TRIzol LS (Ambion, cat# 10296010) and pipetting until homogenous. Tubes were rotated at room temp for 5 min before proceeding with chloroform extraction and ethanol precipitation. Precipitated pellets were dissolved in 20 µl H₂O and incubated at 65°C for 40 sec before placing on ice. For base hydrolysis, 5 µl 1N NaOH was added to each sample. Samples were incubated on ice for 10 min before neutralizing with 25 µl 1M Tris pH 6.8. Samples were passed through Bio-Spin P-30 gel columns (BIO-RAD, cat# 7326231) to remove excess nucleotides, and 1 µl SUPERase-In RNase inhibitor was added.

Dynabeads M-280 streptavidin magnetic beads (Invitrogen, cat# 11205D) were washed once with 0.1N NaOH + 50 mM NaCl then twice with 100 mM NaCl. Beads were then resuspended in binding buffer (10 mM Tris pH 7.4, 300 mM NaCl, 0.1% Triton X-100). Beads were mixed with RNA samples in a 1:1 ratio (50 μ l each) and rotated at room temp for 20 min. Tubes were placed against magnet, and liquid was removed. Beads were washed with 3 sequential washes: 500 μ l high salt wash (50 mM Tris pH 7.4, 2 M NaCl, 0.5% Triton X-100), 500 μ l binding buffer, 500 μ l low salt wash (5 mM Tris pH 7.4, 0.1% Triton X-100). Beads were TRIzol extracted twice, using 300 μ l TRIzol (Ambion, cat# 15596018) each time. Aqueous portions were pooled and ethanol precipitated. RNA pellets were resuspended in 5 μ l 2 μ M reverse 3' RNA adapter (5'-GAUCGUCGGACUGUAGAACUCUGAAC-3') and incubated at room temp for 5 min. Samples were incubated at 65°C for 20 sec then placed on ice. Ligation buffer (T4 RNA ligase buffer, T4 RNA ligase I (NEB, cat# M0204S), 1 mM ATP, 2 U/ μ l SUPERase-In RNase inhibitor) was added, and samples were incubated overnight at 20°C.

Samples were diluted with H₂O to volume of 50 μ l. Streptavidin bead binding and TRIzol extractions were carried out as described above. After ethanol precipitation, RNA pellets were dissolved in 5 μ l H₂O. Samples were incubated at 65°C for 1 min then placed on ice. RNA was incubated with 5' repair mix (1X CAP-CLIP buffer, 0.25 U/ μ l CAP-CLIP enzyme (CellScript, cat# C-CC15011H), 1 U/ μ l SUPERase-In RNase inhibitor) in total volume of 10 μ l for 2 hrs at 37°C. RNA was TRIzol extracted and ethanol precipitated. RNA pellets were dissolved in 5 μ l H₂O. Samples were incubated at 65°C for 1 min then placed on ice. RNA was incubated with PNK mix (1X PNK buffer, 1 mM ATP, T4 PNK (NEB, cat# M0201S), 1 U/ μ l SUPERase-In RNase inhibitor) in total

volume of 10 μ l for 1 hr at 37°C. RNA was TRIzol extracted and ethanol precipitated. RNA pellets were dissolved in 5 μ l of 2 μ M reverse 5' RNA adapter (5'-CCUUGGCACCCGAGAAUUGCA-3') and incubated at room temp for 5 min. Samples were incubated at 65°C for 20 sec then placed on ice. Ligation buffer (T4 RNA ligase buffer, T4 RNA ligase I (NEB, cat# M0204S), 1 mM ATP, 2 U/ μ l SUPERase-In RNase inhibitor) was added, and samples were incubated overnight at 20°C.

Samples were diluted with H₂O to volume of 50 μ l. Streptavidin bead binding and TRIzol extractions were carried out as described above. After ethanol precipitation, RNA pellets were dissolved in 5 μ l of 5 μ M RNA PCR primer RP1 (5'-AATGATACGGCGACCAC CGAGATCTACACGTTTCAGAGTTCTACAGTCCGA-3') and transferred to PCR tubes. Samples were incubated at 65°C for 5 min. Reverse transcription mix (final concentration: 1X first strand synthesis buffer, 10 mM DTT, 625 μ M each dNTP mix, 1 U/ μ l SUPERase-In RNase inhibitor) was added, and samples were incubated at 48°C for 3 min. 1 μ l SuperScript III RTase (Invitrogen, cat # 18080044) was added to each tube, and samples were incubated at 44°C for 20 min then 52°C for 45 min. H₂O was added to each sample to give final volume of 18 μ l, and samples were stored at -80°C overnight.

For library amplification, 16 μ l of cDNA was added to PCR mix (1X HF buffer, 1M betaine, 250 μ M each dNTPs, Phusion polymerase (NEB, cat# M0530S), 250 nM RPIx* barcoded primer). *Each sample received a unique Illumina TruSeq barcode.

Thermocycler protocol was as follows: 95°C for 2 min; 20 cycles of 95°C for 30 sec, 56°C for 30 sec, 72°C for 30 sec; 72°C for 3 min. H₂O was added to each PCR product to give total volume of 200 μ l, and DNA was ethanol precipitated and resuspended in 12

μl H_2O . Samples were run on native 8% polyacrylamide gels stained with SYBR Gold (Invitrogen, cat# S11494). DNA fragments sized between ~ 150 to ~ 400 bp were excised from gel, crushed with pestle, and incubated in soaking buffer (TE + 150 mM NaCl + 0.02% Tween-20) overnight while shaking at 37°C . Samples were centrifuged at top speed for 5 min, and eluate was removed. Additional soaking buffer was added to gel pieces, and samples were incubated while shaking at 37°C for 4 more hours. Samples were centrifuged again, and eluates were pooled and passed through Costar Spin-X centrifuge tube filters (Corning, cat# 8162) to remove gel debris. DNA was extracted with phenol:chloroform:isoamyl alcohol, ethanol precipitated, and resuspended in $10 \mu\text{l}$ 1 mM EDTA. Samples were submitted to VANTAGE for sequencing on Illumina NextSeq500.

Reads were trimmed with Trimmomatic to remove adapter sequences. Reads were converted to their reverse complements using FASTX-Toolkit. Reads were aligned to hg19 genome using bowtie2. Samtools was used to convert sam files to bam files and remove low-quality sequences (mapping quality score < 10). Nascent RNA Sequencing Analysis (NRSA) software package (Wang et al., 2018) was used to quantify changes in transcription. Gene Set Enrichment Analysis software v3.0 (Subramanian et al., 2005) was used to identify gene signatures associated with transcriptional changes. HOMER software (Heinz et al., 2010) was used for motif analysis.

H3K4me1/2 ChIP-seq and analysis

THP-1 cells were seeded at 0.4×10^6 /mL before adding drug (DMSO or 25nM INCB059872). After 48 hours, immediately before crosslinking, approximately 0.74 million S2 cells were added to each sample containing 20 million THP-1 cells. DNA and protein were crosslinked by adding 1% formaldehyde and rocking for 10 min at room temperature. Crosslinking reaction was quenched by adding glycine to a concentration of 125mM. Cells were washed twice with cold PBS before freezing pellets at -80°C . Cells were lysed by resuspending in cell lysis buffer (10 mM Tris-HCl pH 8.0, 10 mM NaCl, 0.5% NP-40) and sitting on ice for 10 min. Samples were centrifuged, and nuclei were resuspended in nuclei lysis buffer (50 mM Tris-HCl pH 8.0, 10 mM EDTA pH 8.0, 0.5% SDS) and kept on ice for 10 min before sonication using a Bioruptor (Diagenode) on high setting for 15 cycles (30 sec on, 30 sec off). After removing an aliquot to serve as input, chromatin from each sample was divided between two tubes and diluted 1:4 with ChIP dilution buffer (16.7 mM Tris-HCl pH 8.0, 1.2 mM EDTA pH 8.0, 167 mM NaCl, 1.1% Triton X-100, 0.01% SDS). $3\mu\text{g}$ anti-H3K4me2 (Abcam, ab7766) or anti-H3K4me1 (Abcam, ab8895) was added to each tube. Samples were rotated at 4°C for 2 hours before adding $15\mu\text{l}$ Protein A Dynabeads (Invitrogen cat# 10001D) and $15\mu\text{l}$ Protein G Dynabeads (Invitrogen cat# 10003D). Samples were rotated at 4°C for 1 hour before washing beads 7 times: (twice with low salt buffer (20 mM Tris-HCl pH 8.0, 2 mM EDTA pH 8.0, 150 mM NaCl, 1% Triton X-100, 0.1% SDS), twice with high salt buffer (500 mM NaCl, otherwise same as low salt buffer), once with LiCl buffer (10 mM Tris-HCl pH 8.0, 1 mM EDTA pH 8.0, 250 mM LiCl, 1% NP-40, 1% Na-deoxycholate), and twice with TE. Samples were eluted twice by resuspending beads in elution buffer (10%

SDS, 1 M NaHCO₃) and rotating for 15 min at room temperature. NaCl was added to a concentration of 190mM, and samples were incubated at 65°C overnight. Each sample was treated with 20 µg RNase A (Clontech cat# 740505) by incubating at 37°C for 1 hour. Next, samples were treated with 32 µg Proteinase K (Clontech cat# 740506) by incubating at 45°C for 2 hours. DNA was extracted by phenol:chloroform:isoamyl alcohol extraction. Libraries were prepared by taking 100 ng DNA from each input and IP sample for polishing, A-tailing, and ligation of adapters. Agencourt AMPure XP Beads (Beckman Coulter cat# A63880) were used at 1.8X volume according to manufacturer's instructions for size selection, and eluted material was PCR amplified with Q5 Hot Start DNA Polymerase (NEB cat# M0493S) for 21 cycles. Samples were run on 1.5% agarose gel, and size range of 200-500 bp was extracted and purified using Wizard SV Gel & PCR Cleanup Kit (Promega cat# A9281). Libraries were submitted to VANTAGE for sequencing on Illumina NextSeq500.

Trimmomatic was used to remove adapters and low-quality sequences. Reads were aligned to a combined genome file containing both *Human* hg19 and *Drosophila* dm3 using Bowtie2. Duplicate reads and reads with mapping quality <10 were removed using samtools. Reads aligned to dm3 were separated into their own files, and read counts of these files were used to calculate normalization factors for each sample. MACS2 was used to call peaks with q-value cutoff of 0.001. Count tables were generated using R program DiffBind (Stark and Brown, 2011). Normalization factors were used with DESeq2 to calculate changes in peak size. HOMER software (Heinz et al., 2010) was used for motif analysis.

H3K27ac ChIP-seq and analysis

THP-1 cells were seeded at 0.4×10^6 /mL before adding drug (DMSO or 25nM INCB059872). After 24 hours, 40 million cells per sample were pelleted and washed with PBS. Cells were washed and resuspended in PBS. DNA and protein were crosslinked by adding 1% methanol-free formaldehyde (Thermo cat# 28908) and rocking for 10 min at room temperature. Crosslinking reaction was quenched by adding glycine to a concentration of 125mM and rocking for 5 min at room temperature. Cells were washed twice with cold PBS then resuspended in Buffer 1 (50 mM HEPES pH 7.5, 140 mM NaCl, 1 mM EDTA, 10% glycerol, 0.5% NP-40, 0.25% Triton X-100, 0.2% aprotinin, 1 mM PMSF) and rocked at 4°C for 10 min. Samples were centrifuged and resuspended in Buffer 2 (10 mM Tris pH 8.0, 200 mM NaCl, 1 mM EDTA, 0.5 mM EGTA, 0.2% aprotinin, 1 mM PMSF) then rocked at 4°C for 5 min. Samples were centrifuged then resuspended in Buffer 3 (10 mM Tris pH 8.0, 100 mM NaCl, 1 mM EDTA, 0.5 mM EGTA, 0.1% Na deoxycholate, 0.5% sarkosyl, 0.2% aprotinin, 1 mM PMSF, Complete mini protease inhibitor cocktail (Roche cat# 4693159001)). Samples were sonicated using a Bioruptor (Diagenode) on high setting for 25 cycles (30 sec on, 30 sec off). Next, 1% Triton X-100 was added, and samples were vortexed for 10 sec. Debris was pelleted by centrifuging at 20,000 xg for 10 min, and cleared lysates were transferred to new tubes. At this point, aliquots of chromatin were removed to serve as input controls. One quarter of each sample volume (corresponding to ~10 million cells equivalent) was used for immunoprecipitation. Samples were incubated overnight with 10 µg anti-H3K27ac (Abcam, ab4729). Protein A (Invitrogen cat# 10001D) and Protein G (Invitrogen cat# 10003D) Dynabeads were mixed at 1:1 ratio and washed with

equilibration buffer (10 mM Tris pH 8.0, 100 mM NaCl, 1 mM EDTA, 0.5 mM EGTA, 0.1% Na-deoxycholate, 1% Triton X-100). Samples were rotated at 4°C for 1 hour after adding 60 µl Dynabeads mix per sample. Beads were washed four times (once in each buffer) by rotating for 5 min at 4°C in the following buffers: low salt wash (20 mM Tris pH 8.0, 150 mM NaCl, 2 mM EDTA, 1% Triton X-100), high salt wash (20 mM Tris pH 8.0, 500 mM NaCl, 2 mM EDTA, 1% Triton X-100), LiCl wash (10 mM Tris pH 8.0, 25 mM LiCl, 1 mM EDTA, 1% Triton X-100), TE. Beads were washed a second time in TE by rotating for 5 min at room temperature. Beads were resuspended in 50 µl elution buffer (TE with 0.1% SDS, 200 mM NaCl, 0.8 µg/µl Proteinase K (Clontech cat# 740506)). Each sample was treated with 20 µg RNase A (Clontech cat# 740505) by incubating at 37°C for 30 min. Samples were incubated with shaking at 65°C overnight before removing eluates from beads. Agencourt AMPure XP Beads (Beckman Coulter cat# A63880) were used at 1.8X volume according to manufacturer's instructions for size selection. Libraries were preparing by following manufacturer's instructions for NEBNext Ultra II DNA Library Prep Kit for Illumina (cat# E7645) and submitted to VANTAGE for sequencing on Illumina NovaSeq.

Reads were trimmed to remove adapters and low-quality bases using Trimmomatic. Bowtie2 was used to align reads to hg19 genome. Duplicate reads and reads with mapping quality <10 were removed using samtools. MACS2 was used to call peaks with q-value cutoff of 0.001. DiffBind R package (Stark and Brown, 2011) was used to calculate differential peak sizes. HOMER software (Heinz et al., 2010) was used for motif analysis.

Single-cell RNA-seq and analysis

After 48-hr drug treatments, apoptotic cells were removed from the AML patient bone marrow cultures using Miltenyi Annexin V Microbead Kit (cat# 130-090-201) with MACS LS columns (cat# 130-042-401). The Annexin V-negative cells were submitted to VANTAGE for single-cell RNA-seq library prep and processing with 10X Genomics Chromium Controller. Samples were demultiplexed and single-cell gene expression matrices were generated using Cell Ranger software. Seurat R package (Butler et al., 2018) was used for data analysis (see Appendix for R code).

Mouse Experiments

Mice

All animal experiments were conducted in accordance with guidelines approved by the IACUC at Vanderbilt University Medical Center. For the *in vivo* studies, female 6-8 week old C57BL/6J mice (The Jackson Laboratory) were treated daily with 10mg/kg INCB059872 via oral gavage for up to six days. INCB059872 was dissolved in N,N-dimethylacetamide (DMAC; Sigma, cat# 185884) and diluted in 5% methylcellulose (Sigma, cat# M0512).

Platelet counts

For peripheral blood analysis, blood was collected via tail vein into an EDTA microtainer and analyzed for complete blood counts using a Hemavet (Drew Scientific).

Flow cytometry analysis

Bone marrow was flushed from femurs and tibias using PBS with 0.5% BSA. Red blood cells were removed by incubation with Qiagen Buffer EL (cat# 79217) according to manufacturer's protocol. Cells were resuspended in PBS with 0.5% BSA at a density of approximately 10^7 cells/mL before proceeding to staining. For lineage staining, BD Pharmingen Biotin Mouse Lineage Panel (cat# 559971) was used according to manufacturer's instructions and followed by staining with 0.5 μ l streptavidin-Pacific Blue (Invitrogen, cat# S11222) per 10^6 cells. Additional antibodies are listed in Table 6. Data were analyzed using FlowJo (Becton Dickinson and Company) and GraphPad Prism (GraphPad Software).

Protein target	Fluorophore	Company	Catalog #	Volume per 10⁶cells
cKit	PE/Cy7	Invitrogen	25-1172-82	1 µl
Sca1	PerCP/Cy5.5	Invitrogen	45-5981-82	1 µl
Flt3	PE	Invitrogen	12-1351-81	1 µl
CD16/32	PE	Invitrogen	12-0161-81	1 µl
CD34	AlexaFluor647	BD Pharmingen	560230	2 µl
CD41	APC/eFluor780	Invitrogen	47-0411-82	1 µl
CD200r3	PE	BioLegend	142205	1 µl
SiglecH	APC	BioLegend	129611	1 µl
Ly6d	FITC	BioLegend	138605	1 µl
CD36	PE	BioLegend	102605	1 µl
FcgRIV	APC/Fire750	BioLegend	149509	1 µl
Ter119	PE	Invitrogen	12-5921-81	1 µl
B220	eFluor450	Invitrogen	48-0452-82	1 µl
IgM	PE/Cy7	Invitrogen	25-5790-82	1 µl
CD3e	APC	Invitrogen	17-0031-82	1 µl
CD11b	PE	Invitrogen	12-0112-83	1 µl
Ly6g	PE/Cy7	Invitrogen	25-5931-82	1 µl

Table 6. Antibodies for mouse immunophenotyping.

Single-cell RNA-seq and analysis

Bone marrow was harvested as described above and stained with BD Pharmingen Biotin Mouse Lineage Panel (cat# 559971) and streptavidin-PacBlue

(Invitrogen, cat# S11222). Zombie-NIR Fixable Viability Dye (BioLegend cat# 423105) was added to each sample at 1:1000 dilution before sorting alive lineage-negative population (PacBlue-/NIR-). Sorted cells were submitted to VANTAGE for single-cell RNA-seq library prep and processing with 10X Genomics Chromium Controller. Samples were demultiplexed and single-cell gene expression matrices were generated using Cell Ranger software. Seurat R package (Butler et al., 2018) was used for data analysis (see Appendix for R code).

RNA-seq and analysis

Bone marrow was harvested and stained for lineage markers, CD41, and CD200r3 as described above. Lin- CD41+ CD200r3- bone marrow cells from 6 mice (2 replicates of 3 conditions) were flow-sorted directly into Buffer RLT from Qiagen RNeasy Mini Kit (cat# 74104), and RNA was isolated according to manufacturer's protocol. Samples were submitted to HudsonAlpha Genomic Services Laboratory for library preparation with Nugen Ovation RNA-Seq System V2 kit (cat# 7102-08) and sequencing on Illumina NovaSeq6000.

Trimmomatic was used to remove adapters and low-quality sequences. Reads were aligned to mouse mm10 genome using Bowtie2. Samtools was used to convert sam files to bam files and remove low-quality sequences (mapping quality score <10). Cuffdiff (Cufflinks software suite; Trapnell et al., 2010) was used to calculate differential gene expression. Heatmaps were generated using ClustVis web tool (Metsalu and Vilo, 2015). Gene Set Enrichment Analysis software v3.0 (Subramanian et al., 2005) was used to identify gene signatures associated with expression changes.

CHAPTER THREE

INHIBITION OF LSD1 INDUCES DIFFERENTIATION OF ACUTE MYELOID LEUKEMIA CELLS

Background and Significance

Acute myeloid leukemia (AML) is characterized by accumulation of incompletely differentiated hematopoietic progenitor cells in the bone marrow. In general, AML has a lower mutational burden than most other malignancies, though approximately half of new AML diagnoses have readily detectable cytogenetic abnormalities (Mould et al., 2015). As the genetics of AML have been defined over the past 25 years, it is clear that many AML cases are initiated by chromosomal translocations that affect DNA-binding transcription factors that recruit histone deacetylases and acetyltransferases, as well as histone methyltransferases and demethylases, and enzymes that control histone ubiquitination (Yang et al., 2017). Despite advances in our understanding of AML biology, chemotherapy is still the standard treatment for newly diagnosed patients. However, drugs targeting some of the histone-modifying enzymes are now in clinical trials and preclinical studies.

One potential therapeutic target is the histone demethylase Lysine-Specific Demethylase 1 (LSD1), which is overexpressed in several types of malignancies, including AML. This enzyme is found in transcriptional repressor complexes and helps to silence gene expression by removing H3K4 mono- and di-methylation. Inhibitors of

LSD1 are expected to modulate gene expression by de-repressing genes regulated by these complexes. Early studies showed that decreased LSD1 activity could synergize with all-trans retinoic acid to induce differentiation of myeloid leukemia cells (Schenk et al., 2012). Leukemias driven by MLL translocations are especially sensitive to LSD1 knockdown and inhibition (Harris et al., 2012; Feng et al., 2016).

INCB059872 is a selective, orally bioavailable LSD1 inhibitor that has recently entered early clinical trials. In preclinical studies, this compound has shown efficacy in models of small cell lung cancer (Lee et al., 2016a), Ewing sarcoma (Roman et al., 2017), prostate cancer (Civenni et al., 2018), and T-cell acute lymphoblastic leukemia (Diamond et al., 2018). INCB059872 is especially promising for the treatment of AML, as it induced cell differentiation of a murine MLL-AF9 leukemia model and inhibited growth in xenograft models (Lee et al., 2016b). Additionally, in xenografts of poorly differentiated human AML, INCB059872 treatment drove differentiation toward more mature myeloid cell types (Chadderton et al., 2018). In this chapter, I will describe multiple genomic approaches that I used to better understand the molecular effects of INCB059872 in MLL-rearranged AML cell lines and in a bone marrow sample from an AML patient.

Results

AML cell lines are sensitive to INCB059872

First, I tested INCB059872 in two cell lines with MLL rearrangements, THP-1 (MLL-AF9) and MV-4-11 (MLL-AF4). These cell lines had different responses to the

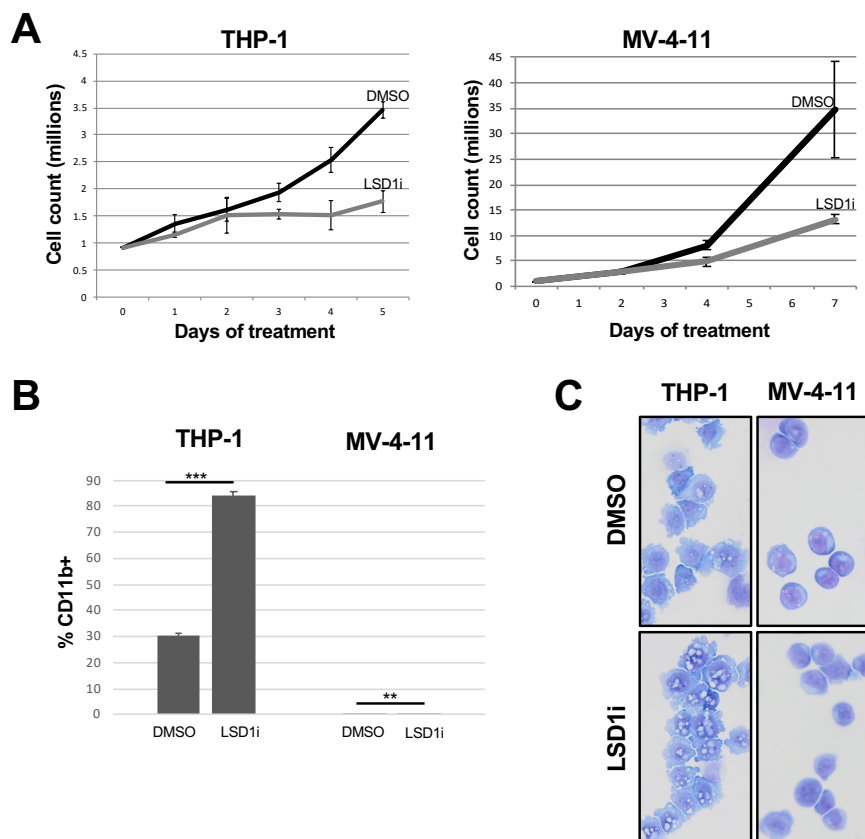


Figure 6. INCB059872 impairs proliferation and induces differentiation of AML cell lines. (A) Growth curves of THP-1 (left) or MV-4-11 (right) following treatment with INCB059872. 25nM in THP-1; 100nM in MV-4-11 (B) Flow cytometry analysis of CD11b expression in THP-1 (left) or MV-4-11 (right) at 3 days after treatment with INCB059872. ** $p < 0.01$, *** $p < 0.001$ (C) Wright-Giemsa staining of THP-1 and MV-4-11 cells after 3-day INCB059872 treatment; images taken at 400X.

inhibitor, as THP-1 showed a growth defect within one cell doubling time (~3 days) while treated MV-4-11 cells continued to grow at the same rate as untreated cells for multiple cell divisions before proliferation became noticeably slower (Fig. 6A). Coincident with the slowing of cell growth, THP-1 cells began expressing CD11b (surface marker found on monocytes and granulocytes) and showed morphological changes indicative of myeloid differentiation (Fig. 6B,C). Conversely, MV-4-11 cells did not show overt signs of differentiation after INCB059872 treatment (Fig. 6B,C). Even if the drug was washed

out after 24hr and replaced with DMSO-containing media for the next 48hr, THP-1 cells still differentiated to nearly the same extent as if continuously exposed to INCB059872 (Fig. 7). This confirms that the compound acts as an irreversible inhibitor.

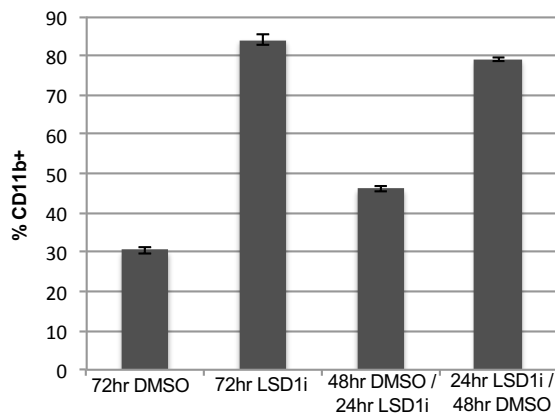


Figure 7. INCB059872 is an irreversible LSD1 inhibitor. Flow cytometry analysis of CD11b expression in THP-1 cells treated with INCB059872 or vehicle control for varying intervals.

Reduced expression of CoREST components mimics INCB059872 treatment

To confirm that the phenotypes observed with INCB059872 in THP-1 cells were on-target, I used shRNA to decrease LSD1 expression for comparison. Indeed, 10 days after infecting THP-1 cells with virus containing shRNA targeting LSD1, the majority of cells began to express CD11b (Fig. 8) At the same time, I wanted to determine if knockdown of proteins that interact with LSD1 would also induce differentiation, as this would provide insight as to which repressor complex modulates expression of differentiation-related genes in THP-1 cells. I tested shRNAs targeting NuRD complex subunits CHD3 and CHD4, as well as CoREST complex subunit RCOR1. KAT8 Regulatory NSL Complex Subunit 1 (KANSL1), a subunit of the MLL histone methyltransferase complex and of the NSL (nonspecific lethal) histone acetyltransferase

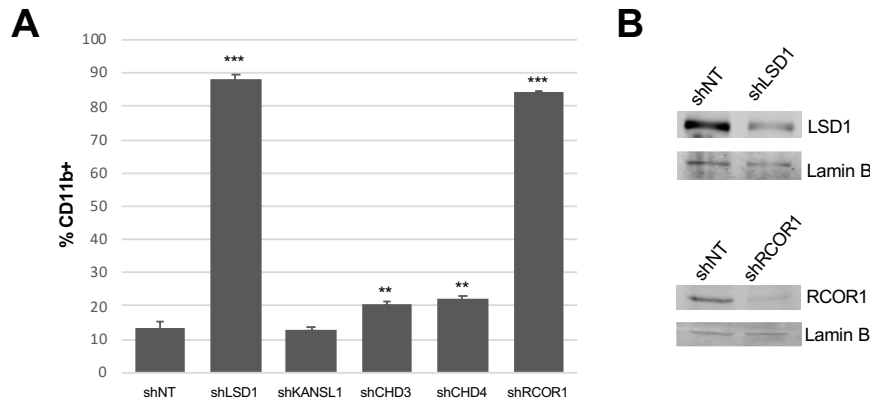


Figure 8. Reduced expression of CoREST components mimics LSD1 inhibition. (A) Flow cytometry analysis of CD11b expression in THP-1 cells 10 days following lentiviral infection with shRNA targeting LSD1 or interacting proteins. shNT, non-targeting control. ** $p < 0.01$, *** $p < 0.001$ (B) Western blot analysis of LSD1 or RCOR1 protein levels in THP-1 cells 5 days following lentiviral infection with indicated shRNA. Lamin B blots included as loading control.

complex, was included in this experiment because yeast two-hybrid results identified it as an interactor with LSD1. Only RCOR1 knockdown induced differentiation of THP-1 cells to the same extent as LSD1 knockdown or inhibitor treatment (Fig. 8), suggesting that the effects of INCB059872 were mediated by inactivation of CoREST rather than by inhibiting other complexes.

RNA-seq identifies differentiation signature associated with INCB059872 treatment

To begin to characterize the changes in gene expression triggered by INCB059872, I performed RNA-seq analysis of the early (3hr) and intermediate (24hr) effects of LSD1 inhibition in THP-1 and MV-4-11 cell lines. At the 3hr timepoint, there were relatively few changes in expression that met the significance cutoff (q -value < 0.05). In THP-1, only 31 transcripts were upregulated and 92 downregulated at least 1.5-fold (Fig. 9, upper left). In contrast, MV-4-11 cells did not have any significantly downregulated genes, but 194 genes were upregulated at least 1.5-fold (Fig. 9, lower

left). The small number of affected transcripts was to be expected because 3 hours is a short window of time for a buildup of histone modifications and subsequent transcription and accumulation of mRNA to occur.

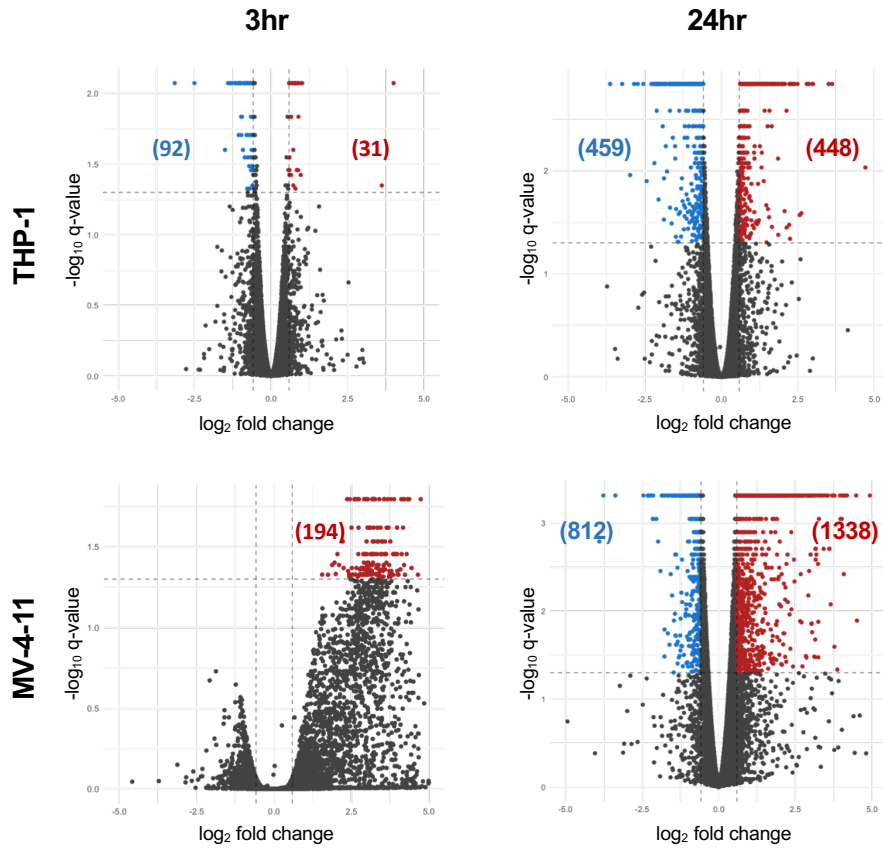


Figure 9. RNA-seq analysis: Volcano plots show gene expression changes caused by 3hr or 24hr INCB059872 treatment in AML cell lines. Genes that were up- or down-regulated >1.5-fold with $q < 0.05$ are indicated by red or blue, respectively.

By 24hr after drug treatment in both cell lines, RNA-seq revealed hundreds of significant changes in gene expression. Surprisingly, more than twice as many genes were induced at least 1.5-fold in MV-4-11 (1338) as compared to THP-1 (448; Fig 9, right), even though THP-1 cells showed a more dramatic phenotype in response to

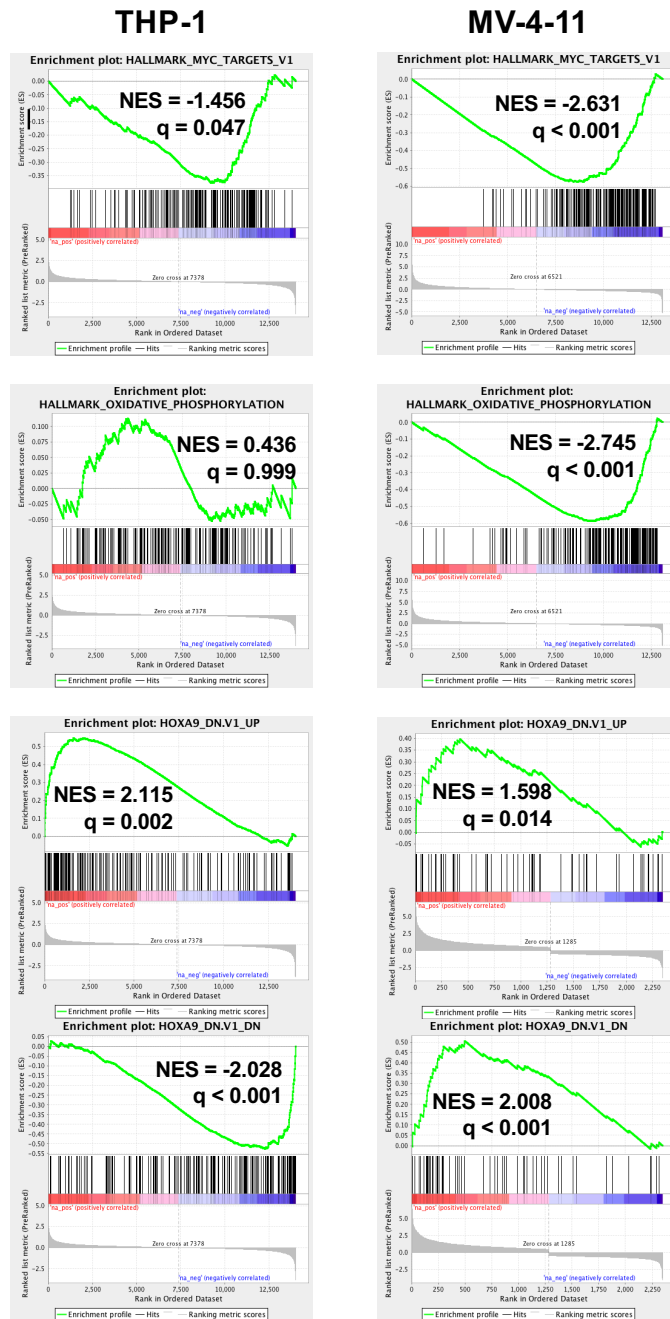


Figure 10. Gene set enrichment analysis of RNA-seq data shows differential response to INCB059872 between THP-1 and MV-4-11 cell lines. Top: MYC target genes; Middle: genes associated with oxidative phosphorylation; Bottom: Gene sets from Faber et al. (2009) that are up- or down-regulated by knockdown of HOXA9 in MOLM-14 cells.

INCB059872. In fact, for THP-1, the number of genes down-regulated genes was approximately equal to the number of up-regulated genes. Consistent with reduced proliferation, gene set enrichment analysis revealed that MYC target genes were downregulated in both cell lines, though to a greater extent in MV-4-11 (Fig. 10, top). Interestingly, an oxidative phosphorylation gene signature was highly downregulated in MV-4-11 but not in THP-1 (Fig. 10, middle). Though it is unclear why this set of genes was not similarly changed in THP-1 cells, decreased oxidative phosphorylation is encouraging from a therapeutic perspective because AML blasts can be more dependent on oxidative phosphorylation than healthy hematopoietic cells (Rashkovan and Ferrando, 2019). Gene set enrichment analysis also showed that INCB059872 induced gene expression changes in THP-1 similar to changes caused by knockdown of Homeobox A9 (HOXA9) (Fig. 10, bottom). Given that HOXA9 drives a gene expression pattern that promotes self-renewal (Vijapurkar et al., 2004), reduced expression of these target genes likely contributed to myeloid differentiation. Gene expression changes in MV-4-11 did not correlate with the HOXA9 signature (Fig. 10, bottom).

As shown by the heatmap in Fig. 11A, the majority of transcripts that were upregulated by INCB059872 treatment in THP-1 were also upregulated in MV-4-11, but downregulated transcripts were mostly unique to each cell line (Fig. 11A,B). KEGG pathway analysis of the 178 genes upregulated in both cell lines indicates that differentiation-related pathways were affected by INCB059872 (Fig. 11C). Categories identified as enriched encompass processes associated with monocyte/granulocyte functions, such as “antigen processing & presentation”, “phagosome”, and “toll-like receptor signaling pathway”. Upregulated genes in the “hematopoietic cell lineage”

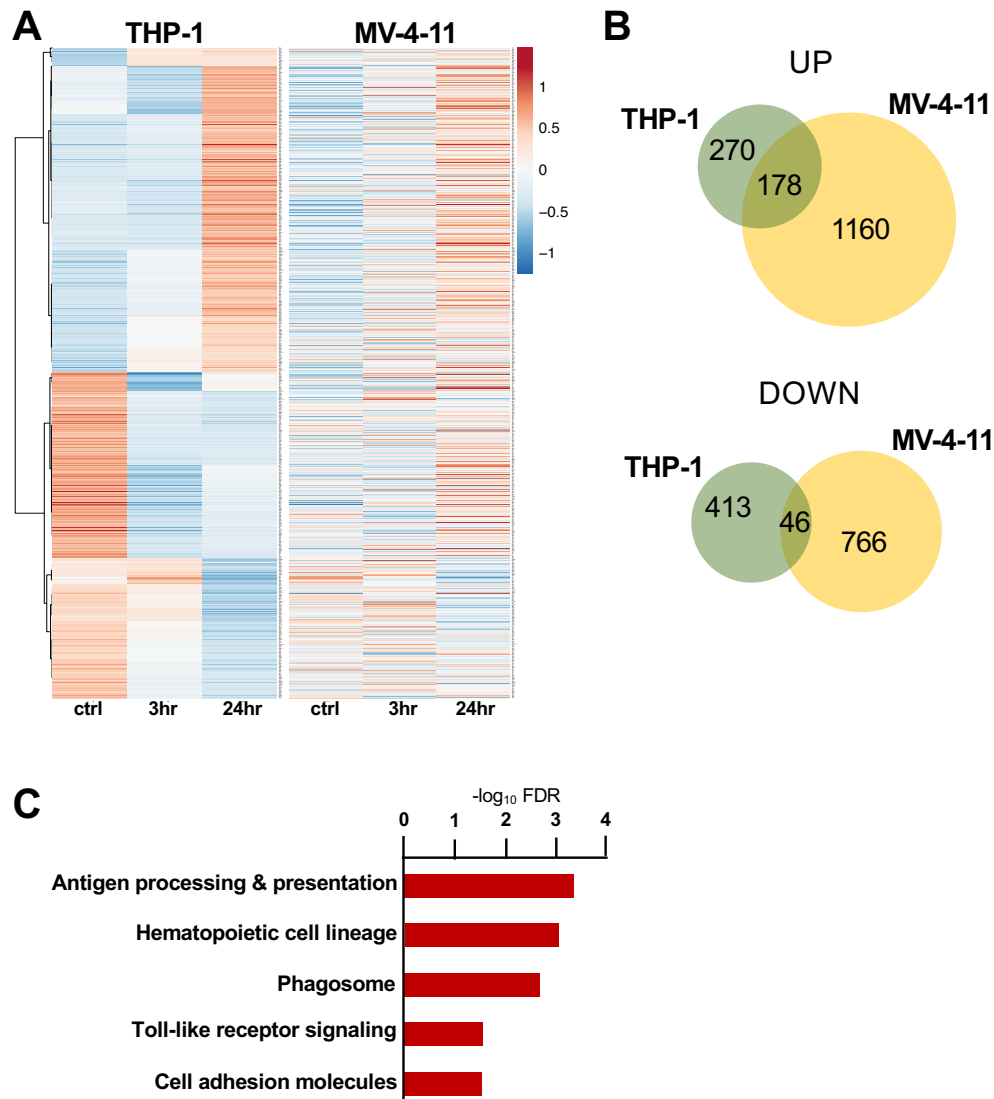


Figure 11. RNA-seq analysis of LSD1i in AML cell lines shows commonly upregulated genes are associated with myeloid differentiation. (A) Clustered heatmaps showing $\ln(\text{RPKM} + 1)$ values with Pareto scaling and row-centering for genes with $\text{FDR} < 0.05$ in THP-1 24hr analysis. (B) Venn diagrams showing genes up- or down-regulated at least 1.5-fold ($q < 0.05$) by 24hr treatment in both cell lines. (C) KEGG overrepresentation analysis of 178 genes commonly upregulated in THP-1 and MV-4-11 cells at 24hr timepoint.

pathway include CD1C/D, colony stimulating factor receptors CSF1R/2RA, major histocompatibility complex class II beta chain HLA-DMB, and Integrin Alpha Subunit M (ITGAM, also known as CD11b). Additionally, KIT expression was decreased in both

cell lines, supporting the evidence that INCB059872 shifts cells toward later stages of hematopoiesis.

PRO-seq of INCB059872-treated cells reveals increased transcription at myeloid differentiation genes

As LSD1 binds to intergenic and intronic regions as well as promoters and can control H3K4 methylation, INCB059872 was expected to affect enhancer activity. Therefore, I used precision nuclear run-on transcription and sequencing (PRO-seq) at 6, 12, and 24hr after addition of INCB059872 to THP-1 cells to measure genome-wide nascent transcription, as this is one of the best methods to identify active enhancers and RNA polymerase pausing and elongation. For this experiment, nuclei are isolated for run-on reactions in which biotinylated CTP is incorporated into nascent transcripts, and biotin-labeled RNA is used to prepare libraries for sequencing. These libraries provide strand-specific maps of active polymerases with near base-pair resolution.

INCB059872 caused upregulation (>1.5-fold) of about 200 genes by 24hr, with several of these changes being detectable at earlier time points as well (Fig. 12A, left). In contrast to the changes in steady-state mRNA levels (Fig. 9), analysis of nascent transcripts indicated that the drug primarily acted as an activator of transcription- only 40 genes showed decreased polymerase density (at least 1.5-fold) within the gene body after 24hr treatment (Fig. 12A, right). By mapping the relative polymerase density in drug-treated versus control cells, we determined that those genes affected by INCB059872 had altered polymerase initiation, rather than changes in promoter-proximal paused polymerase and/or polymerase elongation (Fig. 12B).

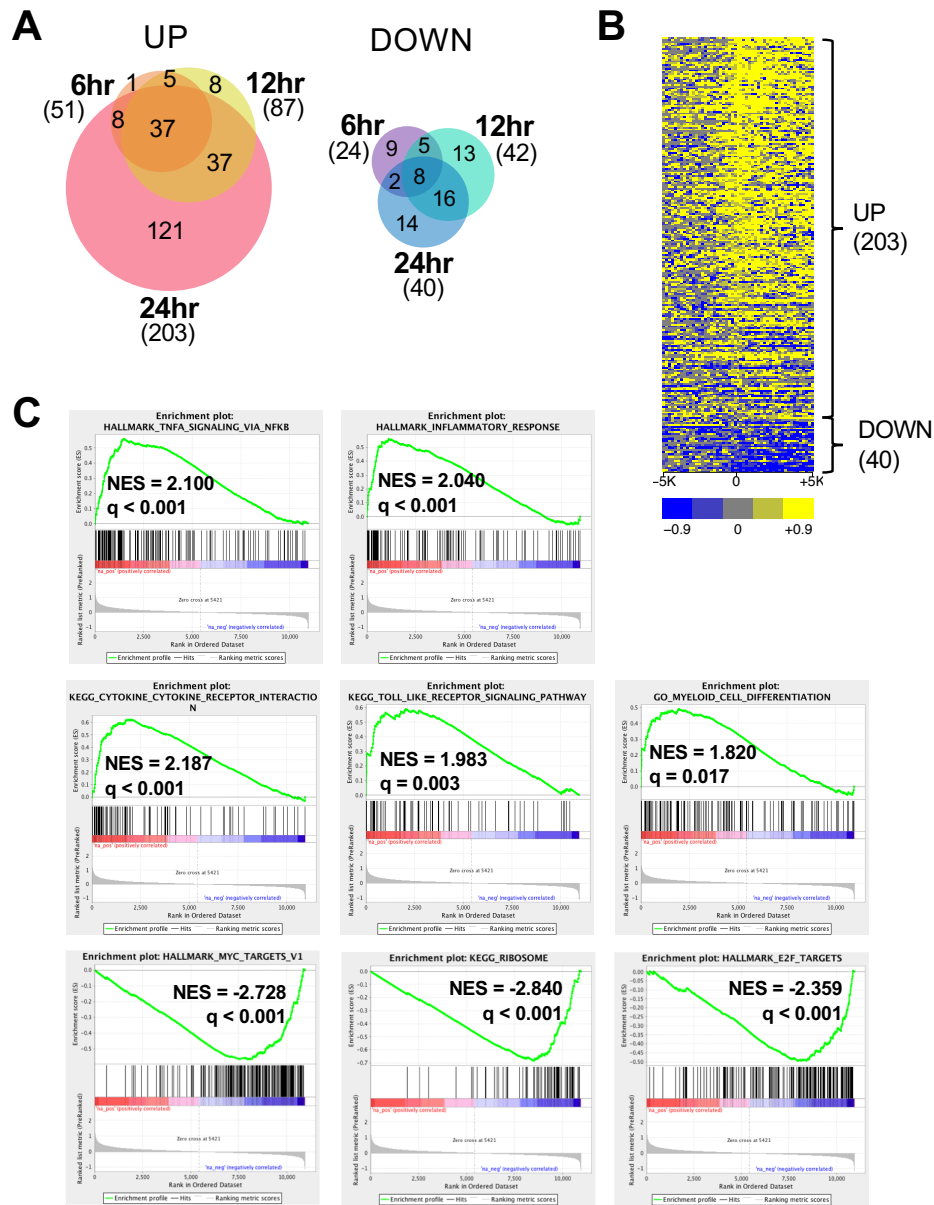


Figure 12. PRO-seq analysis of gene expression changes in THP-1 cells in response to LSD1i. (A) Venn diagrams of genes with > 1.5-fold change ($\text{padj} < 0.05$) in gene body transcription at 6, 12, or 24hr after INCB059872 treatment. Left, upregulated genes; right, downregulated genes. (B) Heatmap of polymerase density surrounding TSSs of genes meeting 1.5-fold change cutoff at 24hr. Yellow indicates higher density of active polymerase at a locus in treated cells relative to control cells. (C) Ranked list gene set enrichment analysis. Top and middle rows show gene lists that are upregulated by 24hr treatment, and bottom row shows gene lists downregulated by 24hr treatment.

Using a ranked list of changes in gene body transcription, gene set enrichment analysis identified several differentiation-related gene sets that were upregulated after 24hr INCB059872 treatment in THP-1 cells. These pathways included NFkB signaling, toll-like receptor signaling, cytokine receptors, inflammation, and myeloid differentiation (Fig. 12C, top and middle rows). Additionally, this analysis indicated that MYC targets, E2F targets, and ribosome genes were downregulated at the transcriptional level (Fig. 12C, bottom row). Though the decreases in polymerase density at individual genes were small, these trends are consistent with the loss of proliferation as THP-1 cells begin the differentiation process.

I also performed PRO-seq on MV-4-11 cells treated with INCB059872 for 24hr, and the results were similar to what I observed in THP-1 cells. There were more genes with an increase in gene body polymerase density (378 with >1.5-fold increase) than decreased genes (91 with >1.5-fold decrease). Plotting a heatmap of polymerase density around transcription start sites showed that transcriptional changes are due to polymerase initiation (Fig. 13A). Gene set enrichment plots show the same overall trends in gene expression as seen in THP-1 cells (compare Fig. 13B to Fig. 12C), with the exception that E2F targets were not significantly downregulated in MV-4-11 at this time point, which is consistent with the delayed effect of the drug on proliferation.

PRO-seq of THP-1 cells treated with INCB059872 reveals increased transcription at GF11-regulated enhancers

The PRO-seq dataset from inhibitor-treated THP-1 cells was also useful for measuring transcriptional changes at enhancers, which were identified by intergenic bidirectional transcription. These changes greatly outnumbered changes within gene

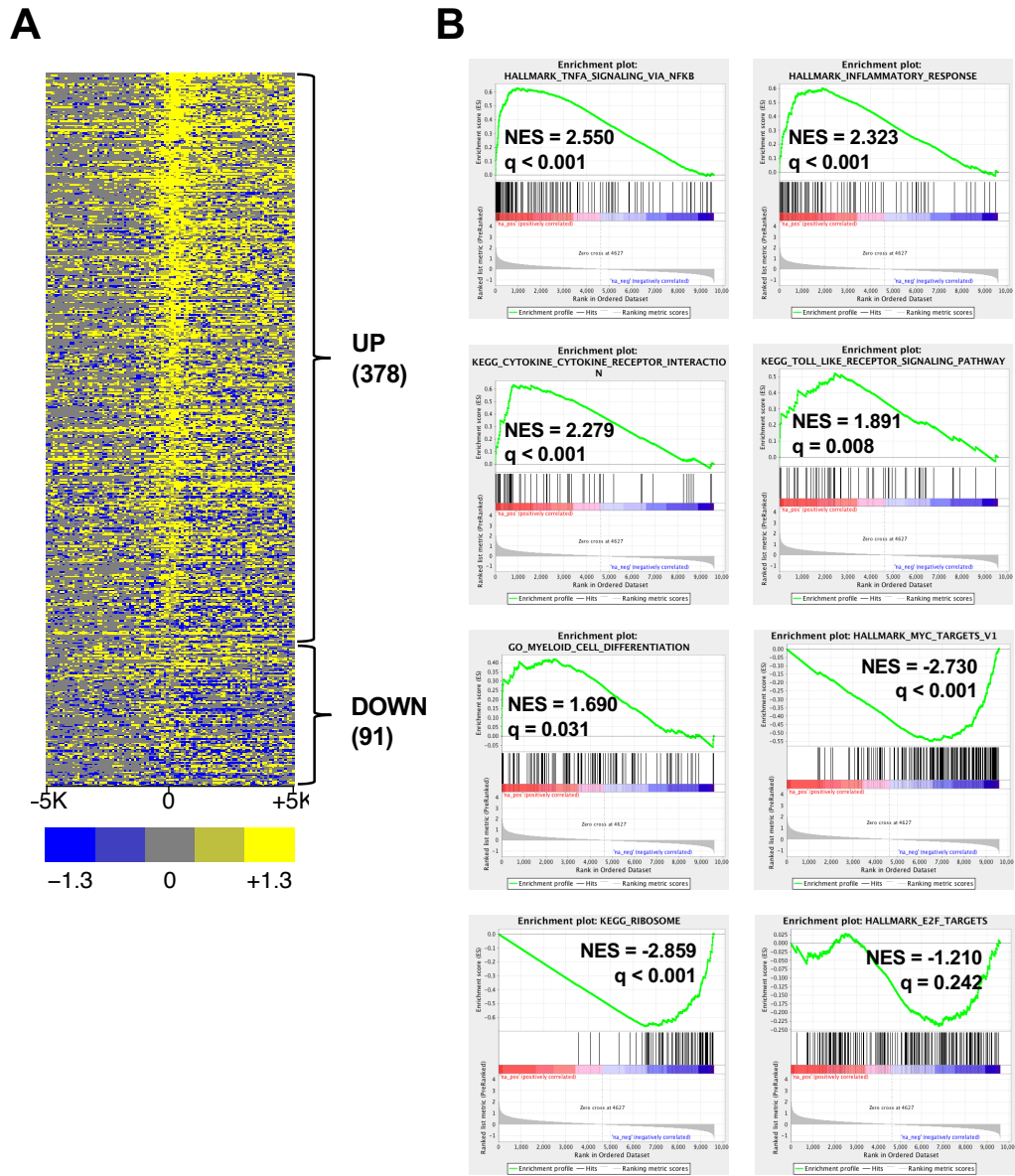


Figure 13. PRO-seq analysis of transcriptional changes in MV-4-11 cells after 24hr INCB059872 treatment. (A) Heatmap of polymerase density surrounding TSSs of genes that had >1.5-fold change in gene body transcription. Yellow indicates higher density of active polymerase at a locus in treated cells relative to control cells. (B) Ranked list gene set enrichment analysis.

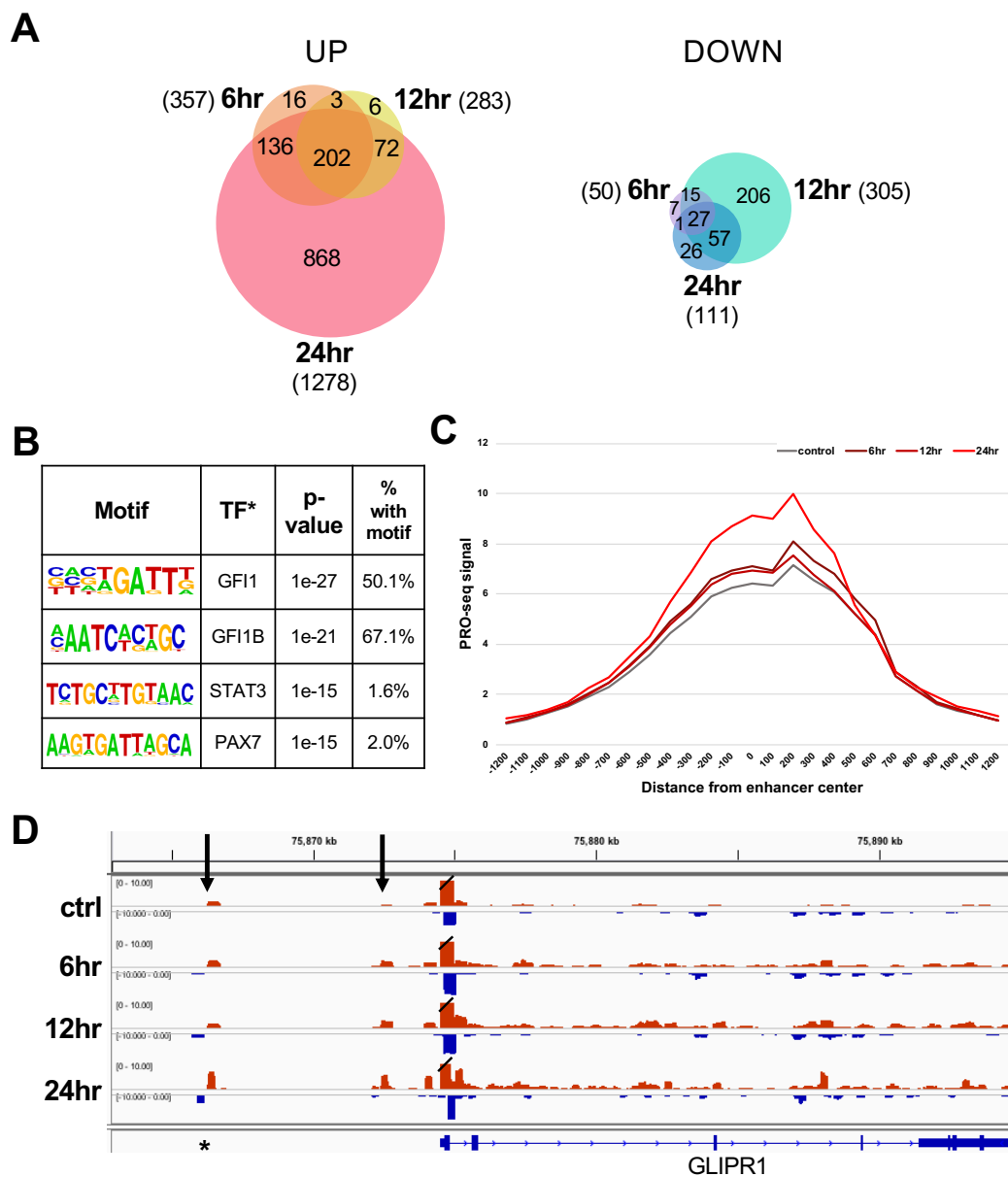


Figure 14. PRO-seq analysis of transcriptional changes at enhancers in THP-1 cells in response to INCB059872. (A) Venn diagrams of enhancers with >1.5-fold change ($p_{adj} < 0.05$) in transcription at 6, 12, or 24hr after INCB059872 treatment. (B) Homer motif analysis of the 1,278 enhancers that are upregulated by 24hr. *Transcription factor identified by Homer as having DNA recognition sequence most similar to the discovered motif. (C) Histogram of PRO-seq signal at active enhancers containing a GFI1 binding motif. (D) IGV screenshot of PRO-seq signal at GLIPR1 gene and upstream enhancers (indicated by arrows). Asterisk indicates GFI1 binding motif.

bodies- at 24hr after INCB059872 treatment, there were nearly 1300 enhancers with at least 1.5-fold increase in transcription (Fig. 14A, left). As expected, enhancers with decreased transcription were relatively few (Fig. 14A, right). Motif analysis of the sequences within the 1278 upregulated enhancers identified the GF11/GF11B recognition sequence as the most highly enriched (Fig. 14B). PRO-seq signal surrounding active enhancers with GF11 binding motifs is plotted in a histogram in Fig. 14C, which shows a slight increase in transcription at these enhancers within 6hr and a greater increase after 24hr of drug treatment. Thus, the primary targets of INCB059872 appeared to be sites at which LSD1 cooperated with GF11/GF11B to repress transcription. An example genome browser track (Fig. 14D) from this dataset shows gradual increases in active polymerase over time throughout the gene body as well as at two upstream enhancers of *GLI Pathogenesis Related 1 (GLIPR1)*, a gene often silenced in AML (Xiao et al., 2011). Within this dataset we pinpointed GF11 as the important factor, as GF11B was not expressed in THP-1 cells. Interestingly, GF11B was not expressed in untreated MV-4-11 cells but had begun to be transcribed at 24hr after drug treatment (Fig. 15A). RT-PCR at 48hr after INCB059872 treatment confirmed that GF11B mRNA was present in MV-4-11 but not THP-1 (Fig. 15B).

Transcriptional changes caused by INCB059872 are consistent with loss of LSD1:CoREST activity at GF11 binding sites

Loss of LSD1 activity was expected to cause a buildup of H3K4 methylation. However, global increases in H3K4me1/2 levels were not detected after INCB059872 treatment of THP-1 cells using western blot analysis (Fig. 16A). Of note, longer treatment times in other cell lines did not reveal methylation changes either. I also used

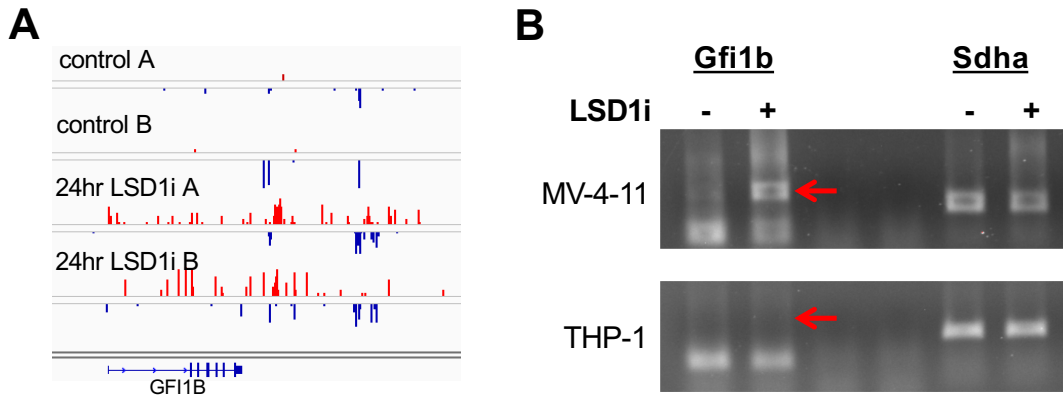


Figure 15. INCB059872 induces expression of GFI1B in MV-4-11 cells.

(A) IGV screenshot of PRO-seq data showing increased transcription around *GFI1B* gene after 24hr INCB059872 in MV-4-11 cells. (B) RT-PCR of *Gfi1b* or *Sdha* mRNA levels after 48hr INCB059872 in MV-4-11 and THP-1 cells. Arrow indicates correct size for *Gfi1b* PCR fragment.

a micrococcal nuclease (MNase) assay to test if INCB059872 would alter the distribution of nucleosomes. After 48hr treatment, there were no obvious changes caused by the drug (Fig. 16B).

Despite the lack of global chromatin changes, I anticipated that inhibition of LSD1 would cause an accumulation of H3K4 mono- and di-methylation at specific, regulated loci. Therefore, I performed ChIP-seq for these marks 48hr after INCB059872 treatment and included a spike-in control of *D. melanogaster* S2 cells to ensure that normalization did not minimize the drug effect. Surprisingly, there were no significant changes (FDR<0.05) in H3K4me1 (Fig. 17A). Only 5 H3K4me2 peaks significantly increased in size, yet there was a trend of increased dimethylation in treated versus control cells (Fig. 17B).

Given that the CoREST complex also mediates removal of histone acetylation, I wanted to determine if INCB059872 would increase H3K27 acetylation. After 24hr treatment in THP-1 cells, ChIP-seq revealed that H3K27ac levels were significantly

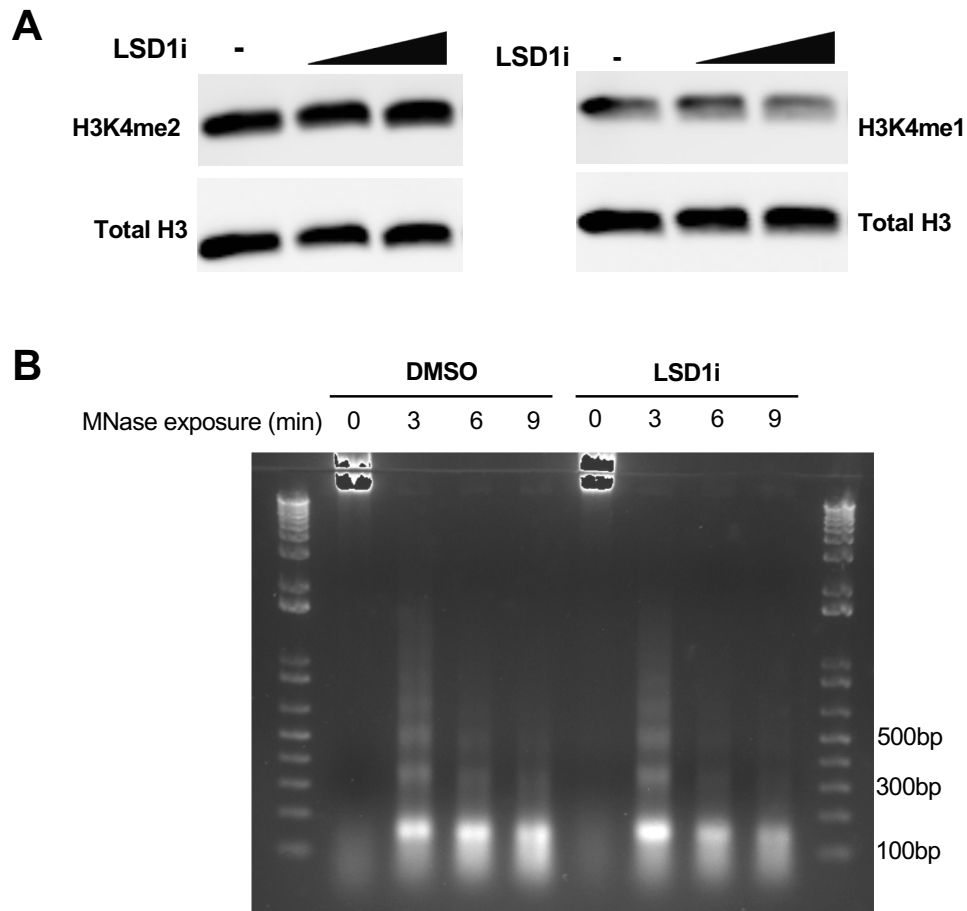


Figure 16. INCB059872 treatment does not change global levels of H3K4 methylation or nucleosome structure. (A) H3K4me2 and H3K4me1 Western blots shown with total histone H3 as loading control. Lysates are from THP-1 cells treated with DMSO, 25nM INCB059872, or 250nM INCB059872 for 24hr. (B) MNase assay comparing nucleosome distribution in THP-1 cells treated with DMSO or 25nM INCB059872 for 48hr.

increased >1.5-fold at 111 loci (Fig. 17C). Overall, H3K27ac patterns correlated better than H3K4me1/2 with the transcriptional changes I observed by PRO-seq. Histograms of ChIP-seq signal at the 1278 upregulated enhancers show only minor increases in methylation (Fig. 17D) but a large increase in H3K27ac (Fig. 17E). These effects are further illustrated by a genome browser screenshot (Fig.17F) of *Cytochrome B-245 Beta Chain (CYBB)*, a gene that encodes a component of the oxidase system of phagocytes

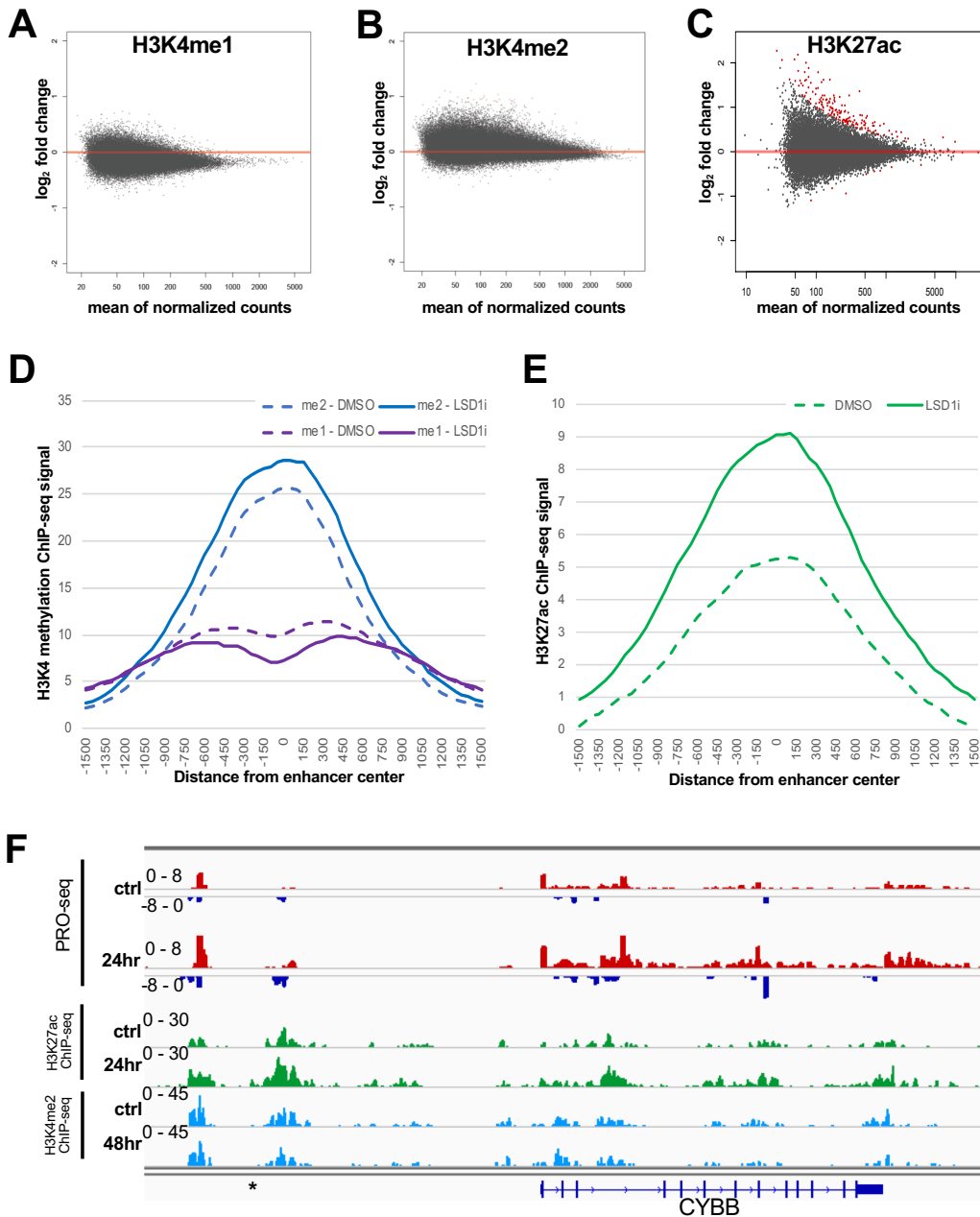


Figure 17. CHIP-seq analysis shows INCB059872 causes more dramatic changes in histone acetylation than methylation. (A-C) MA plots of ChIP-seq changes after INCB059872 treatment in THP-1 cells. Red dots indicate FDR<0.1 (A) H3K4me1 after 48hr (B) H3K4me2 after 48hr (C) H3K27ac after 24hr (D-E) Histograms showing ChIP-seq coverage (per bp per peak) for H3K4 methylation (D) or H3K27ac (E) at 1,278 intergenic enhancers that were upregulated by 24hr INCB059872. (F) IGV screenshot of CYBB locus and upstream enhancers; top: PRO-seq signal +/- 24h INCB059872; middle: H3K27ac ChIP-seq signal +/- 24h INCB059872; bottom: H3K4me2 ChIP-seq signal +/- 48h INCB059872. Asterisk indicates GFI1 binding motif.

and has a GFI1 binding motif ~27 kb upstream of its start site, coinciding with an enhancer. These genome browser tracks show increases in transcription and acetylation throughout gene body and at the upstream enhancers compared to histone methylation that was unchanged.

Of the genes and enhancers identified by PRO-seq as upregulated by INCB059872, more of these loci showed increases in H3K27ac than H3K4me2 (Fig. 18A). Motif analysis of the 500 peaks with greatest increase in ChIP-seq signal from both H3K4me2 (Fig. 18B) and H3K27ac (Fig. 18C) experiments identified GFI1/1B consensus binding motifs as the most enriched. Thus, the histone modification changes are consistent with loss of LSD1:CoREST activity at GFI1 binding sites.

The genomics datasets described above pointed to the possibility that INCB059872 disrupts the interaction between LSD1 and GFI1. I tested this hypothesis by co-immunoprecipitation. As expected, GFI1 was present in the anti-LSD1 immunoprecipitate of control cells, but its association with LSD1 was substantially decreased in cells treated with INCB059872 for 48hr (Fig. 19A). Additionally, the INCB059872 PRO-seq dataset correlated very highly with gene expression data (from Maiques-Diaz et al., 2018) in which THP-1 cells were treated with OG86, a compound known to disrupt the LSD1:GFI1 interaction (Fig. 19B).

Single-cell RNA-seq analysis of AML patient bone marrow reveals gene expression changes caused by INCB059872

INCB059872 is in early phase trials for clinical development. Although few patients have been treated with INCB059872, one patient with new diagnosis, poor risk treatment-related acute myeloid leukemia (t-AML) with *TP53* mutation and complex

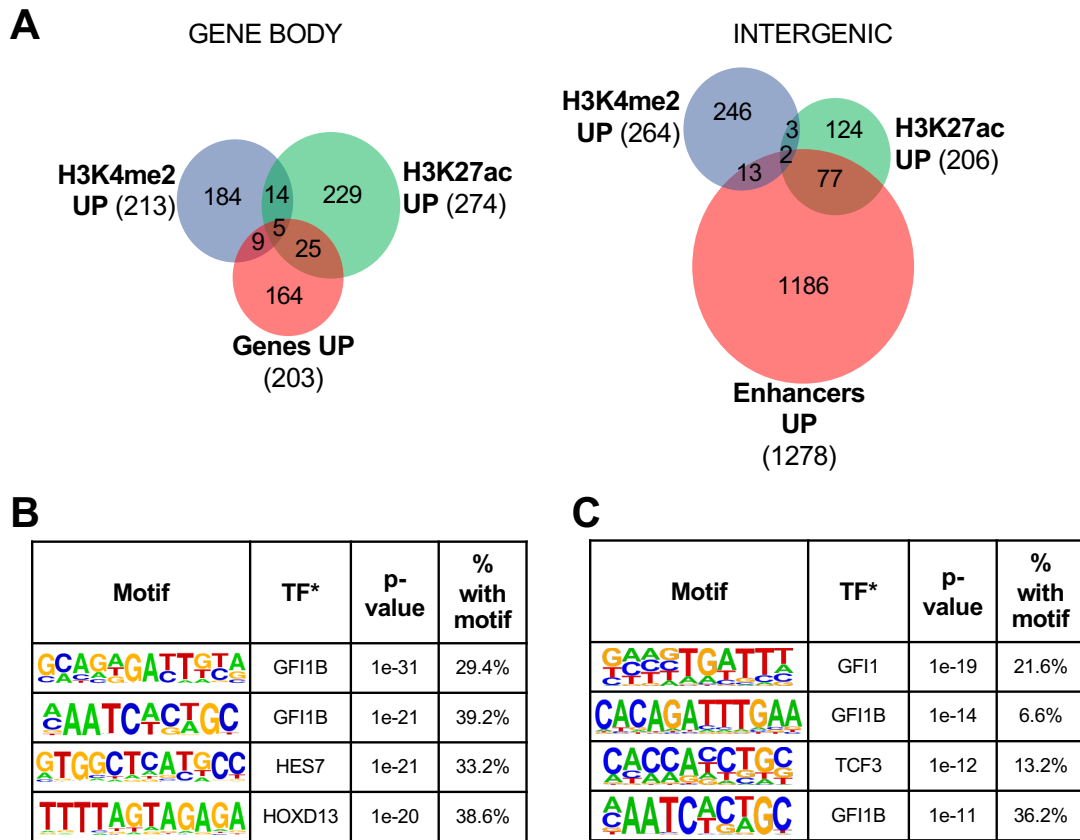


Figure 18. Histone modification changes caused by INCB059872 are consistent with loss of LSD1:CoREST activity at GF1 binding sites. (A) Venn diagrams showing overlap of transcriptional changes (PRO-seq) with changes in H3K4me2 and H3K27ac after treatment with INCB059872. Left diagram includes genes with >1.5-fold increase in gene body transcription and genes that contain increased H3K4me2 peaks or H3K27ac peaks (within top 500 most upregulated). Right diagram includes intergenic enhancers with >1.5-fold increase in transcription, intergenic H3K4me2 peaks (within top 500 most upregulated), and intergenic H3K27ac peaks (within top 500 most upregulated). (B) Homer motif analysis of the 500 H3K4me2 peaks with greatest increase in signal after 48hr INCB059872. (C) Homer motif analysis of the 500 H3K27ac peaks with greatest increase in signal after 24hr INCB059872. *Transcription factor identified by Homer as having DNA recognition sequence most similar to the discovered motif.

genetics showed a remarkable response with INCB059872 + azacitidine (AZA) therapy. This provided a unique opportunity to study the gene expression changes in the bone marrow of an AML patient who responded to treatment with INCB059872 + AZA.

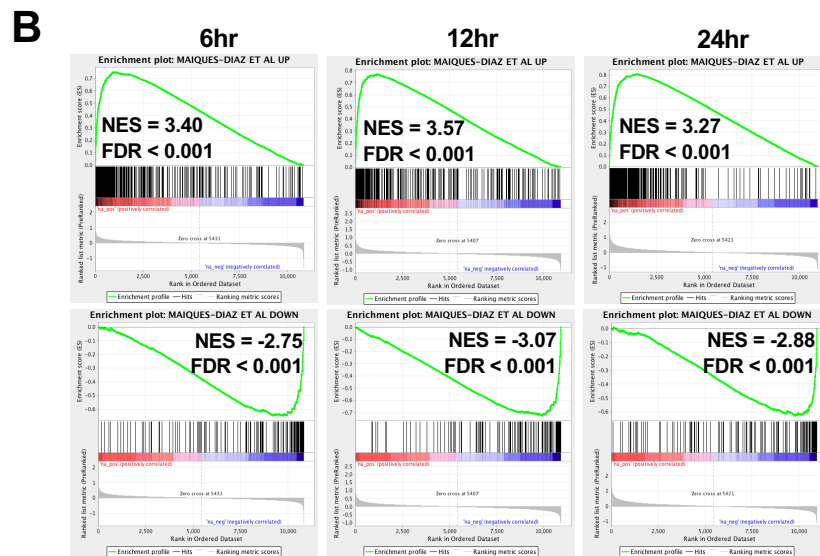
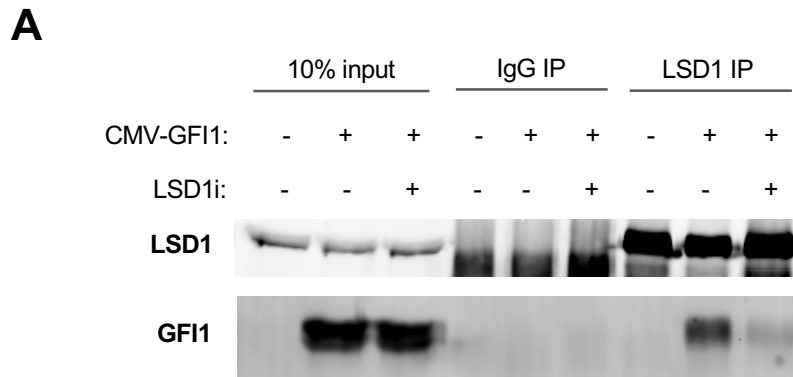


Figure 19. INCB059872 disrupts the LSD1:GFI1 interaction.

(A) 293T cells were transfected with CMV-GFI1 and treated with DMSO or 250nM INCB059872 for 48hr. Cell lysates were immunoprecipitated with anti-LSD1 or IgG control. Western blots representative of three experiments are shown. (B) Ranked list gene set enrichment analysis of INCB059872-induced gene expression changes detected by PRO-seq at multiple timepoints. Gene sets (from Maiques-Diaz et al. 2018) include genes with >1.5-fold change in 24hr OG86 RNA-seq dataset.

Subpopulations within a sample are likely to have variable responses to drug treatment, so we chose single-cell RNA-seq (scRNA-seq) to be able to observe these effects. For this experiment, a pre-INCB059872 treatment bone marrow sample was divided and treated *ex vivo* in duplicate with vehicle, INCB059872, AZA, or INCB059872 + AZA.

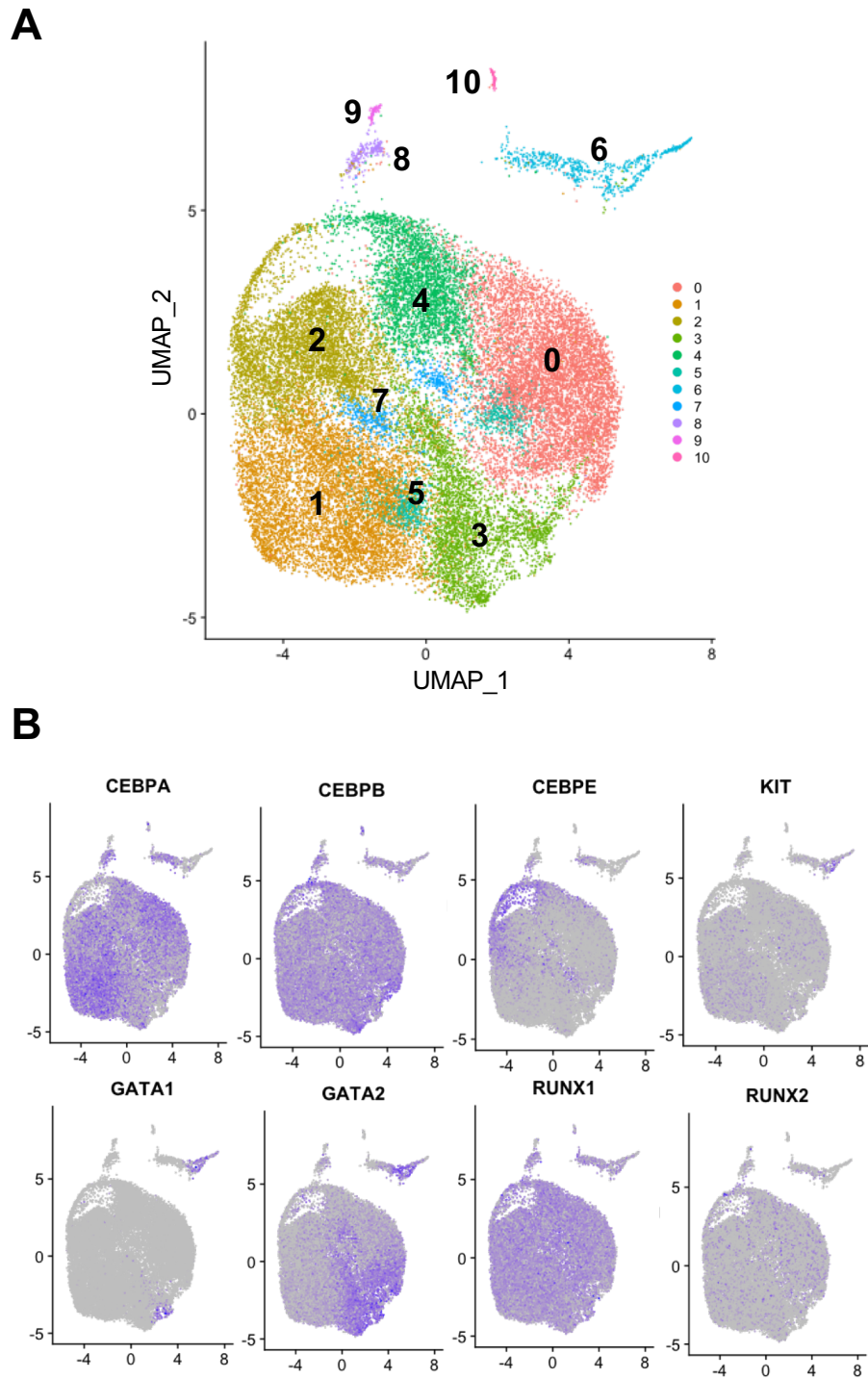


Figure 20. Single-cell RNA-seq analysis of AML patient bone marrow. (A) UMAP plot shows unsupervised clustering of 29,278 patient bone marrow cells. (B) Heatmaps of individual gene expression displayed on UMAP plots. Intensity of blue color corresponds to level of expression.

Though a longer treatment duration would have been ideal to detect differentiation-related changes, a 48hr timepoint was chosen to avoid measuring drug-independent cell death. Cells were passed over Annexin V depletion columns to exclude dying cells from the experiment.

Unsupervised clustering of nearly 30,000 cells identified 11 different populations (“clusters”) based on mRNA expression of 1500 to 5500 genes per cell. In the UMAP (uniform manifold approximation and projection) plot (Fig. 20A), each dot corresponds to a cell, and the distance between dots represents the difference in their overall gene expression patterns. Despite this patient sample having a relatively low blast count (32 percent), the majority of the cells in this experiment expressed myeloid markers (Fig. 20B), likely due to leukemic cells being able to withstand culture conditions better than untransformed primary cells.

Displaying the data as UMAP plots in which cells are separated according to treatment groups reveals dramatic differences caused by LSD1 inhibition. Surprisingly, the majority of INCB059872- and combination-treated cells were assigned to clusters that were not found in control- or AZA-treated samples (Fig. 21A). Clustering patterns of non-leukemic cells (including lymphoid and erythroid populations; clusters 6, 8-10) were unchanged. Within this treatment window, AZA had a negligible effect on gene expression compared to INCB059872.

Consistent with the results in THP-1 cells, AML blasts exposed to INCB059872 dramatically upregulated GFI1 and GFI1B (Fig. 21B). Additionally, several of the most highly increased transcripts (e.g. ANXA2, GLIPR1) measured in LSD1i-treated AML cell lines were also upregulated in this patient sample (Fig. 21B), which suggests that the

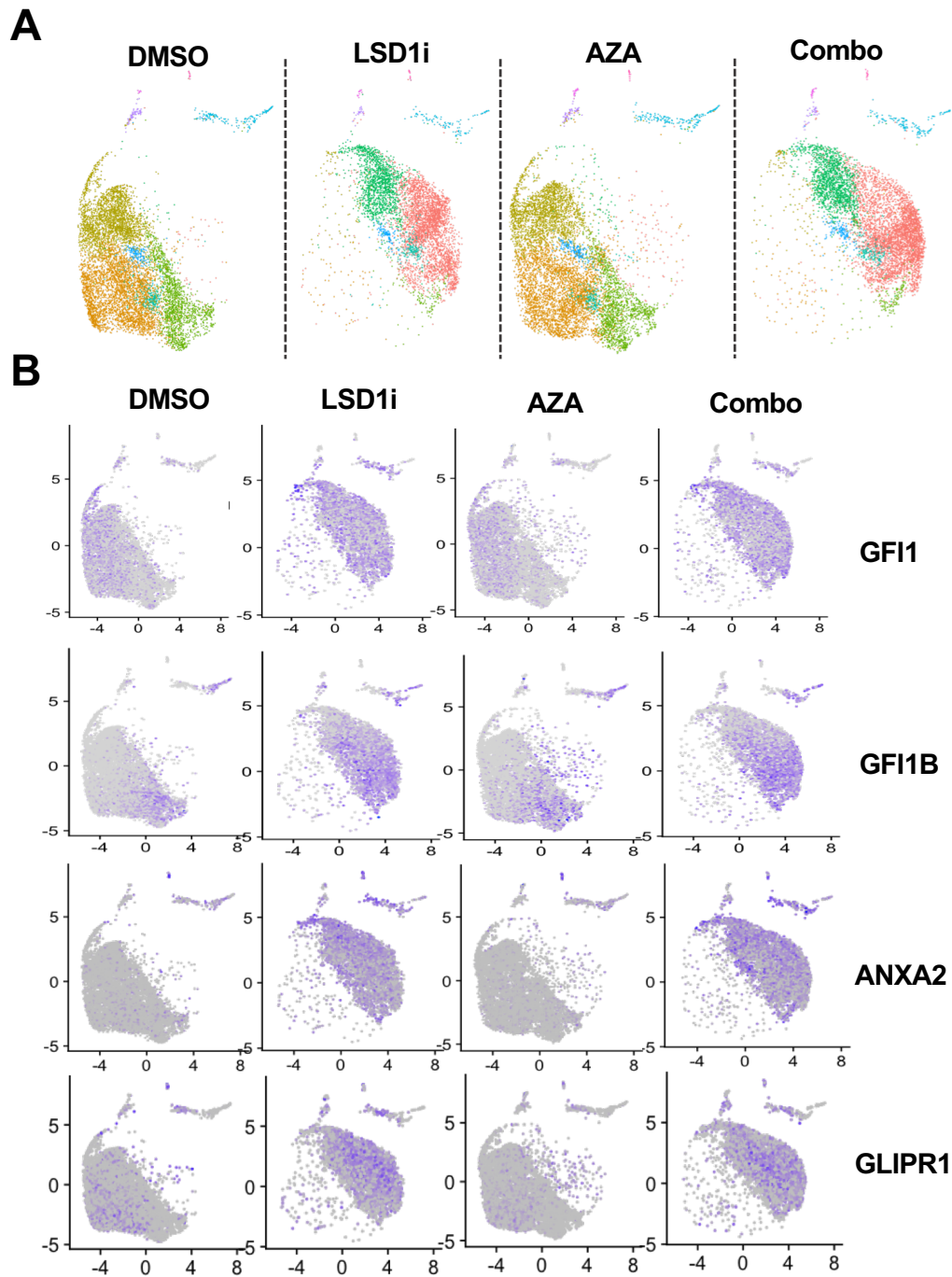


Figure 21. Single-cell RNA-seq analysis of AML patient bone marrow reveals gene expression changes caused by INCB059872. (A) UMAP plots separated by treatment group. Cells are colored according to assigned cluster. (B) Heatmaps of individual gene expression displayed on UMAP plots, separated by treatment group. Intensity of blue color corresponds to level of expression.

leukemic blasts from this patient were pushed toward myeloid differentiation, likely via the same mechanism as in THP-1 cells.

Discussion

Current treatment options for AML consist mostly of cytotoxic agents, though targeted therapies for certain genetic backgrounds have recently become available. Aside from PML-RARA-driven APL and, possibly, IDH mutant AML, there is a lack of differentiation therapies available for most subtypes. Inhibitors of LSD1 have been developed as a potential therapeutic strategy for myeloid malignancies, as LSD1 inhibition was discovered to synergize with ATRA to promote myeloid differentiation in non-APL cell lines. Here, I have shown that a potent, selective inhibitor of LSD1, INCB059872, activates a gene expression program consistent with myeloid differentiation in MLL-rearranged AML cell lines. The results described in this chapter provide rationale for the use of INCB059872 to treat human AML.

Though THP-1 cells were more sensitive to the drug than MV-4-11 cells (Fig. 6), RNA-seq analysis revealed a set of commonly upregulated genes that are associated with myeloid differentiation-related processes (Fig. 11). PRO-seq analysis of INCB059872 treatment at multiple timepoints in THP-1 cells showed that the drug primarily activates transcription and most of these effects are at enhancers (Figs. 12,14). As chromatin-associated LSD1 is primarily located at intergenic/intronic regions, it makes sense that the earliest, likely direct effects of LSD1 inhibition would be at enhancers.

The PRO-seq data was also useful for overlapping with genomic maps of histone modifications, as I was able to see that transcriptional changes more closely match H3K27 acetylation than H3K4 methylation (Fig. 17). Though LSD1 inhibition was expected to increase H3K4 methylation, ChIP-seq analysis of H3K4me1 and H3K4me2 marks in THP-1 cells treated with INCB059872 revealed only subtle changes in methylation. Co-immunoprecipitation experiments showed that the drug disrupted the interaction between LSD1 and GFI1 (Fig. 19). Consistent with the role of GFI1 to recruit the CoREST complex to deacetylate histones, ChIP-seq analysis showed that accumulation of H3K27ac at GFI1-regulated loci was the primary effect of INCB059872. As suggested by LSD1 inhibition in murine AML models (Cusan et al., 2018; Barth et al., 2019), the loss of repressor activity can allow lineage-defining transcription factors such as PU.1 or CEBPA to activate transcription of genes that had been repressed by GFI1.

In addition to AML cell lines, I was also able to test INCB059872 in a pre-treatment bone marrow sample from an AML patient who responded to AZA + INCB059872. ScRNA-seq analysis of cells treated *ex vivo* showed that the LSD1 inhibitor had a greater effect on gene expression than AZA did within a 48hr timeframe (Fig. 21). Although we cannot rule out the possibility that the patient would have responded to AZA without the addition of INCB059872, these scRNA-seq data demonstrated that INCB059872 was able to induce expression of genes associated with myeloid differentiation in primary leukemic blasts.

CHAPTER FOUR

INHIBITION OF LSD1 IMPAIRS MATURATION OF MEGAKARYOCYTE PROGENITORS

Background and Significance

Patients with hematologic malignancies are at risk of thrombocytopenia prior to treatment, and platelet counts are usually further reduced by chemotherapy. In these cases, platelet transfusions are often needed to prevent or treat severe bleeding (Castaman and Pieri, 2018). Thrombocytopenia is also an issue observed with LSD1 inhibitors. In preclinical and early clinical studies, the primary dose-limiting toxicity caused by INCB059872 was thrombocytopenia. The loss of platelets is likely an on-target effect, as the transcription factor GFI1B, which recruits LSD1, is essential for megakaryopoiesis. Deletion of *Gfi1b* in bone marrow of adult mice resulted in death within three weeks due to extreme decreases in hemoglobin levels and platelet counts (Foudi et al., 2014). Additional hematopoietic lineages could be affected by INCB059872 because the drug disrupts the interaction of LSD1 with GFI1, which modulates granulocyte/monocyte gene expression programs and contributes to development of lymphoid lineages. *Gfi1*-deficient mice had severe neutropenia and accumulation of immature monocytic cells in their bone marrow (Karsunky et al., 2002). Moreover, conditional deletion of *Kdm1a* (*Lsd1*) in hematopoietic cells caused multi-

lineage cytopenia due to defects in early HSC differentiation and in terminal blood cell maturation (Kerenyi et al., 2013).

To explore how INCB059872 affects normal hematopoiesis, we used single-cell RNA-seq (scRNA-seq) to analyze the lineage-negative bone marrow of wild-type mice treated with the drug. This method provides detailed insights into the differentiation trajectories of hematopoiesis and allows for deep phenotyping of progenitor populations (Dahlin et al., 2018). As shown in the analysis of an AML bone marrow sample (Chapter III), scRNA-seq can highlight population-specific changes in gene expression in response to drug treatment, e.g. more dramatic effects in myeloid blasts than in lymphoid cells.

Results

Single-cell RNA-seq reveals changes in bone marrow progenitor populations following INCB059872 treatment in mice

In mice treated daily with INCB059872, circulating platelet counts began to drop within 4 days and continued to fall by the sixth day (data from Haley Ramsey).

Therefore, these timepoints were selected for scRNA-seq analysis. C57BL/6 mice (3 per treatment group) were treated daily with 10 mg/kg INCB059872 via oral gavage for 0, 4, or 6 days before bone marrow was harvested. We chose to sort lineage-negative cells, which account for approximately 5 percent of the total bone marrow, for this experiment to focus on immature populations. This excluded cells with surface expression of CD3, B220, Ter119, Mac1, or Gr1.

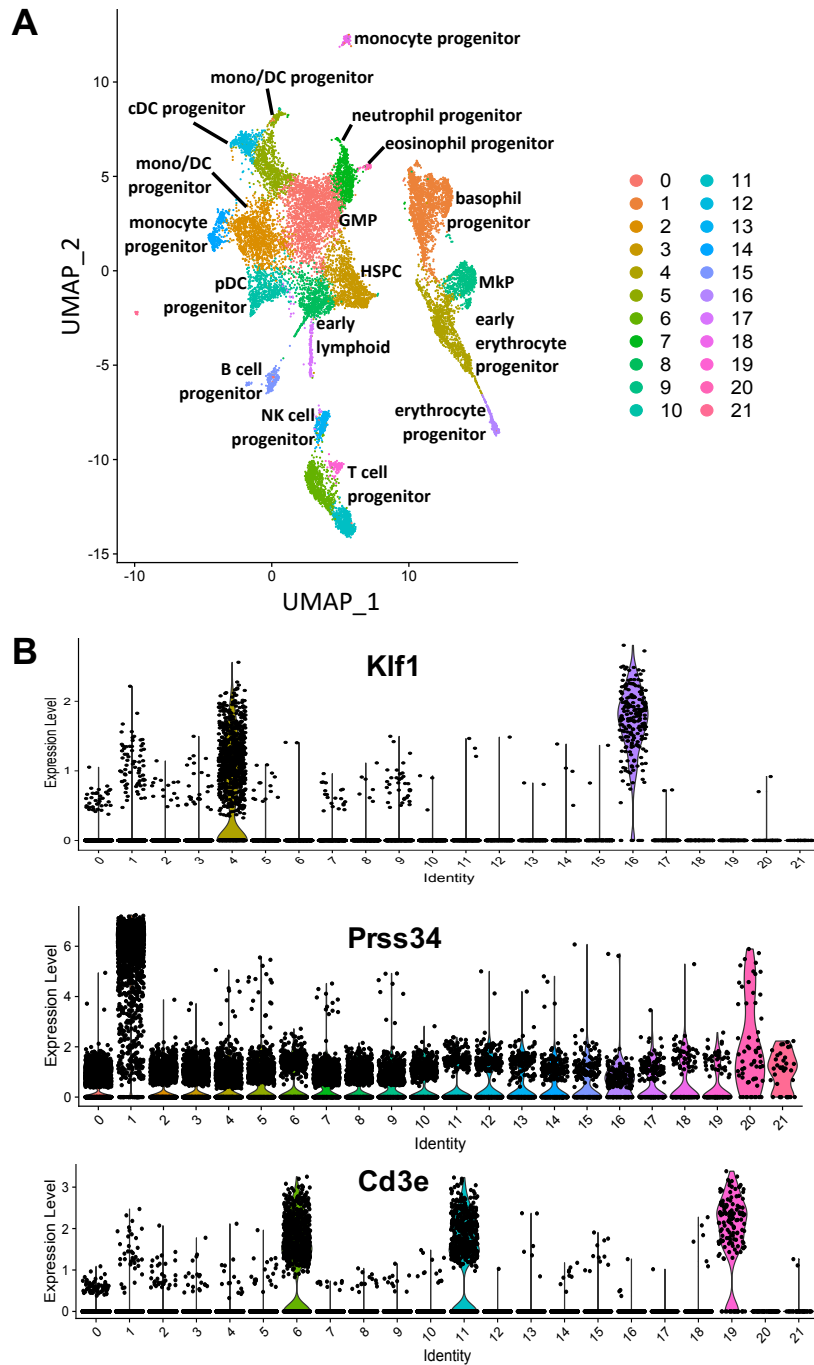


Figure 22. Single-cell RNA-seq defines distinct subpopulations within murine Lin- bone marrow. (A) UMAP plot shows unsupervised clustering of 15,046 cells from all treatment groups (9 total mice). HSPC, hematopoietic stem progenitor cell; GMP, granulocyte-monocyte progenitor; Mkp, megakaryocytic progenitor; cDC, conventional dendritic cell; pDC, plasmacytoid dendritic cell. (B) Violin plots show expression levels of lineage-defining genes across clusters; top: *Klf1* is an erythroid marker; middle: *Prss34* is a basophil marker; bottom: *Cd3e* is a T cell marker.

After quality control filtering, the dataset consisted of 15,046 individual cells (from 9 mice), with 750 to 4000 transcripts detected per cell. Unsupervised clustering divided these cells into 22 unique clusters (Fig. 22A), which were identified by expression levels of known lineage-defining genes. For example, erythrocyte progenitors were divided into two clusters, 4 and 16, with the latter being a slightly more mature population having higher Klf1 (Kruppel-like factor 1) expression (Fig. 22B). Basophil progenitors were identified by high Prss34 (serine protease 34) expression, and T cell progenitors were identified by Cd3e expression (Fig. 22B). The proximity of cells (dots) on the UMAP plot represents the similarity in their gene expression patterns, so as expected, less mature populations are located in the center while cells that have begun to differentiate toward specific lineages are nearer to the edges of the plot.

While the distribution of cells into different progenitor populations was largely unaffected by drug treatment, there were a few clusters with significant changes (Fig. 23A). The most striking effect of INCB059872 was the increase in the number of cells assigned to a megakaryocyte progenitor (MkP) cluster (Fig 23B, solid circle). Cells within this expanded cluster expressed stem cell markers, such as Mycn and Pbx1 (pre B cell leukemia homeobox 1), but also expressed Vwf (von Willebrand factor) (Fig. 24). This result suggests that a block in megakaryocyte differentiation could have caused thrombocytopenia in the mice.

LSD1 inhibition also altered the distribution of cells in non-megakaryocytic clusters. Cells in cluster 10 were classified as plasmacytoid dendritic cell progenitors (pDCP) based on expression of Siglech (sialic acid binding Ig-like lectin H) and Ly6d (lymphocyte antigen 6 complex, locus D) (Rodrigues et al., 2018). After 4 days of

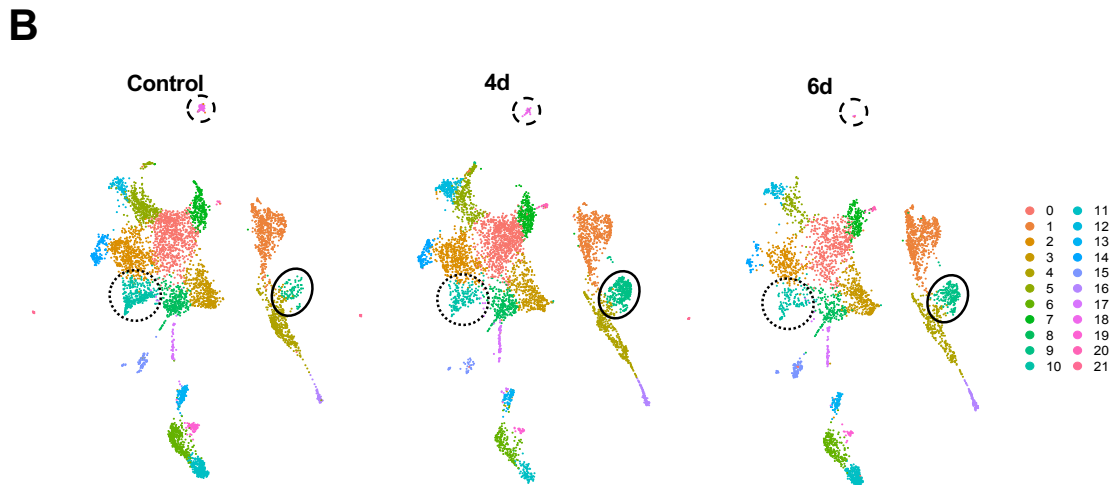
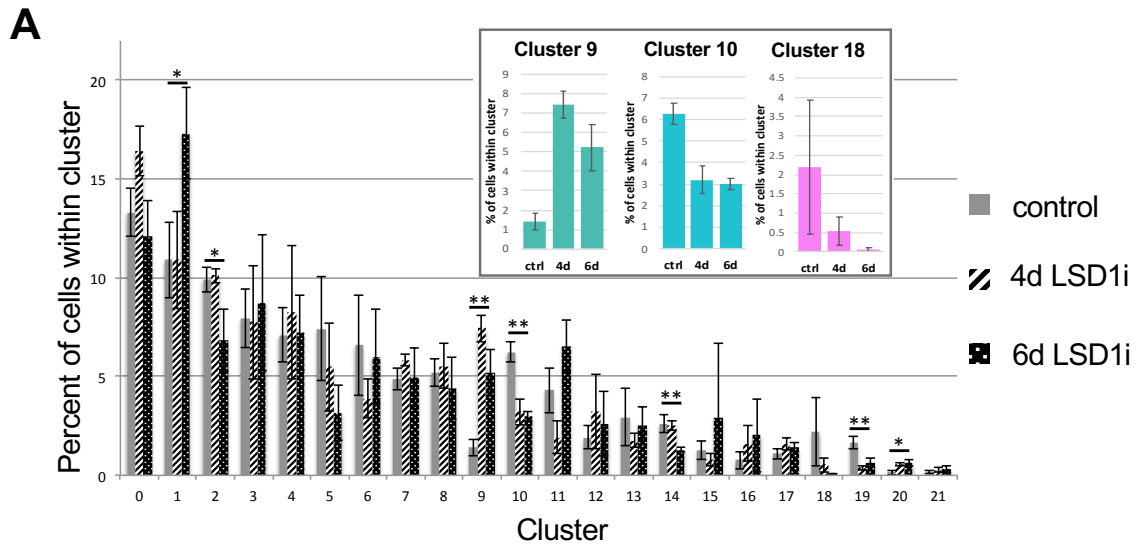


Figure 23. Single-cell RNA-seq reveals changes in bone marrow progenitor populations following INCB059872 treatment in mice. (A) Bar graph shows percentages of cells from each mouse that were assigned to each cluster. Populations with dramatic shifts are shown in colored inset graphs. (B) UMAP plots, cells separated by treatment group. Solid circle indicates cluster 9; dotted circle indicates cluster 10; dashed circle indicates cluster 18.

INCB059872 treatment, mice had fewer cells with this identity (Fig. 23). Cluster 18, a Csf1r+ Cd36+ pre-monocyte population, was almost completely absent after 6 days of treatment (Fig. 23).

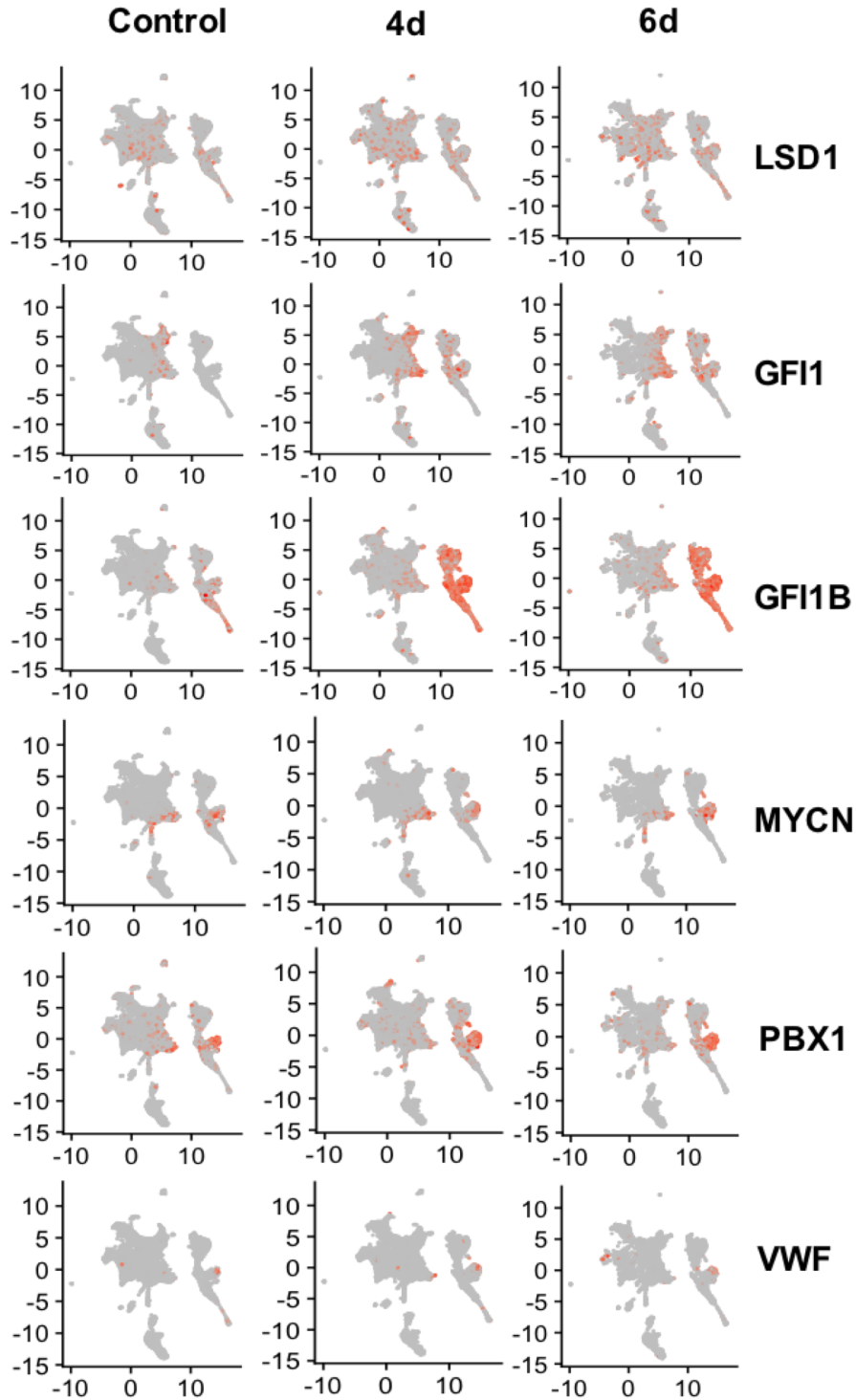


Figure 24. Single-cell RNA-seq reveals gene expression changes in murine bone marrow caused by INCB059872 treatment. Heatmaps of individual gene expression displayed on UMAP plots, separated by treatment group. Intensity of red color corresponds to level of expression.

Notably, gene expression changes in response to INCB059872 were variable between clusters. Though cells with detectable levels of *Lsd1* are scattered throughout the populations, *Gfi1* and *Gfi1b* were dramatically upregulated in clusters 1, 3, 4, and 9 after drug treatment (Fig. 24). Additionally, *Gfi1* expression increased within neutrophil progenitor cells (cluster 7), and *Gfi1b* expression increased within erythrocyte progenitor cells (cluster 16), suggesting that the disrupting the interaction of LSD1 with GFI1/GFI1B prevented the auto- and trans-repression of GFI family members.

Flow cytometry analysis of bone marrow from INCB059872-treated mice confirms lineage defects

To confirm the changes in lineage distribution seen in the scRNA-seq data, we repeated the experimental design but this time distributed the bone marrow between different flow cytometry antibody panels for multi-lineage analysis. There were no significant changes in the total numbers of erythrocyte-depleted bone marrow cells between treated and control animals. Populations of mature lymphoid cells (B220+ B cells or CD3+ T cells) were not substantially affected by INCB059872 (Fig. 25A, B). Interestingly, drug treatment transiently altered the distribution of granulocyte/monocyte and erythroid cells. After 4 days of INCB059872, the Ter119+ erythroid population had significantly decreased while the Gr1+/Mac1+ population showed a compensatory increase (Fig. 25C, D). After 6 days of treatment, there were no longer differences in these populations between treated and control mice. As for classically defined progenitor populations, we did not observe any significant changes in the size of these populations in response to INCB059872. The Lin- Sca1+ cKit+ stem and progenitor population (LSK), lymphoid-primed multi-potent progenitor cells (LMPP, LSK Flt3^{high}),

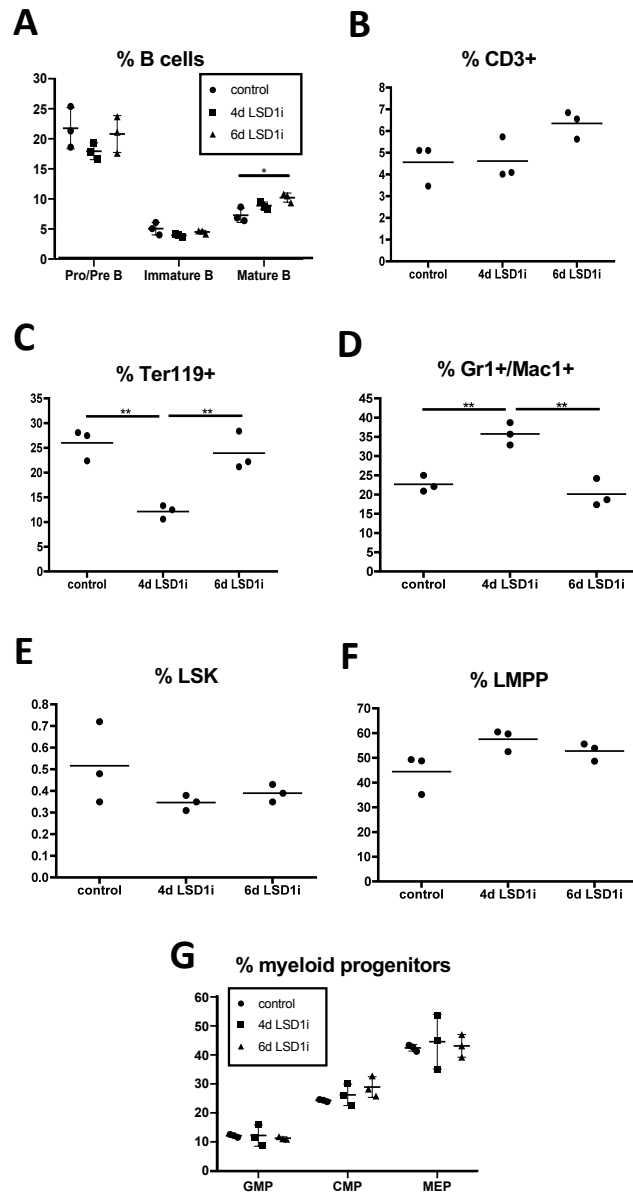


Figure 25. INCB059872 has little effect on most murine bone marrow populations. Flow cytometry analysis of bone marrow from mice treated with INCB059872 for 0, 4, or 6 days. 3 mice per group. (A-D) Percentages of mature hematopoietic lineages out of total bone marrow. (A) B cell subsets defined by levels of B220 and IgM. (B) T cells defined by CD3 expression. (C) Erythroid cells defined by Ter119 expression. (D) Mature myeloid cells defined by Mac-1/Gr-1 expression. (E) LSK population defined as percentage of Sca-1+/c-Kit+ cells out of Lin- population. (F) LMPP population defined as percentage of Flt3^{high} cells out of LSK population. (G) Percentage of myeloid progenitor populations within Lin-/c-Kit+/Sca-1- subset; populations defined by levels of CD34 and CD16/32. *p<0.05, **p<0.01, ***p<0.001

common myeloid progenitor cells (CMP, Lin⁻ Sca1⁻ cKit⁺ CD34⁺ CD16/32^{low}), granulocyte/monocyte progenitor cells (GMP, Lin⁻ Sca1⁻ cKit⁺ CD34⁺ CD16/32^{high}), and megakaryocyte/erythroid progenitor cells (MEP, Lin⁻ Sca1⁻ cKit⁺ CD34⁻ CD16/32⁻) populations remained the same size after treatment (Fig. 25E-G).

To be able to use flow cytometry to study populations that correspond to scRNA-seq clusters, I identified two cluster-defining genes from each cluster of interest that encode cell surface markers. CD41 (encoded by *Itga2b*) marked basophil progenitors as well as the MkP cluster, so I also used the basophil marker CD200r3 to distinguish these populations. Thus, the population corresponding to MkP is Lin⁻ CD41⁺ CD200r3⁻ (Fig. 26A). Cluster 10 (pDCP) was defined as Lin⁻ Ly6D⁺ SiglecH⁺ (Fig. 26B), and cluster 18 (monocyte progenitors) was defined as Lin⁻ CD36⁺ FCGR4⁺ (Fig. 26C).

As expected, mice from both treatment timepoints had a dramatically higher percentage of cells that fell into the MkP population as compared to vehicle control mice (Fig. 26D). Importantly, the percentage of cells within this population that expressed Kit was roughly doubled by INCB059872 (Fig. 26E), supporting the notion that the drug caused the expansion of a stem-like population. When measured by flow cytometry, the size of the pDCP population was not reduced until the sixth day of treatment (Fig. 26F), though a reduction in this population was detectable by the fourth day using scRNA-seq (Fig 23A). Consistent with the gene expression data, the CD36⁺ monocyte population was also dramatically reduced by INCB059872 within 4 days (Fig. 26G).

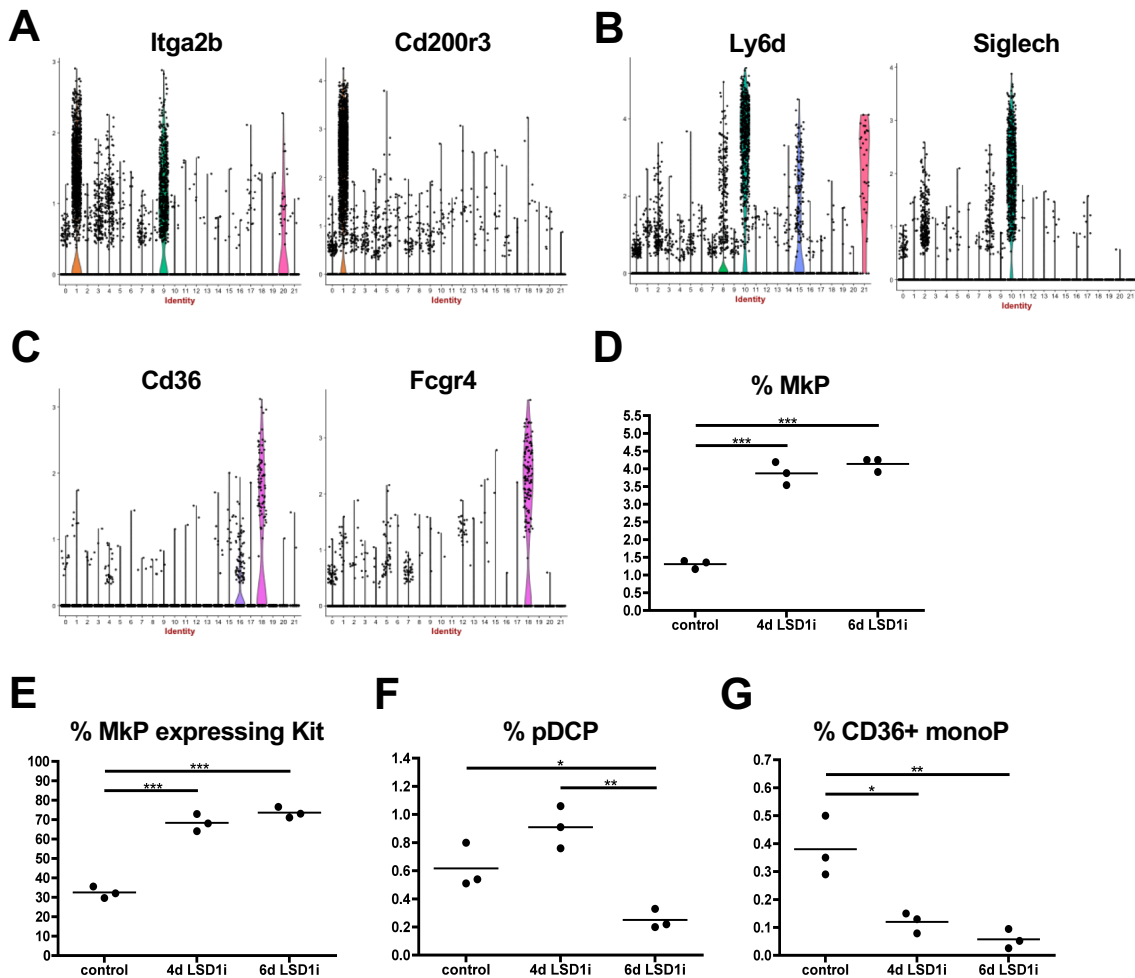


Figure 26. INCB059872 treatment expands megakaryocyte progenitor population and decreases plasmacytoid dendritic cell progenitor and monocyte progenitor populations. (A-C) Violin plots of scRNA-seq data show expression of markers used to define populations. (A) Megakaryocyte progenitor (MkP) population, based on cluster 9, is defined as *Itga2b*⁺ *Cd200r3*⁻. (B) Plasmacytoid dendritic cell progenitor (pDCP) population, based on cluster 10, is defined as *Ly6d*⁺ *Siglech*⁺. (C) Monocyte progenitor population, based on cluster 18, is defined as *Cd36*⁺ *Fcgr4*⁺. (D-G) Flow cytometry analysis of bone marrow from mice treated with INCB059872 for 0, 4, or 6 days. 3 mice per group. (D) Percentage of CD41⁺/CD200r3⁻ megakaryocyte progenitors within Lin⁻ subset. (E) Percentage of c-Kit⁺ cells within megakaryocyte progenitor population. (F) Percentage of Ly6D⁺/Siglech⁺ plasmacytoid dendritic cell progenitors within Lin⁻ subset. (G) Percentage of CD36⁺/Fcgr4⁺ monocyte progenitors within Lin⁻ subset. *p<0.05, **p<0.01, ***p<0.001

RNA-seq analysis of MkP suggests that INCB059872 impairs platelet production

Additionally, we sorted the MkP population (Lin- CD41+ CD200r3-) for bulk RNA-seq to measure gene expression changes after 4 or 6 days of INCB059872 treatment. This analysis indicated that most of the changes in gene expression had occurred by day 4 (Fig. 27A). While there were many transcripts affected by the drug treatment, only a few dozen met statistical significance with 61 genes up and 113 down by at least 1.5-fold after 6 days of treatment (Fig. 27B). Importantly, gene set enrichment analysis revealed that a gene signature associated with platelet function was significantly downregulated at both time points (Fig. 27C). This signature included factors that are critical for platelet aggregation (P2ry12 (purinergic receptor P2Y, G-protein coupled 12), Thbs1 (thrombospondin 1), Pf4 (platelet factor 4)), as well as receptors for thrombopoietin (Mpl (myeloproliferative leukemia virus oncogene)) and vWF (glycoproteins Gp1ba, Gp5, Gp9). These data further support our finding that the population of cells expanded after INCB059872 treatment consisted of megakaryocyte-biased stem cells that failed to mature into efficient platelet producers.

Discussion

Sc-RNA-seq is a powerful tool for deep phenotyping of heterogeneous biological samples. This approach is especially valuable in the context of hematopoiesis, in which certain progenitor populations make up very low percentages of total bone marrow. Measuring gene expression at the single-cell level allows for detection of drug responses that are specific to distinct populations. The scRNA-seq data described in

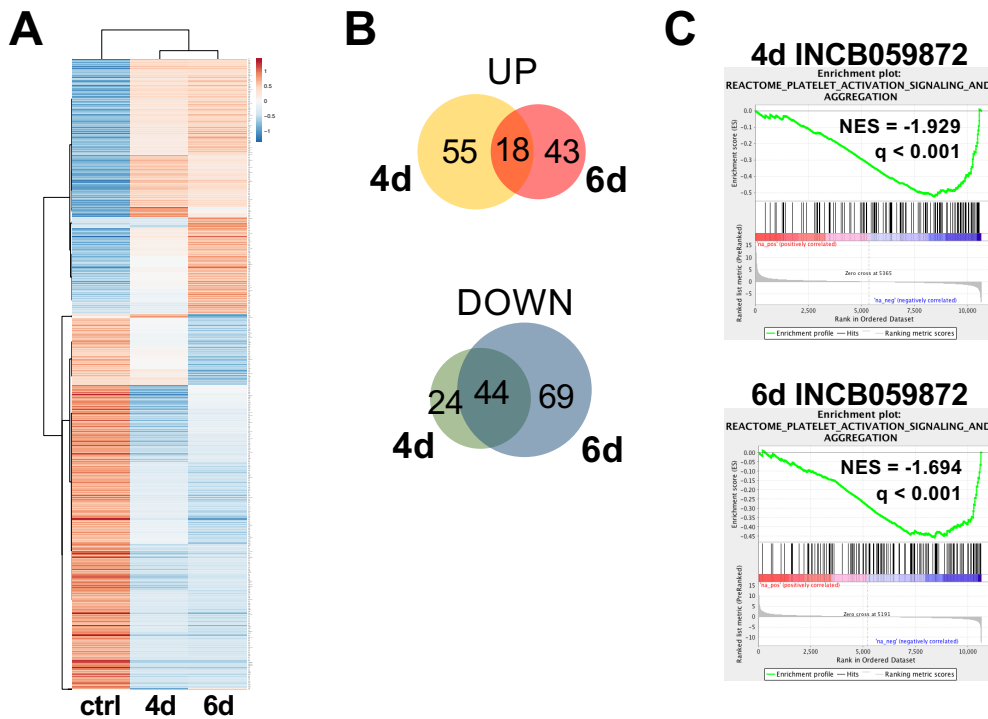


Figure 27. RNA-seq analysis of megakaryocyte progenitors shows that INCB059872 impairs platelet production. Mice were treated with INCB059872 for 0, 4, or 6 days; two mice per group. Megakaryocyte progenitor population was harvested for RNA-seq. (A) Clustered heatmaps showing $\ln(\text{RPKM} + 1)$ values with Pareto scaling and row-centering for 1000 genes with lowest FDR. (B) Venn diagrams show number of genes meeting 1.5-fold change cutoff (with q value < 0.05) at each time point. (C) Ranked list gene set enrichment analysis shows “platelet activation signaling and aggregation” gene signature is downregulated at both timepoints.

this chapter demonstrate that INCB059872 alters the size of certain progenitor populations in murine bone marrow. Additionally, these results were corroborated by flow cytometry analysis.

Preclinical studies have indicated that thrombocytopenia is a serious adverse event that could result from treating AML patients with LSD1 inhibitors. Our scRNA-seq

data point to a defect in megakaryocyte progenitor differentiation as a likely mechanism for this effect. After INCB059872 treatment, a cluster of MkP cells within murine bone marrow that expressed *Mycn*, *Pbx1*, and *Vwf* was expanded (Fig. 23-24). This population is likely to be the same as the “platelet-biased HSC” population described by Sanjuan-Pla et al. (2013), which was defined by expression of vWF. Platelet-biased HSCs showed multipotent potential *in vitro* yet exclusively adopted a megakaryocytic lineage upon transplantation into primary recipients (Carrelha et al., 2018). Interestingly, these megakaryocyte lineage-restricted cells displayed reduced platelet output when compared to other less restricted HSC populations. The expansion of a progenitor population with lower platelet yield is consistent with the lack of mature platelets in INCB059872-treated mice.

These results also highlight the importance of LSD1:CoREST recruitment by GFI family members. Expression of *Lsd1* itself was not a predictor of how clusters would respond to treatment, as *Lsd1*-expressing cells were evenly scattered throughout the lineage-negative populations we observed. The most dramatic changes in gene expression after INCB059872 treatment were the upregulation of *Gfi1* and/or *Gfi1b*, which only occurred in certain clusters (Fig. 24). GFI1 and GFI1B normally trans- and auto-repress. Thus, the deficit of CoREST activity at sites of GFI1/GFI1B binding appears to be the primary mechanism driving gene expression changes. These results are consistent with THP-1 data, in which accumulation of histone methylation was secondary to increased histone acetylation and enhancer activation.

Another discovery from our scRNA-seq data was the reduced proportion of a pDC progenitor population within 4 days of INCB059872 treatment. PDCs promote

innate immune responses by producing large amounts of type I interferon. They can also promote adaptive immunity by acting as antigen presenting cells. When we used flow cytometry to verify that these cells were affected by INCB059872 treatment, the progenitor population (Lin⁻ Ly6D⁺ SiglecH⁺) was significantly decreased in size by the sixth day. Mature pDCs would have been excluded from this analysis because they express B220 (part of the lineage panel). Flipping the gating strategy to first look at Ly6D and SiglecH expression showed that Ly6D⁺ SiglecH⁺ cells made up a slightly higher percentage of total bone marrow in treated mice, but a lower fraction of these were Lin⁻ (~6% in control mice versus ~2% in 6d treated mice). This suggests that INCB059872 treatment could have promoted differentiation of pDCs. Although there is a report that LSD1 inhibition promoted differentiation of a cDC population in certain MDS patient samples (Srivastava et al., 2020), further work is needed to understand the exact function(s) of LSD1 in dendritic cells.

Another population affected by INCB059872 treatment was a small cluster of monocyte progenitors marked by expression of Cd36 and Fcgr4. These cells appear to be precursors of “non-classical” monocytes, which patrol along vascular endothelial cells, because they highly expressed the characteristic markers Cx3cr1, Cebpb, Nr4a1, and Csf1r (Guilliams et al., 2018). In the scRNA-seq dataset, this population was dramatically reduced in size within 4 days of INCB059872 treatment and nearly absent at day 6. This result was also observed by flow cytometry analysis. It is possible that this monocyte progenitor population, a subset of Lin⁻ cells, appeared to decrease in size after drug treatment because the cells had differentiated and acquired expression of Mac1. Though the percentage of Cd36⁺ Fcgr4⁺ cells in total bone marrow did not

significantly change after INCB059872 treatment, a lower fraction of these were Lin- (~3% in control mice versus 0.5% in 6d treated mice). These results are consistent with data obtained from the monocytic leukemia cell line THP-1, in which genes associated with monocytic differentiation were upregulated by INCB059872.

Overall, the data presented in this chapter support the understanding of LSD1 as an important regulator of multiple stages of hematopoiesis. In addition to the desired effect of LSD1 inhibitors to promote differentiation of myeloid leukemic blasts, these compounds also cause thrombocytopenia that limits their usefulness as therapeutic agents. Our data suggest that INCB059872 impaired the maturation of murine megakaryocyte progenitors into efficient platelet-producing cells.

CHAPTER FIVE

CONCLUSIONS AND FUTURE DIRECTIONS

Epigenetic deregulation is a common feature of myeloid malignancies. Thus, inhibitors of chromatin-modifying enzymes are being developed as therapeutic options. The histone demethylase LSD1 is overexpressed in multiple cancer types, including AML. Given that its expression correlates with the self-renewal capacity of leukemic cells, LSD1 likely has a role in maintaining the transformed state of an AML blast. Inhibition of LSD1 became especially interesting as a therapeutic strategy after the inhibitor TCP was found to synergize with ATRA to induce differentiation of leukemia cells (Schenk et al., 2012). Multiple inhibitors of LSD1 have now been developed, and the focus of this dissertation is the use of one such compound, INCB059872, for the treatment of AML.

INCB059872 is an orally bioavailable compound that has reached early stage clinical trials. I first tested the transcriptional effects of this drug in MLL-rearranged AML cell lines and found that THP-1 cells were especially sensitive and could be induced to differentiate at a low concentration (25 nM). RNA-seq analysis of treated cell lines showed a gene expression pattern consistent with myeloid differentiation, and similar changes were observed in the bone marrow of an AML patient. Additionally, PRO-seq experiments established that earliest effects of INCB059872 treatment were increases in transcription at enhancers.

Inhibition of LSD1 was expected to turn on transcription of target genes by causing a buildup of H3K4 mono- and di-methylation, which are associated with active transcription. Surprisingly, ChIP-seq analysis revealed only subtle changes in H3K4 methylation by 48 hours after treating THP-1 cells with INCB059872. However, H3K27 acetylation was significantly increased at over 100 loci within 24 hours of treatment. These increased H3K27ac peaks (as well as upregulated enhancers identified by PRO-seq) were enriched for GFI1 binding motifs, which led to the hypothesis that INCB059872 disrupts the interaction of LSD1 with GFI1 and GFI1B. Indeed, immunoprecipitation experiments confirmed that drug treatment limited the interaction of LSD1 with GFI1. This is consistent with preliminary data that showed knockdown of components of the CoREST complex induced myeloid differentiation but knockdown of other LSD1-interacting proteins did not.

In the context of AML, the disruption of the LSD1:GFI1 interaction by INCB059872 appears to be more influential than the direct effects of LSD1 inhibition on histone methylation. This result is supported by CRISPR-suppressor scanning, which identified mutations within LSD1 that confer resistance to LSD1 inhibitors yet abolish the enzymatic activity, indicating that the demethylase activity is not required for survival of AML cells (Vinyard et al., 2019). At GFI1 binding sites where the CoREST complex would normally be recruited, drug treatment prevents this interaction, resulting in buildup of H3K27 acetylation and activation of transcription (Fig. 28). Our data provide evidence that increases in H3K4 methylation occur after these initial effects. This is consistent with *in vitro* experiments that showed LSD1 catalytic activity is greatly reduced when the substrate H3 peptide was acetylated (Forneris et al., 2006), implying

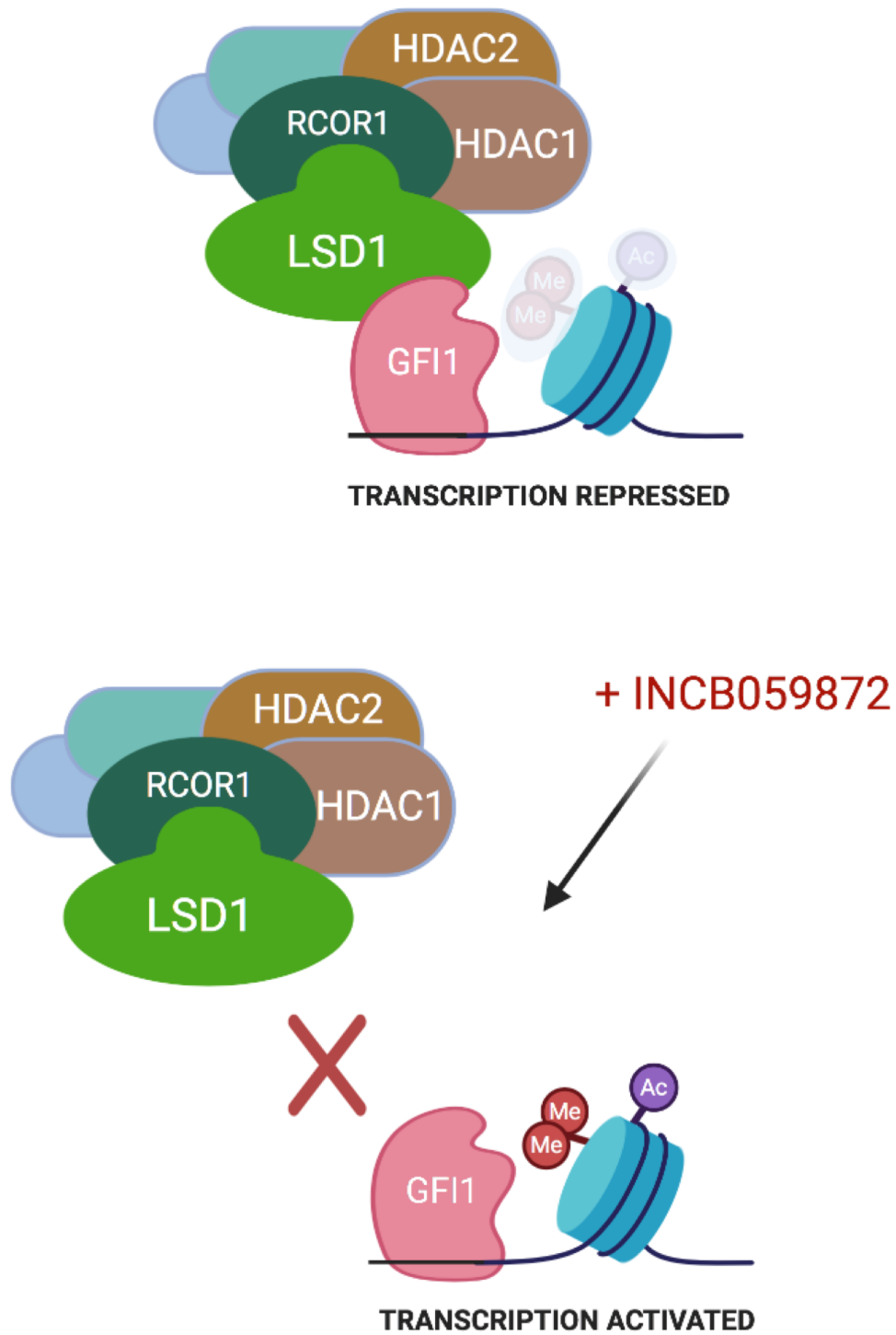


Figure 28. Model of INCB059872 disrupting the LSD1:GFI1 interaction to prevent CoREST activity at GFI1 binding sites.

that HDACs within the CoREST complex act first to deacetylate a histone before LSD1-mediated demethylation occurs.

The drawback of disrupting the interaction of LSD1 with GFI family members is that certain steps of hematopoiesis are dependent on these proteins. The primary adverse event associated with LSD1 inhibitor treatment is thrombocytopenia, which is unsurprising given the crucial role of GFI1B in megakaryopoiesis. Our murine scRNA-seq data showed that INCB059872 treatment caused expansion of a megakaryocyte progenitor population. Impairment of megakaryocytic differentiation at an early stage could explain the low platelet counts observed in treated mice.

The subset of cells that was expanded after drug treatment appears to be the platelet-primed HSC population described by Sanjuan-Pla et al. (2013). This population is characterized by the megakaryocytic marker *Vwf* and by the stem cell markers *Mycn* and *Pbx1*. Also, the proportion of *Kit*⁺ cells within this cluster was increased by INCB059872 treatment, giving further evidence that disruption of the LSD1:GFI1B interaction kept the cells in a more stem-like state as opposed to differentiating toward the megakaryocyte lineage.

One possible explanation for expansion of megakaryocyte-biased hematopoietic stem cells is that platelet production could have been impaired at a later stage, triggering a feedback mechanism that prompts stem cells to enter the cell cycle. This could be true, as our experiments did not address late-stage megakaryopoiesis. However, increased cycling does not seem to be the only cause of the expansion. Further analysis of gene expression within these cells revealed that a gene signature associated with platelet function was downregulated by the fourth day of INCB059872

treatment, suggesting that lineage-specific transcripts, not just cell cycle changes, are directly altered.

INCB059872 is not the only compound known to disrupt the interaction of LSD1 with GF11/1B. The LSD1 inhibitor T-3775440 was tested in a variety of leukemia cell lines, and erythroleukemia and megakaryoblastic leukemias were found to be among the most sensitive (Ishikawa et al., 2017). T-3775440 induced expression of myeloid markers in these cell lines, indicative of transdifferentiation, and immunoprecipitation experiments showed that this drug disrupted the association of GF11B with LSD1. Similarly, the compound OG86 was shown to disrupt the LSD1:GF11 interaction and induce differentiation of AML cell lines (Maiques-Diaz et al., 2018). INCB059872, OG86, and T-3775440 are all derivatives of TCP, so it is likely that other TCP-derived compounds disrupt this interaction as well.

In a small molecule screen to find LSD1 inhibitors that would not cause thrombocytopenia, the compound T-448 was discovered (Matsuda et al., 2019). *In vitro* assays showed that T-448 inhibited the enzymatic activity of LSD1, and it caused accumulation of H3K4me2 at a target gene in rat neurons. However, T-448 did not induce expression of GF11 mRNA in an erythroblast cell line. Structural analyses determined that T-448 forms an FAD-adduct like other TCP-based compounds, but this adduct is compact and has minimal impact on the interaction between LSD1 and GF11B. In mice, the drug increased H3K4 methylation in brain tissues but did not cause thrombocytopenia. Though T-448 could be a therapeutic option for neurodevelopmental disorders in which histone methylation is altered, it has not been tested in the context of leukemia. Based on our studies of INCB059872 in THP-1 cells, it seems unlikely that T-

448 would induce differentiation of AML cells, given that the gene expression changes that led to differentiation were dependent on loss CoREST activity at GFI1 binding sites.

Dependence on the LSD1:GFI1 interaction does not appear to be limited to hematological malignancies. Approximately 15 percent of Group 3 and Group 4 medulloblastomas overexpress GFI1 or GFI1B (Northcott et al., 2017). Coexpression of Myc and Gfi1 in murine neural progenitors caused transformation into medulloblastoma cells, but a SNAG domain mutation in Gfi1 (which mediates binding to LSD1) prevented tumorigenesis (Lee et al., 2019). Gfi1/Myc-driven tumors were especially sensitive to conditional deletion of *Lsd1* or treatment with LSD1 inhibitors. Conversely, TCP-based LSD1 inhibitors did not impair growth of Ewing sarcoma cells (Romo-Morales et al., 2019). This was an unexpected result given the high expression of LSD1 within these tumors (Theisen et al., 2016). The majority of Ewing sarcomas are driven by the EWS-FLI1 fusion protein, which recruits the NuRD complex to repress target genes (Sankar et al., 2013). Thus, it seems plausible that INCB059872 is better suited to treat tumors that depend on CoREST:LSD1:GFI1 activity more than those dependent on NuRD:LSD1.

Even among AML subtypes, the extent to which LSD1 inhibition can induce differentiation is variable. Though MV-4-11 and THP-1 cell lines are both driven by MLL translocations, the effects of INCB059872 differed between the two. Treatment with the inhibitor caused the majority of THP-1 cells to become CD11b⁺ and undergo morphological changes, but MV-4-11 cells did not display a differentiation phenotype. The influence of genetic background on sensitivity to LSD1 loss has also been reported in murine models. Conditional deletion of *Kdm1a* caused granulocytic/monocytic

differentiation in AML with Hoxa9/Meis1 overexpression but not in AML driven by MN1 overexpression (Barth et al., 2019). Despite the contrasting phenotypic changes (both in THP-1 versus MV-4-11 and in Hoxa9/Meis1 versus MN1), gene expression analyses revealed considerable overlap of the transcripts upregulated by LSD1 loss/inhibition. This suggests that the LSD1i-induced gene expression changes that promote differentiation are insufficient to overcome the differentiation block driven by certain oncogenic transcriptional programs.

The potential for clinical use of LSD1 inhibitors depends on their combinatorial effects with other therapeutic agents. A wide variety of compounds are being tested preclinically for synergy with LSD1 inhibitors. As previously mentioned, LSD1 inhibition cooperated with ATRA to induce differentiation in AML cell lines that were insensitive to ATRA alone (Schenk et al., 2012), and in a few cases the combination promoted caspase-mediated cell death (Smitheman et al., 2019). Clinical trials in which different LSD1 inhibitor compounds are combined with ATRA are currently underway.

Other signaling pathways could also be targeted for synergy with LSD1 inhibitors. The FLT3 inhibitor quizartinib showed synergy with the LSD1 inhibitor ORY-1001 in FLT3-ITD cell lines (Maes et al., 2018). A CRISPR dropout screen identified components of the mTORC1 signaling pathway as important for the survival of AML cells that had been treated with the LSD1 inhibitor OG86 (Deb et al., 2019). Combination treatment of MLL-rearranged AML cells with OG86 and the selective mTORC1 inhibitor RAD001 synergistically increased expression of a differentiation-related set of genes. Additionally, there are reports that reduced LSD1 activity can sensitize tumors to immunotherapy. In a mouse model of melanoma in which tumors

are insensitive to PD-1 blockade, deletion of *Kdm1a* conferred sensitivity to the treatment and prolonged survival (Sheng et al., 2018). Similarly, in triple-negative breast cancer xenografts, LSD1 inhibition combined with PD-1 antibody increased T cell infiltration within tumors and suppressed tumor growth (Qin et al., 2019).

Perhaps the most promising use of LSD1 inhibitors is in combination with other epigenetic therapies. Early studies of INCB059872 found that administration of this compound prior to BET inhibition in AML xenograft models more effectively reduced tumor growth than either agent alone (Liu et al., 2016). Targeting histone methylation at other residues could also be useful in combination with LSD1 inhibitors. Inhibition of the H3K79 methyltransferase DOT1L is an appealing strategy for MLL-rearranged leukemias because DOT1L is recruited by the oncogenic fusion protein. Interestingly, DOT1L inhibitors (SYC-522 or EPZ5676) showed synergy with LSD1 inhibitors in these cells (Feng et al., 2016; Maes et al., 2018). LSD1 and the H3K27 methyltransferase EZH2 are often simultaneously overexpressed in AML cells (Wen et al., 2018), suggesting that combined inhibition of both enzymes could be a therapeutic strategy. Indeed, co-treatment of AML cells with LSD1 and EZH2 inhibitors synergistically impaired viability and colony formation (Wen et al., 2018).

Because LSD1 acts as part of chromatin remodeling complexes (CoREST and NuRD) that also have HDAC activity, targeting both of these enzymatic activities could have therapeutic benefit in certain malignancies. A pan-HDAC inhibitor combined with the LSD1 inhibitor pargyline synergistically inhibited growth of breast cancer cell lines (Huang et al., 2012). Combined pan-HDAC and LSD1 inhibition improved survival in a patient-derived xenograft model of AML compared to either inhibitor alone (Fiskus et al.,

2014). Additionally, ORY-1001 plus the pan-HDAC inhibitor panobinostat demonstrated synergy in MLL-rearranged AML cell lines (Maes et al., 2018). Recently, bifunctional molecules that inhibit both LSD1 and HDACs have been developed. Corin, a hybrid TCP analog and class I HDAC inhibitor, caused nearly irreversible inhibition of CoREST complex HDAC activity, whereas individual HDAC and LSD1 inhibitors did not, indicating the possibility of a conformational change in the CoREST complex that allows one molecule to bind both active sites (Kalin et al., 2018). Corin impaired tumor growth in models of melanoma and cutaneous squamous cell carcinoma (Kalin et al. 2018) and induced neuronal differentiation of diffuse intrinsic pontine glioma (Anastas et al., 2019). However, dual inhibitors have yet to be tested in hematological malignancies.

LSD1 inhibition could also be therapeutically advantageous in cases of epigenetic resistance to other treatments. In a CRISPR screen, targeting LSD1 in combination with a BET inhibitor was found to induce differentiation of AML cells that had developed non-genetic resistance to BET inhibition (Bell et al., 2019). Surprisingly, LSD1 inhibition did not reverse the gene expression changes associated with resistance to BET inhibition. Instead, treatment with an LSD1 inhibitor opened new PU.1/IRF8-bound enhancers that were not affected by short- or long-term BET inhibition. These data support an “enhancer switching” model in which loss of LSD1 at certain enhancer loci allows PU.1/IRF8 to activate these enhancers, making the cells dependent on different survival genes than were previously used, so that BET inhibition would now kill the cells by preventing transcription of these survival genes. Thus, INCB059872 could be effective when incorporated into maintenance strategies to combat therapeutic resistance.

Targeting epigenetic dysregulation in cancer is a promising therapeutic approach. The work in this dissertation demonstrated that the LSD1 inhibitor INCB059872 prevented the CoREST complex from repressing transcription at GFI1-regulated enhancers, leading to downstream gene expression changes that promoted differentiation of AML cells. However, INCB059872 should be used with caution, as its use impaired early megakaryopoiesis, leading to thrombocytopenia. The data presented here provide support for the continued investigation of LSD1 inhibitors for the treatment of malignancies dependent on the LSD1:GFI1/GFI1B interaction.

APPENDIX

R code for scRNA-seq analysis:

```
> library(Seurat)

> library(dplyr)

> zeroA.data <- Read10X(data.dir = "1433-HR-1_count/filtered_gene_bc_matrices/mm10")
> zeroB.data <- Read10X(data.dir = "1433-HR-2_counts/filtered_gene_bc_matrices/mm10")
> zeroC.data <- Read10X(data.dir = "1433-HR-3_count/filtered_gene_bc_matrices/mm10")
> fourA.data <- Read10X(data.dir = "1433-HR-4_count/filtered_gene_bc_matrices/mm10")
> fourB.data <- Read10X(data.dir = "1433-HR-8_count/filtered_gene_bc_matrices/mm10")
> fourC.data <- Read10X(data.dir = "1433-HR-9_count/filtered_gene_bc_matrices/mm10")
> sixA.data <- Read10X(data.dir = "1433-HR-5_count/filtered_gene_bc_matrices/mm10")
> sixB.data <- Read10X(data.dir = "1433-HR-6_count/filtered_gene_bc_matrices/mm10")
> sixC.data <- Read10X(data.dir = "1433-HR-7_count/filtered_gene_bc_matrices/mm10")

> zeroA <- CreateSeuratObject(raw.data = zeroA.data, min.cells = 5, min.genes = 300, project = "zero")
> zeroB <- CreateSeuratObject(raw.data = zeroB.data, min.cells = 5, min.genes = 300, project = "zero")
> zeroC <- CreateSeuratObject(raw.data = zeroC.data, min.cells = 5, min.genes = 300, project = "zero")
> fourA <- CreateSeuratObject(raw.data = fourA.data, min.cells = 5, min.genes = 300, project = "four")
> fourB <- CreateSeuratObject(raw.data = fourB.data, min.cells = 5, min.genes = 300, project = "four")
> fourC <- CreateSeuratObject(raw.data = fourC.data, min.cells = 5, min.genes = 300, project = "four")
> sixA <- CreateSeuratObject(raw.data = sixA.data, min.cells = 5, min.genes = 300, project = "six")
> sixB <- CreateSeuratObject(raw.data = sixB.data, min.cells = 5, min.genes = 300, project = "six")
> sixC <- CreateSeuratObject(raw.data = sixC.data, min.cells = 5, min.genes = 300, project = "six")

> mito.genes0a <- grep(pattern = "^mt-", x = rownames(x = zeroA@data), value = TRUE)
> mito.genes0b <- grep(pattern = "^mt-", x = rownames(x = zeroB@data), value = TRUE)
> mito.genes0c <- grep(pattern = "^mt-", x = rownames(x = zeroC@data), value = TRUE)
> mito.genes4a <- grep(pattern = "^mt-", x = rownames(x = fourA@data), value = TRUE)
> mito.genes4b <- grep(pattern = "^mt-", x = rownames(x = fourB@data), value = TRUE)
> mito.genes4c <- grep(pattern = "^mt-", x = rownames(x = fourC@data), value = TRUE)
> mito.genes6a <- grep(pattern = "^mt-", x = rownames(x = sixA@data), value = TRUE)
> mito.genes6b <- grep(pattern = "^mt-", x = rownames(x = sixB@data), value = TRUE)
> mito.genes6c <- grep(pattern = "^mt-", x = rownames(x = sixC@data), value = TRUE)

> percent.mito0a <- Matrix::colSums(zeroA@raw.data[mito.genes0a,
])/Matrix::colSums(zeroA@raw.data)
> percent.mito0b <- Matrix::colSums(zeroB@raw.data[mito.genes0b,
])/Matrix::colSums(zeroB@raw.data)
> percent.mito0c <- Matrix::colSums(zeroC@raw.data[mito.genes0c,
])/Matrix::colSums(zeroC@raw.data)
> percent.mito4a <- Matrix::colSums(fourA@raw.data[mito.genes4a, ])/Matrix::colSums(fourA@raw.data)
> percent.mito4b <- Matrix::colSums(fourB@raw.data[mito.genes4b, ])/Matrix::colSums(fourB@raw.data)
> percent.mito4c <- Matrix::colSums(fourC@raw.data[mito.genes4c, ])/Matrix::colSums(fourC@raw.data)
> percent.mito6a <- Matrix::colSums(sixA@raw.data[mito.genes6a, ])/Matrix::colSums(sixA@raw.data)
> percent.mito6b <- Matrix::colSums(sixB@raw.data[mito.genes6b, ])/Matrix::colSums(sixB@raw.data)
> percent.mito6c <- Matrix::colSums(sixC@raw.data[mito.genes6c, ])/Matrix::colSums(sixC@raw.data)

> zeroA <- AddMetaData(object = zeroA, metadata = percent.mito0a, col.name = "percent.mito")
> zeroB <- AddMetaData(object = zeroB, metadata = percent.mito0b, col.name = "percent.mito")
```

```

> zeroC <- AddMetaData(object = zeroC, metadata = percent.mito0c, col.name = "percent.mito")
> fourA <- AddMetaData(object = fourA, metadata = percent.mito4a, col.name = "percent.mito")
> fourB <- AddMetaData(object = fourB, metadata = percent.mito4b, col.name = "percent.mito")
> fourC <- AddMetaData(object = fourC, metadata = percent.mito4c, col.name = "percent.mito")
> sixA <- AddMetaData(object = sixA, metadata = percent.mito6a, col.name = "percent.mito")
> sixB <- AddMetaData(object = sixB, metadata = percent.mito6b, col.name = "percent.mito")
> sixC <- AddMetaData(object = sixC, metadata = percent.mito6c, col.name = "percent.mito")

> zeroA <- FilterCells(object = zeroA, subset.names = c("nGene", "percent.mito"), low.thresholds = c(750, -Inf), high.thresholds = c(4000, 0.05))
> zeroB <- FilterCells(object = zeroB, subset.names = c("nGene", "percent.mito"), low.thresholds = c(750, -Inf), high.thresholds = c(4000, 0.05))
> zeroC <- FilterCells(object = zeroC, subset.names = c("nGene", "percent.mito"), low.thresholds = c(750, -Inf), high.thresholds = c(4000, 0.05))
> fourA <- FilterCells(object = fourA, subset.names = c("nGene", "percent.mito"), low.thresholds = c(750, -Inf), high.thresholds = c(4000, 0.05))
> fourB <- FilterCells(object = fourB, subset.names = c("nGene", "percent.mito"), low.thresholds = c(750, -Inf), high.thresholds = c(4000, 0.05))
> fourC <- FilterCells(object = fourC, subset.names = c("nGene", "percent.mito"), low.thresholds = c(750, -Inf), high.thresholds = c(4000, 0.05))
> sixA <- FilterCells(object = sixA, subset.names = c("nGene", "percent.mito"), low.thresholds = c(750, -Inf), high.thresholds = c(4000, 0.05))
> sixB <- FilterCells(object = sixB, subset.names = c("nGene", "percent.mito"), low.thresholds = c(750, -Inf), high.thresholds = c(4000, 0.05))
> sixC <- FilterCells(object = sixC, subset.names = c("nGene", "percent.mito"), low.thresholds = c(750, -Inf), high.thresholds = c(4000, 0.05))

> zeroA <- NormalizeData(zeroA)
> zeroB <- NormalizeData(zeroB)
> zeroC <- NormalizeData(zeroC)
> fourA <- NormalizeData(fourA)
> fourB <- NormalizeData(fourB)
> fourC <- NormalizeData(fourC)
> sixA <- NormalizeData(sixA)
> sixB <- NormalizeData(sixB)
> sixC <- NormalizeData(sixC)

> zeroA <- ScaleData(zeroA, display.progress = F)
> zeroB <- ScaleData(zeroB, display.progress = F)
> zeroC <- ScaleData(zeroC, display.progress = F)
> fourA <- ScaleData(fourA, display.progress = F)
> fourB <- ScaleData(fourB, display.progress = F)
> fourC <- ScaleData(fourC, display.progress = F)
> sixA <- ScaleData(sixA, display.progress = F)
> sixB <- ScaleData(sixB, display.progress = F)
> sixC <- ScaleData(sixC, display.progress = F)

> zeroAB <- MergeSeurat(object1 = zeroA, object2 = zeroB, add.cell.id1 = "zeroA", add.cell.id2 = "zeroB", do.normalize = FALSE)
> fourAB <- MergeSeurat(object1 = fourA, object2 = fourB, add.cell.id1 = "fourA", add.cell.id2 = "fourB", do.normalize = FALSE)
> sixAB <- MergeSeurat(object1 = sixA, object2 = sixB, add.cell.id1 = "sixA", add.cell.id2 = "sixB", do.normalize = FALSE)
> zeroall <- MergeSeurat(object1 = zeroAB, object2 = zeroC, add.cell.id2 = "zeroC", do.normalize = FALSE)
> fourall <- MergeSeurat(object1 = fourAB, object2 = fourC, add.cell.id2 = "fourC", do.normalize = FALSE)

```

```
> sixall <- MergeSeurat(object1 = sixAB, object2 = sixC, add.cell.id2 = "sixC", do.normalize = FALSE)
> mergedzerofour <- MergeSeurat(object1 = zeroall, object2 = fourall, do.normalize = FALSE)
> mergedcells <- MergeSeurat(object1 = mergedzerofour, object2 = sixall, do.normalize = FALSE)

(txt file containing list of cell cycle genes was downloaded from
https://satijalab.org/seurat/cell\_cycle\_vignette.html#assign-cell-cycle-scores)
> cc.genes <- readLines(con = "regev_lab_cell_cycle_genes.txt")
> s.genes <- cc.genes[1:43]
> g2m.genes <- cc.genes[44:97]

> n_allcells <- NormalizeData(mergedcells)

> nv_allcells <- FindVariableGenes(n_allcells, do.plot = F)

> nv_allcells <- CellCycleScoring(object = nv_allcells, s.genes = s.genes, g2m.genes = g2m.genes)

> nvs_allcells <- ScaleData(object = nv_allcells, vars.to.regress = c("S.Score", "G2M.Score"),
display.progress = FALSE)

> allcellsr_pca <- RunPCA(object = nvs_allcells, pc.genes = nvs_allcells@var.genes, pcs.compute = 40)

> allcellsr_tsne30 <- RunTSNE(allcellsr_pca, dims.use = 1:30, do.fast = T)

> allcellsr_30_08 <- FindClusters(allcellsr_tsne30, resolution = 0.8, dims.use = 1:30)
```

REFERENCES

- Adamo A, Sese B, Boue S, Castano J, Paramonov I, Barrero MJ *et al.* LSD1 regulates the balance between self-renewal and differentiation in human embryonic stem cells. *Nat Cell Biol* 2011; 13(6): 652-660.
- Allfrey VG, Faulkner R, Mirsky AE. Acetylation and methylation of histones and their possible role in the regulation of RNA synthesis. *Proc Natl Acad Sci USA* 1964; 51: 786-794.
- Amann JM, Nip J, Strom DK, Lutterbach B, Harada H, Lenny N *et al.* ETO, a target of t(8;21) in acute leukemia, makes distinct contacts with multiple histone deacetylases and binds mSin3A through its oligomerization domain. *Mol Cell Biol* 2001; 21(19): 6470-6483.
- Anastas JN, Zee BM, Kalin JH, Kim M, Guo R, Alexandrescu S *et al.* Re-programming chromatin with a bifunctional LSD1/HDAC inhibitor induces therapeutic differentiation in DIPG. *Cancer Cell* 2019; 36(5): 528-544.
- Andres ME, Burger C, Peral-Rubio MJ, Battaglioli E, Anderson ME, Grimes J *et al.* CoREST: a functional corepressor required for regulation of neural-specific gene expression. *Proc Natl Acad Sci USA* 1999; 96(17): 9873-9878.
- Anguita E, Gupta R, Olariu V, Valk PJ, Peterson C, Delwel R *et al.* A somatic mutation of GFI1B identified in leukemia alters cell fate via a SP1 (PU.1) centered genetic regulatory network. *Dev Biol* 2016; 411(2): 277-286.
- Bannister AJ, Zegerman P, Partridge JF, Miska EA, Thomas JO, Allshire RC *et al.* Selective recognition of methylated lysine 9 on histone H3 by the HP1 chromo domain. *Nature* 2001; 410(6824): 120-124.
- Bannister AJ, Schneider R, Kouzarides T. Histone methylation: dynamic or static? *Cell* 2002; 190(7): 801-806.
- Baron B, Binda C, Tortorici M, McCammon JA, Mattevi A. Molecular mimicry and ligand recognition in binding and catalysis by the histone demethylase LSD1-CoREST complex. *Structure* 2011; 19(2): 212-220.
- Barth J, Abou-El-Ardat K, Dalic D, Kurrle N, Maier AM, Mohr S *et al.* LSD1 inhibition by tranylcypromine derivatives interferes with GFI1-mediated repression of PU.1 target genes and induces differentiation in AML. *Leukemia* 2019; 33(6): 1411-1426.
- Barth TK, Imhof A. Fast signals and slow marks: the dynamics of histone modifications. *Trends Biochem Sci* 2010; 35(11): 618-626.
- Bell CC, Fennell KA, Chan YC, Rambow F, Yeung MM, Vassiliadis D *et al.* Targeting enhancer switching overcomes non-genetic drug resistance in acute myeloid leukaemia. *Nat Commun* 2019; 10(1): 2723.
- Benayoun BA, Pollina EA, Ucar D, Mahmoudi S, Karra K, Wong ED *et al.* H3K4me3 breadth is linked to cell identity and transcriptional consistency. *Cell* 2014; 158(3): 673-688.
- Botezatu L, Michel LC, Makishima H, Schroeder T, Germing U, Haas R *et al.* GFI1(36N) as a therapeutic and prognostic marker for myelodysplastic syndrome. *Exp Hematol* 2016; 44(7): 590-595.

- Bouchard C, Sahu P, Meixner M, Notzold RR, Rust MB, Kremmer E *et al.* Genomic location of PRMT6-dependent H3R2 methylation is linked to the transcriptional outcome of associated genes. *Cell Rep* 2018; 24(12): 3339-3352.
- Bradner JE, West N, Grachan ML, Greenberg EF, Haggarty SJ, Warnow T *et al.* Chemical phylogenetics of histone deacetylases. *Nat Chem Biol* 2010; 6(3): 238-243.
- Brownell JE, Allis CD. An activity gel assay detects a single, catalytically active histone acetyltransferase subunit in *Tetrahymena* macronuclei. *Proc Natl Acad Sci USA* 1995; 92(14): 6364-6368.
- Butler A, Hoffman P, Smibert P, Papalexi E, Satija R. Integrating single-cell transcriptomic data across different conditions, technologies, and species. *Nat Biotechnol* 2018; 36(5): 411-420.
- Cao R, Wang L, Wang H, Xia L, Erdjument-Bromage H, Tempst P *et al.* Role of histone H3 lysine 27 methylation in polycomb-group silencing. *Science* 2002; 298(5595): 1039-1043.
- Carnesecchi J, Forcet C, Zhang L, Tribollet V, Barenton B, Boudra R *et al.* ERR α induces H3K9 demethylation by LSD1 to promote cell invasion. *Proc Natl Acad Sci USA* 2017; 114(15): 3909-3914.
- Carrelha J, Meng Y, Kettyle LM, Luis TC, Norfo R, Alcolea V *et al.* Hierarchically related lineage-restricted fates of multipotent haematopoietic stem cells. *Nature* 2018; 554(7690): 106-111.
- Castaman G, Pieri L. Management of thrombocytopenia in cancer. *Thromb Res* 2018; 164(Suppl 1): S89-S93.
- Chadderton A, Ye M, Diamond M, Roman V, Weber M, He C *et al.* The FAD-directed LSD1-specific inhibitor INCB059872 is a promising epigenetic agent for AML therapy by inducing differentiation of leukemic stem/progenitor cells. *Cancer Res* 2018; 78(13 Suppl):Abstract 1888.
- Chen D, Ma H, Hong H, Koh SS, Huang SM, Schurter BT *et al.* Regulation of transcription by a protein methyltransferase. *Science* 1999; 284(5423): 2174-2177.
- Chen Y, Anastassiadis K, Kranz A, Stewart AF, Arndt K, Waskow C *et al.* MLL2, not MLL1, plays a major role in sustaining MLL-rearranged acute myeloid leukemia. *Cancer Cell* 2017; 31(6): 755-770.
- Chen Y, Yang Y, Wang F, Wan K, Yamane K, Zhang Y *et al.* Crystal structure of human histone lysine-specific demethylase 1 (LSD1). *Proc Natl Acad Sci USA* 2006; 103(38): 13956-13961.
- Cismasiu VB, Adamo K, Gecewicz J, Duque J, Lin Q, Avram D. BCL11B functionally associates with the NuRD complex in T lymphocytes to repress targeted promoter. *Oncogene* 2005; 24(45): 6753-6764.
- Civenni G, Zoppi G, Vazquez R, Shinde D, Paganoni A, Kokanovic A *et al.* INCB059872, a novel FAD-directed LSD1 inhibitor, is active in prostate cancer models and impacts prostate cancer stem-like cells. *Cancer Res* 2018; 78(13 Suppl):Abstract 1379.
- Creyghton MP, Cheng AW, Welstead GG, Kooistra T, Carey BW, Steine EJ *et al.* Histone H3K27ac separates active from poised enhancers and predicts developmental state. *Proc Natl Acad Sci USA* 2010; 107(50): 21931-21936.

- Cui S, Lim KC, Shi L, Lee M, Jearawiriyapaisarn N, Myers G *et al.* The LSD1 inhibitor RN-1 induces fetal hemoglobin synthesis and reduces disease pathology in sickle cell mice. *Blood* 2015; 126(3): 386-396.
- Cusan M, Cai SF, Mohammad HP, Krivtsov A, Chramiec A, Loizou E *et al.* LSD1 inhibition exerts its antileukemic effect by recommissioning PU.1- and C/EBP α -dependent enhancers in AML. *Blood* 2018; 131(15): 1730-1742.
- Da G, Lenkart J, Zhao K, Shiekhattar R, Cairns BR, Marmorstein R. Structure and function of the SWIRM domain, a conserved protein module found in chromatin regulatory complexes. *Proc Natl Acad Sci USA* 2006; 103(7): 2057-2062.
- Dahlin JS, Hamey FK, Pijuan-Sala B, Shepherd M, Lau WWY, Nestorowa S *et al.* A single-cell hematopoietic landscape resolves 8 lineage trajectories and defects in Kit mutant mice. *Blood* 2018; 131(21): e1-e11.
- Daigle SR, Olhava EJ, Therkelsen CA, Majer CR, Sneeringer CJ, Song J *et al.* Selective killing of mixed lineage leukemia cells by a potent small-molecule DOT1L inhibitor. *Cancer Cell* 2011; 20(1): 53-65.
- Deb G, Wingelhofer B, Amaral FMR, Maiques-Diaz A, Chadwick JA, Spencer GJ *et al.* Pre-clinical activity of combined LSD1 and mTORC1 inhibition in MLL-translocated acute myeloid leukaemia. *Leukemia* 2019; 34: 1266-1277.
- Delmore JE, Issa GC, Lemieux ME, Rahl PB, Shi J, Jacobs HM *et al.* BET bromodomain inhibition as a therapeutic strategy to target c-Myc. *Cell* 2011; 146(6): 904-917.
- Diamond M, Lo Y, Chadderton A, Ye M, Roman V, Weber M *et al.* The evaluation of INCB059872, an FAD-directed inhibitor of LSD1, in preclinical models of T-ALL. *Cancer Res* 2018; 78(13 Suppl):Abstract 1893.
- DiNardo CD, Stein EM, de Botton S, Roboz GJ, Altman JK, Mims AS *et al.* Durable remissions with ivosidenib in IDH1-mutated relapsed or refractory AML. *N Engl J Med* 2018; 378(25): 2386-2398.
- Doan LL, Porter SD, Duan Z, Flubacher MM, Montoya D, Tschlis PN *et al.* Targeted transcriptional repression of Gfi1 by GFI and GFI1B in lymphoid cells. *Nucleic Acids Res* 2004; 32(8): 2508-2519.
- Duan YC, Ma YC, Qin WP, Ding LN, Zheng YC, Zhu YL *et al.* Design and synthesis of novel tranlycypromine derivatives as novel LSD1/HDACs dual inhibitors for cancer treatment. *Eur J Med Chem* 2017; 140: 392-402.
- Faber J, Krivtsov AV, Stubbs MC, Wright R, Davis TN, van den Heuvel-Eibrink M *et al.* HOXA9 is required for survival in human MLL-rearranged acute leukemias. *Blood* 2009; 113(11): 2375-2385.
- Fang J, Ying H, Mao T, Fang Y, Lu Y, Wang H *et al.* Upregulation of CD11b and CD86 through LSD1 inhibition promotes myeloid differentiation and suppresses cell proliferation in human monocytic leukemia cells. *Oncotarget* 2017; 8(49): 85085-85101.
- Feng Z, Yao Y, Zhou C, Chen F, Wu F, Wei L *et al.* Pharmacological inhibition of LSD1 for the treatment of MLL-rearranged leukemia. *J Hematol Oncol* 2016; 9(1): 24.
- Filippakopoulos P, Qi J, Picaud S, Shen Y, Smith WB, Fedorov O *et al.* Selective inhibition of BET bromodomains. *Nature* 2010; 468(7327): 1067-1073.

- Fiolka K, Hertzano R, Vassen L, Zeng H, Hermesh O, Avraham KB *et al.* Gfi1 and Gfi1b act equivalently in hematopoiesis, but have distinct, non-overlapping functions in inner ear development. *EMBO Rep* 2006; 7(3): 326-333.
- Fiskus W, Sharma S, Shah B, Portier BP, Devaraj SG, Liu K *et al.* Highly effective combination of LSD1 (KDM1A) antagonist and pan-histone deacetylase inhibitor against human AML cells. *Leukemia* 2014; 28(11): 2155-2164.
- Fornieris F, Binda C, Dall'Aglio A, Fraaije MW, Battaglioli E, Mattevi A. A highly specific mechanism of histone H3-K4 recognition by histone demethylase LSD1. *J Biol Chem* 2006; 281(46): 35289-35295.
- Fornieris F, Binda C, Vanoni MA, Mattevi A, Battaglioli E. Histone demethylation catalyzed by LSD1 is a flavin-dependent oxidative process. *FEBS Lett* 2005; 579(10): 2203-2207.
- Foudi A, Kramer DJ, Qin J, Ye D, Behlich AS, Mordecai S *et al.* Distinct, strict requirements for Gfi-1b in adult bone marrow red cell and platelet generation. *J Exp Med* 2014; 211(5): 909-927.
- Fujita S, Honma D, Adachi N, Araki K, Takamatsu E, Katsumoto T *et al.* Dual inhibition of EZH1/2 breaks the quiescence of leukemia stem cells in acute myeloid leukemia. *Leukemia* 2018; 32(4): 855-864.
- Gambacourta V, Gnani D, Vago L, Di Micco R. Epigenetic therapies for acute myeloid leukemia and their immune-related effects. *Front Cell Dev Biol* 2019; 7: 207.
- Gardin C, Dombret H. Hypomethylating agents as a therapy for AML. *Curr Hematol Malign Rep* 2017; 12(1): 1-10.
- Gilks CB, Bear SE, Grimes HL, Tschlis PN. Progression of interleukin-2 (IL-2)-dependent rat T cell lymphoma lines to IL-2-independent growth following activation of a gene (Gfi-1) encoding a novel zinc finger protein. *Mol Cell Biol* 1993; 13(3): 1759-1768.
- Grimes HL, Chan TO, Zweidler-McKay PA, Tong B, Tschlis PN. The Gfi-1 proto-oncoprotein contains a novel transcriptional repressor domain, SNAG, and inhibits G1 arrest induced by interleukin-2 withdrawal. *Mol Cell Biol* 1996; 16(11): 6263-6272.
- Guilliams M, Mildner A, Yona S. Developmental and functional heterogeneity of monocytes. *Immunity* 2018; 49(4): 595-613.
- Guo Y, Fu X, Huo B, Wang Y, Sun J, Meng L *et al.* GATA2 regulates GATA1 expression through LSD1-mediated histone modification. *Am J Transl Res* 2016; 8(5): 2265-2274.
- Hamey FK, Nestorowa S, Kinston SJ, Kent DG, Wilson NK, Gottgens B. Reconstructing blood stem cell regulatory network models from single-cell molecular profiles. *Proc Natl Acad Sci* 2017; 114(23): 5822-5829.
- Harris WJ, Huang X, Lynch JT, Spencer GJ, Hitchin JR, Li Y *et al.* The histone demethylase KDM1A sustains the oncogenic potential of MLL-AF9 leukemia stem cells. *Cancer Cell* 2012; 21(4): 473-487.
- Hayami S, Kelly JD, Cho HS, Yoshimatsu M, Unoki M, Tsunoda T *et al.* Overexpression of LSD1 contributes to human carcinogenesis through chromatin regulation in various cancers. *Int J Cancer* 2011; 128(3): 574-586.

- He X, Zhu Y, Lin YC, Li M, Du J, Dong H *et al.* PRMT1-mediated FLT3 arginine methylation promotes maintenance of FLT3-ITD+ acute myeloid leukemia. *Blood* 2019; 134(6): 548-560.
- Heinz S, Benner C, Spann N, Bertolino E, Lin YC, Laslo P *et al.* Simple combinations of lineage-determining transcription factors prime cis-regulatory elements required for macrophage and B cell identities. *Mol Cell* 2010; 38(4): 576-589.
- Helin K, Dhanak D. Chromatin proteins and modifications as drug targets. *Nature* 2013; 502(7472): 480-488.
- Hock H, Hamblen MJ, Rooke HM, Schindler JW, Saleque S, Fujiwara Y *et al.* Gfi-1 restricts proliferation and preserves functional integrity of hematopoietic stem cells. *Nature* 2004; 431(7011): 1002-1007.
- Hojfeldt JW, Agger K, Helin K. Histone lysine demethylases as targets for anticancer therapy. *Nat Rev Drug Discov* 2013; 12(12): 917-930.
- Hong W, Nakazawa M, Chen YY, Kori R, Vakoc CR, Rakowski C *et al.* FOG-1 recruits the NuRD repressor complex to mediate transcriptional repression by GATA-1. *EMBO J* 2005; 24(13): 2367-2378.
- Hosseini A, Minucci S. A comprehensive review of lysine-specific demethylase 1 and its roles in cancer. *Epigenomics* 2017; 9(8): 1123-1142.
- Hu X, Li X, Valverde K, Fu X, Noguchi C, Qiu Y *et al.* LSD1-mediated epigenetic modification is required for TAL1 function and hematopoiesis. *Proc Natl Acad Sci USA* 2009; 106(25): 10141-10146.
- Hu D, Shilatifard A. Epigenetics of hematopoiesis and hematological malignancies. *Genes Dev* 2016; 30(18): 2021-2041.
- Huang J, Sengupta R, Espejo AB, Lee MG, Dorsey JA, Richter M *et al.* p53 is regulated by the lysine demethylase LSD1. *Nature* 2007; 449(7158): 105-108.
- Huang Y, Vasilatos SN, Boric L, Shaw PG, Davidson NE. Inhibitors of histone demethylation and histone deacetylation cooperate in regulating gene expression and inhibiting growth in human breast cancer cells. *Breast Cancer Res Treat* 2012; 131(3): 777-789.
- Humphrey GW, Wang Y, Russanova VR, Hirai T, Qin J, Nakatani Y *et al.* Stable histone deacetylase complexes distinguished by the presence of SANT domain proteins CoREST/kiaa0071 and Mta-L1. *J Biol Chem* 2001; 276(9): 6817-6824.
- Ishikawa Y, Gamo K, Yabuki M, Takagi S, Toyoshima K, Nakayama K *et al.* A novel LSD1 inhibitor T-3775440 disrupts GFI1B-containing complex leading to transdifferentiation and impaired growth of AML cells. *Mol Cancer Ther* 2017; 16(2): 273-284.
- Jain AK, Barton MC. Bromodomain histone readers and cancer. *J Mol Biol* 2017; 429(13): 2003-2010.
- Johnston G, Ramsey HE, Liu Q, Wang J, Stengel KR, Sampathi S *et al.* Nascent transcript and single-cell RNA-seq analysis defines the mechanism of action of the LSD1 inhibitor INCB059872 in myeloid leukemia. *Gene* 2020; 752: 144758.
- Jones PA, Taylor SM. Cellular differentiation, cytidine analogs and DNA methylation. *Cell* 1980; 20: 85-93.
- Jutzi JS, Kleppe M, Dias J, Staehle HF, Shank K, Teruya-Feldstein J *et al.* LSD1 inhibition prolongs survival in mouse models of MPN by selectively targeting the disease clone. *Hemasphere* 2018; 2(3): e54.

- Kalin JH, Wu M, Gomez AV, Song Y, Das J, Hayward D *et al.* Targeting the CoREST complex with dual histone deacetylase and demethylase inhibitors. *Nat Commun* 2018; 9(1): 53.
- Karakaidos P, Verigos J, Magklara A. LSD1/KDM1A, a gatekeeper of cancer stemness and a promising therapeutic target. *Cancers (Basel)* 2019; 11(12): 1821.
- Karsunky H, Zeng H, Schmidt T, Zevnik B, Kluge R, Schmid KW *et al.* Inflammatory reactions and severe neutropenia in mice lacking the transcriptional repressor Gfi1. *Nat Genet* 2002; 30(3): 295-300.
- Kassim AA, Savani BN. Hematopoietic stem cell transplantation for acute myeloid leukemia: a review. *Hematol Oncol Stem Cell Ther* 2017; 10(4): 245-251.
- Kerenyi MA, Shao Z, Hsu Y, Guo G, Luc S, O'Brien K *et al.* Histone demethylase Lsd1 represses hematopoietic stem and progenitor cell signatures during blood cell maturation. *eLife* 2013; 2: e00633.
- Khandanpour C, Sharif-Askari E, Vassen L, Gaudreau MC, Zhu J, Paul WE *et al.* Evidence that the growth factor independence 1b regulates dormancy and peripheral blood mobilization of hematopoietic stem cells. *Blood* 2010; 116(24): 5149-5161.
- Khandanpour C, Thiede C, Valk PJ, Sharif-Askari E, Nuckel H, Lohmann D *et al.* A variant allele of Growth Factor Independence 1 (GFI1) is associated with acute myeloid leukemia. *Blood* 2010; 115(12): 2462-2472.
- Khandanpour C, Krongold J, Schutte J, Bouwman F, Vassen L, Gaudreau MC *et al.* The human GFI136N variant induces epigenetic changes at the Hoxa9 locus and accelerates K-RAS driven myeloproliferative disorder in mice. *Blood* 2012; 120(19): 4006-4017.
- Kontaki H, Talianidis I. Lysine methylation regulates E2F1-induced cell death. *Mol Cell* 2010; 39(1): 152-160.
- Krivtsov AV, Evans K, Gadrey JY, Eschle BK, Hatton C, Uckelmann HJ *et al.* A Menin-MLL inhibitor induces specific chromatin changes and eradicates disease in models of MLL-rearranged leukemia. *Cancer Cell* 2019; 36(6): 660-673.
- Lai AY, Wade PA. Cancer biology and NuRD: a multifaceted chromatin remodelling complex. *Nat Rev Cancer* 2011; 11(8): 588-596.
- Laslo P, Spooner CJ, Warmflash A, Lancki DW, Lee HJ, Sciammas R *et al.* Multilineage transcriptional priming and determination of alternate hematopoietic cell fates. *Cell* 2006; 126(4): 755-766.
- Laugesen A, Helin K. Chromatin repressive complexes in stem cells, development, and cancer. *Cell Stem Cell* 2014; 14(6): 735-751.
- Laurent B, Ruitu L, Murn J, Hempel K, Ferrao R, Xiang Y *et al.* A specific LSD1/KDM1A isoform regulates neuronal differentiation through H3K9 demethylation. *Mol Cell* 2015; 57(6): 957-970.
- Lee C, Rudneva VA, Erkek S, Zapatka M, Chau LQ, Tacheva-Grigorova SK *et al.* Lsd1 as a therapeutic target in Gfi1-activated medulloblastoma. *Nat Commun* 2019; 10(1): 332.
- Lee MG, Wynder C, Cooch N, Shiekhattar R. An essential role for CoREST in nucleosomal histone 3 lysine 4 demethylation. *Nature* 2005; 437(7057): 432-435.

- Lee MG, Wynder C, Schmidt DM, McCafferty DG, Shiekhattar R. Histone H3 lysine 4 demethylation is a target of nonselective antidepressive medications. *Chem Biol* 2006; 13(6): 563-567.
- Lee SH, Liu XM, Diamond M, Dostalík V, Favata M, He C *et al.* The evaluation of INCB059872, an FAD-directed inhibitor of LSD1, in preclinical models of human small cell lung cancer. *Cancer Res* 2016; 76(14 Suppl):Abstract 4704.
- Lee SH, Stubbs M, Liu XM, Diamond M, Dostalík V, Ye M *et al.* Discovery of INCB059872, a novel FAD-directed LSD1 inhibitor that is effective in preclinical models of human and murine AML. *Cancer Res* 2016; 76(14 Suppl):Abstract 4712.
- Li H, Ji M, Klarmann KD, Keller JR. Repression of Id2 expression by Gfi-1 is required for B-cell and myeloid development. *Blood* 2010; 116(7): 1060-1069.
- Lin Y, Wu Y, Li J, Dong C, Ye X, Chi YI *et al.* The SNAG domain of Snail1 functions as a molecular hook for recruiting lysine-specific demethylase 1. *EMBO J* 2010; 29(11): 1803-1816.
- Liu X, Stubbs M, Ye M, Collins R, Favata M, Yang G *et al.* Combination of BET inhibitor INCB054329 and LSD1 inhibitor INCB059872 is synergistic for the treatment of AML in vitro and in vivo. *Cancer Res* 2016; 76(14 Supplement): 4702.
- Macinkovic I, Theofel I, Hundertmark T, Kovac K, Awe S, Lenz J *et al.* Distinct CoREST complexes act in a cell-type-specific manner. *Nucleic Acids Res* 2019; 47(22): 11649-11666.
- Maes T, Mascaro C, Tirapu I, Estiarte A, Ciceri F, Lunardi F *et al.* ORY-1001, a potent and selective KDM1A inhibitor, for the treatment of acute leukemia. *Cancer Cell* 2018; 33(3): 495-511.
- Magliulo D, Bernardi R, Messina S. Lysine-specific demethylase 1A as a promising target in acute myeloid leukemia. *Front Oncol* 2018; 8: 255.
- Mahat DB, Kwak H, Booth GT, Jonkers IH, Danko CG, Patel RK *et al.* Base-pair-resolution genome-wide mapping of active RNA polymerases using precision nuclear run-on (PRO-seq). *Nat Protoc* 2016; 11(8): 1455-1476.
- Maiques-Diaz A, Somerville TCP. LSD1: Biologic roles and therapeutic targeting. *Epigenomics* 2016; 8(8): 1103-1116.
- Maiques-Diaz A, Spencer GJ, Lynch JT, Ciceri F, Williams EL, Amaral FMR *et al.* Enhancer activation by pharmacological displacement of LSD1 from GF11 induces differentiation in acute myeloid leukemia. *Cell Reports* 2018; 22(13): 3641-3659.
- Marchi E, Zullo KM, Amengual JE, Kalac M, Bongero D, McIntosh CM *et al.* The combination of hypomethylating agents and histone deacetylase inhibitors produce marked synergy in preclinical models of T-cell lymphoma. *Br J Haematol* 2015; 171(2): 215-226.
- Marmorstein R, Zhou MM. Writers and readers of histone acetylation: structure, mechanism, and inhibition. *Cold Spring Harb Perspect Biol* 2014; 6(7): a018762.
- Marneth AE, Botezatu L, Hones JM, Israel JCL, Schutte J, Vassen L *et al.* GF11 is required for RUNX1/ETO positive acute myeloid leukemia. *Haematologica* 2018; 103(9): e395-e399.

- Masse A, Roulin L, Pasanisi J, Penneroux J, Gachet S, Delord M *et al.* BET inhibitors impair leukemic stem cell function only in defined subgroups of acute myeloid leukaemias. *Leuk Res* 2019; 87: 106269.
- Matsuda S, Baba R, Oki H, Morimoto S, Toyofuku M, Igaki S, *et al.* T-448, a specific inhibitor of LSD1 enzyme activity, improves learning function without causing thrombocytopenia in mice. *Neuropsychopharmacology* 2019; 44(8): 1505-1512.
- McClure JJ, Li X, Chou CJ. Advances and challenges of HDAC inhibitors in cancer therapeutics. *Adv Cancer Res* 2018; 138: 183-211.
- McGhee L, Bryan J, Elliott L, Grimes HL, Kanzanjian A, Davis JN *et al.* Gfi-1 attaches to the nuclear matrix, associates with ETO (MTG8) and histone deacetylase proteins, and represses transcription using a TSA-sensitive mechanism. *J Cell Biochem* 2003; 89(5): 1005-1018.
- Metsalu T, Vilo J. ClustVis: a web tool for visualizing clustering of multivariate data using Principal Component Analysis and heatmap. *Nucleic Acid Res* 2015; 43(Web Server issue): W566-W570.
- Metzger E, Wissmann M, Yin N, Muller JM, Schneider R, Peters AHFM *et al.* LSD1 demethylates repressive histone marks to promote androgen-receptor-dependent transcription. *Nature* 2005; 437: 25-28.
- Mizzen CA, Allis CD. Linking histone acetylation to transcriptional regulation. *Cell Mol Life Sci* 1998; 54(1): 6-20.
- Mohan M, Lin C, Guest E, Shilatifard A. Licensed to elongate: a molecular mechanism for MLL-based leukaemogenesis. *Nat Rev Cancer* 2010; 10(10): 721-728.
- Monteferrario D, Bolar NA, Marneth AE, Hebeda KM, Bergevoet SM, Veenstra H *et al.* A dominant-negative GF11B mutation in the gray platelet syndrome. *N Engl J Med* 2014; 370(3): 245-253.
- Moroy T, Vassen L, Wilkes B, Khandanpour C. From cytopenia to leukemia: the role of Gfi1 and Gfi1b in blood formation. *Blood* 2015; 126(24): 2561-2570.
- Mould DP, McGonagle AE, Wiseman DH, Williams EL, Jordan AM. Reversible inhibitors of LSD1 as therapeutic agents in acute myeloid leukemia: clinical significance and progress to date. *Med Res Rev* 2015; 35(3): 586-618.
- Mulligan P, Yang F, Di Stefano L, Ji J, Ouyang J, Nishikawa JL *et al.* A SIRT1-LSD1 corepressor complex regulates Notch target gene expression and development. *Mol Cell* 2011; 42(5): 689-699.
- Murn J, Shi Y. The winding path of protein methylation research: milestones and new frontiers. *Nat Rev Mol Cell Biol* 2017; 18(8): 517-527.
- Murray K. The occurrence of epsilon-N-methyl lysine in histones. *Biochemistry* 1964; 3: 10-15.
- Nagase R, Inoue D, Pastore A, Fujino T, Hou HA, Yamasaki N *et al.* Expression of mutant Asxl1 perturbs hematopoiesis and promotes susceptibility to leukemic transformation. *J Exp Med* 2018; 215(6): 1729-1747.
- Northcott PA, Buchhalter I, Morrissy AS, Hovestadt V, Weischenfeldt J, Ehrenberger T *et al.* The whole-genome landscape of medulloblastoma subtypes. *Nature* 2017; 547(7663): 311-317.
- Norsworthy KJ, Ko CW, Lee JE, Liu J, John CS, Przepiorka D *et al.* FDA approval summary: Mylotarg for treatment of patients with relapsed or refractory CD33-positive acute myeloid leukemia. *Oncologist* 2018; 23(9): 1103-1108.

- Ossenkoppele G, Montesinos P. Challenges in the diagnosis and treatment of secondary acute myeloid leukemia. *Crit Rev Oncol Hematol* 2019; 138: 6-13.
- Paik WK, Kim S. Enzymatic demethylation of calf thymus histones. *Biochem Biophys Res Commun* 1973; 51(3): 781-788.
- Pandey MR, Wang ES. What potential is there for LSD1 inhibitors to reach approval for AML? *Expert Opin Emerg Drugs* 2019; 24(4): 205-212.
- Park S, Yoon B, Kim S, Kim S. GENT2: an updated gene expression database for normal and tumor tissues. *BMC Med Genomics* 2019; 12(5): 101.
- Person RE, Li FQ, Duan Z, Benson KF, Wechsler J, Papadaki HA *et al*. Mutations in proto-oncogene GFI1 cause human neutropenia and target ELA2. *Nat Genet* 2003; 34(3): 308-312.
- Pervaiz M, Mishra P, Gunter S. Bromodomain drug discovery – the past, the present, and the future. *Chem Rec* 2018; 18(12): 1808-1817.
- Pleyer L, Greil R. Digging deep into “dirty” drugs- modulation of the methylation machinery. *Drug Metab Rev* 2015; 47(2): 252-279.
- Pollyea DA, Amaya M, Strati P, Konopleva MY. Venetoclax for AML: changing the treatment paradigm. *Blood Adv* 2019; 3(24): 4326-4335.
- Qin Y, Vasilatos SN, Chen L, Wu H, Cao Z, Fu Y *et al*. Inhibition of histone lysine-specific demethylase 1 elicits breast tumor immunity and enhances antitumor efficacy of immune checkpoint blockade. *Oncogene* 2019; 38(3): 390-405.
- Qureshi IA, Gokhan S, Mehler MF. REST and CoREST are transcriptional and epigenetic regulators of seminal neural fate decisions. *Cell Cycle* 2010; 9(22): 4477-4486.
- Rashkovan M, Ferrando A. Metabolic dependencies and vulnerabilities in leukemia. *Genes Dev* 2019; 33: 1460-1474.
- Rathinam C, Geffers R, Yucel R, Buer J, Welte K, Moroy T *et al*. The transcriptional repressor Gfi1 controls STAT3-dependent dendritic cell development and function. *Immunity* 2005; 22(6): 717-728.
- Ray SK, Li HJ, Metzger E, Schule R, Leiter AB. CtBP and associated LSD1 are required for transcriptional activation by NeuroD1 in gastrointestinal endocrine cells. *Mol Cell Biol* 2014; 34(12): 2308-2317.
- Rea S, Eisenhaber F, O’Carroll D, Strahl BD, Sun ZW, Schmid M *et al*. Regulation of chromatin structure by site-specific histone H3 methyltransferases. *Nature* 2000; 406(6796): 593-599.
- Reed D, DuBois SG, Gorlick R, Mascarenhas L, Harrison D, Metts J *et al*. A phase I dose escalation and expansion study of seclidemstat (SP-2577) a first-in-class reversible LSD1 inhibitor for patients with relapsed or refractory Ewing sarcoma. *Cancer Res* 2019; 79(13 Suppl):Abstract CT109.
- Richon VM, Webb Y, Merger R, Sheppard T, Jursic B, Ngo L *et al*. Second generation hybrid polar compounds are potent inducers of transformed cell differentiation. *Proc Natl Acad Sci USA* 1996; 93(12): 5705-5708.
- Rodrigues PF, Alberti-Servera L, Eremin A, Grajales-Reyes GE, Ivanek R, Tussiwand R. Distinct progenitor lineages contribute to the heterogeneity of plasmacytoid dendritic cells. *Nat Immunol* 2018; 19(7): 711-722.

- Roman VD, Ye M, Liu H, Diamond M, Chadderton A, Lo Y *et al.* The evaluation of INCB059872, an FAD-directed covalent inhibitor of LSD1, in preclinical models of Ewing sarcoma. *Cancer Res* 2017; 77(13 Suppl):Abstract 1162.
- Romo-Morales A, Aladowicz E, Blagg J, Gatz SA, Shipley JM. Catalytic inhibition of KDM1A in Ewing sarcoma is insufficient as a therapeutic strategy. *Pediatr Blood Cancer* 2019; 66(9): e27888.
- Ryan QC, Headlee D, Acharya M, Sparreboom A, Trepel JB, Ye J *et al.* Phase I and pharmacokinetic study of MS-275, a histone deacetylase inhibitor, in patients with advanced and refractory solid tumors or lymphoma. *J Clin Oncol* 2005; 23(17): 3912-3922.
- Saleque S, Cameron S, Orkin SH. The zinc-finger proto-oncogene Gfi-1b is essential for development of the erythroid and megakaryocytic lineages. *Genes Dev* 2002; 16(3): 301-306.
- Saleque S, Kim J, Rooke HM, Orkin SH. Epigenetic regulation of hematopoietic differentiation by Gfi-1 and Gfi-1b is mediated by the cofactors CoREST and LSD1. *Mol Cell* 2007; 27(4): 562-572.
- San Jose-Eneriz E, Gimenez-Camino N, Agirre X, Prosper F. HDAC inhibitors in acute myeloid leukemia. *Cancers (Basel)* 2019; 11(11): 1794.
- San-Miguel JF, Hungria VT, Yoon SS, Beksac M, Dimopoulos MA, Elghandour A *et al.* Overall survival of patients with relapsed multiple myeloma treated with panobinostat or placebo plus bortezomib and dexamethasone (the PANORAMA 1 trial): a randomized, placebo-controlled, phase 3 trial. *Lancet Haematol* 2016; 3(11): e506-e515.
- Sanjuan-Pla A, Macaulay IC, Jensen CT, Woll PS, Luis TC, Mead A *et al.* Platelet-biased stem cells reside at the apex of the hematopoietic stem-cell hierarchy. *Nature* 2013; 502(7470): 232-236.
- Sankar S, Bell R, Stephens B, Zhuo R, Sharma S, Bearss DJ *et al.* Mechanism and relevance of EWS/FLI-mediated transcriptional repression in Ewing sarcoma. *Oncogene* 2013; 32(42): 5089-5100.
- Sashida G, Harada H, Matsui H, Oshima M, Yui M, Harada Y *et al.* Ezh2 loss promotes development of myelodysplastic syndrome but attenuates its predisposition to leukaemic transformation. *Nat Commun* 2014; 23(5): 4177.
- Schenk T, Chen WC, Gollner S, Howell L, Jin L, Hebestreit K *et al.* Inhibition of the LSD1 (KDM1A) demethylase reactivates the all-trans-retinoic acid differentiation pathway in acute myeloid leukemia. *Nature Medicine* 2012; 18(4): 605-611.
- Sheng W, LaFleur MW, Nguyen TH, Chen S, Chakravarthy A, Conway JR *et al.* LSD1 ablation stimulates anti-tumor immunity and enables checkpoint blockade. *Cell* 2018; 174(3): 549-563.
- Shi LZ, Kalupahana NS, Turnis ME, Neale G, Hock H, Vignali DA *et al.* Inhibitory role of the transcription repressor Gfi1 in the generation of thymus-derived regulatory T cells. *Proc Natl Acad Sci USA* 2013; 110(34): E3198-3205.
- Shi Y, Lan F, Matson C, Mulligan P, Whetstine JR, Cole PA *et al.* Histone demethylation mediated by the nuclear amine oxidase homolog LSD1. *Cell* 2004; 7: 941-953.
- Smitheman KN, Severson TM, Rajapurkar SR, McCabe MT, Karpinich N, Foley J *et al.* Lysine specific demethylase 1 inactivation enhances differentiation and promotes

- cytotoxic response when combined with all-trans retinoic acid in acute myeloid leukemia across subtypes. *Haematologica* 2019; 104(6): 1156-1167.
- Sprussel A, Schulte JH, Weber S, Necke M, Handschke K, Thor T *et al.* Lysine-specific demethylase 1 restricts hematopoietic progenitor proliferation and is essential for terminal differentiation. *Leukemia* 2012; 26(9): 2039-2051.
- Srivastava P, Tzetzio SL, Gomez EC, Eng KH, Jani Sait SN, Kuechle JB *et al.* Inhibition of LSD1 in MDS progenitors restores differentiation of CD141^{Hi} conventional dendritic cells. *Leukemia* 2020; doi: 10.1038/s41375-020-0765-5.
- Stark R, Brown GD. DiffBind: Differential binding analysis of ChIP-seq peak data. 2011. Bioconductor; available online at <http://bioconductor.org/packages/release/bioc/html/Diffbind.html>
- Stein EM, DiNardo CD, Pollyea DA, Fathi AT, Roboz GJ, Altman JK *et al.* Enasidenib in mutant IDH2 relapsed or refractory acute myeloid leukemia. *Blood* 2017; 130(6): 722-731.
- Stein EM, Garcia-Manero G, Rizzieri DA, Tibes R, Berdeja JG, Savona MR *et al.* The DOT1L inhibitor pinometostat reduces H3K79 methylation and has modest clinical activity in adult acute leukemia. *Blood* 2018; 131(24): 2661-2669.
- Stevenson WS, Morel-Kopp MC, Chen Q, Liang HP, Bromhead CJ, Wright S *et al.* GF11B mutation causes a bleeding disorder with abnormal platelet function. *J Thromb Haemost* 2013; 11(11): 2039-2047.
- Stone RM, Mandrekar SJ, Sanford BL, Laumann K, Geyer S, Bloomfield CD *et al.* Midostaurin plus chemotherapy for acute myeloid leukemia with a FLT3 mutation. *N Engl J Med* 2017; 377(5): 454-464.
- Strahl BD, Allis CD. The language of covalent histone modifications. *Nature* 2000; 403(6765): 41-45.
- Subramanian A, Tamayo P, Mootha VK, Mukherjee S, Ebert BL, Gillette MA *et al.* Gene set enrichment analysis: a knowledge-based approach for interpreting genome-wide expression profiles. *Proc Natl Acad Sci USA* 2005; 102(43): 15545-15550.
- Sugino N, Kawahara M, Tatsumi G, Kanai A, Matsui H, Yamamoto R *et al.* A novel LSD1 inhibitor NCD38 ameliorates MDS-related leukemia with complex karyotype by attenuating leukemia programs via activating super-enhancers. *Leukemia* 2017; 31(11): 2303-2314.
- Suzuki J, Maruyama S, Tamauchi H, Kuwahara M, Horiuchi M, Mizuki M *et al.* Gfi1, a transcriptional repressor, inhibits the induction of the T helper type 1 programme in activated CD4 T cells. *Immunology* 2016; 147(4): 476-487.
- Tabé Y, Jin L, Contractor R, Gold D, Ruvolo P, Radke S *et al.* Novel role of HDAC inhibitors in AML1/ETO AML cells: activation of apoptosis and phagocytosis through induction of annexin A1. *Cell Death Differ* 2007; 14(8): 1443-14456.
- Takeuchi M, Fuse Y, Watanabe M, Andrea CS, Takeuchi M, Nakajima H *et al.* LSD1/KDM1A promotes hematopoietic commitment of hemangioblasts through downregulation of Etv2. *Proc Natl Acad Sci USA* 2015; 112(45): 13922-13927.
- Taunton J, Hassig CA, Schreiber SL. A mammalian histone deacetylase related to the yeast transcriptional regulator Rpd3p. *Science* 1996; 272(5260): 408-411.
- Thambyrajah R, Mazan M, Patel R, Moignard V, Stefanska M, Marinopoulou E *et al.* GF11 proteins orchestrate the emergence of hematopoietic stem cells through recruitment of LSD1. *Nat Cell Biol* 2016; 18(1): 21-32.

- Theisen ER, Pishas KI, Saund RS, Lessnick SL. Therapeutic opportunities in Ewing sarcoma: EWS-FLI inhibition via LSD1 targeting. *Oncotarget* 2016; 7(14): 17616-17630.
- Tochio N, Umehara T, Koshiba S, Inoue M, Yabuki T, Aoki M *et al.* Solution structure of the SWIRM domain of human histone demethylase LSD1. *Structure* 2006; 14(3): 457-468.
- Tong B, Grimes HL, Yang TY, Bear SE, Qin Z, Du K *et al.* The Gfi-1B proto-oncoprotein represses p21WAF1 and inhibits myeloid cell differentiation. *Mol Cell Biol* 1998; 18(5): 2462-2473.
- Tong JK, Hassig CA, Schnitzler GR, Kingston RE, Schreiber SL. Chromatin deacetylation by an ATP-dependent nucleosome remodeling complex. *Nature* 1998; 395: 917-921.
- Trapnell C, Williams BA, Pertea G, Mortazavi A, Kwan G, van Baren MJ *et al.* Transcript assembly and quantification by RNA-seq reveals unannotated transcripts and isoform switching during cell differentiation. *Nat Biotechnol* 2010; 28(5): 511-515.
- Vassen L, Okayama T, Moroy T. Gfi1b:green fluorescent protein knock-in mice reveal a dynamic expression pattern of Gfi1b during hematopoiesis that is largely complementary to Gfi1. *Blood* 2007; 109(6): 2356-2364.
- van Bergen MGJM, van der Reijden BA. Targeting the GFI1/1B-CoREST complex in acute myeloid leukemia. *Front Oncol* 2019; 9: 1027.
- van Oorschot R, Hansen M, Koornneef JM, Marneth AE, Bergevoet SM, van Bergen MGJM *et al.* Molecular mechanisms of bleeding disorder-associated GFI1B^{Q287*} mutation and its affected pathways in megakaryocytes and platelets. *Haematologica* 2019; 104(7): 1460-1472.
- Velinder M, Singer J, Bareyan D, Mezmarich J, Tracy CM, Fulcher JM *et al.* GFI1 functions in transcriptional control and cell fate determination require SNAG domain methylation to recruit LSD1. *Biochem J* 2016; 473(19): 3355-3369.
- Vijapurkar U, Fischbach N, Shen W, Brandts C, Stokoe D, Lawrence HJ *et al.* Protein kinase C-mediated phosphorylation of the leukemia-associated HOXA9 protein impairs its DNA binding ability and induces myeloid differentiation. *Mol Cell Biol* 2004; 24(9): 3827-3837.
- Vinyard ME, Su C, Siegenfeld AP, Waterbury AL, Freedy AM, Gosavi PM *et al.* CRISPR-suppressor scanning reveals a nonenzymatic role of LSD1 in AML. *Nat Chem Biol* 2019; 15(5): 529-539.
- Volpe G, Walton DS, Grainger DE, Ward C, Cauchy P, Blakemore D *et al.* Prognostic significance of high GFI1 expression in AML of normal karyotype and its association with a FLT3-ITD signature. *Sci Rep* 2017; 7(1): 11148.
- Wang J, Hevi S, Kurash JK, Lei H, Gay F, Bajko J *et al.* The lysine demethylase LSD1 (KDM1) is required for maintenance of global DNA methylation. *Nat Genet* 2009; 41(1): 125-129.
- Wang J, Scully K, Zhu X, Cai L, Zhang J, Prefontaine GG *et al.* Opposing LSD1 complexes function in developmental gene activation and repression programmes. *Nature* 2007; 446(7138): 882-887.
- Wang J, Telese F, Tan Y, Li W, Jin C, He X *et al.* LSD1n is an H4K20 demethylase regulating memory formation via transcriptional elongation control. *Nat Neurosci* 2015; 18(9): 1256-1264.

- Wang J, Zhao Y, Zhou X, Hiebert SW, Liu Q, Shyr Y. Nascent RNA sequencing analysis provides insights into enhancer-mediated gene regulation. *BMC Genomics* 2018; 19(1): 633.
- Wang Y, Zhang H, Chen Y, Sun Y, Yang F, Yu W *et al.* LSD1 is a subunit of the NuRD complex and targets the metastasis programs in breast cancer. *Cell* 2009; 138(4): 660-672.
- Wen S, Wang J, Liu P, Li Y, Lu W, Hu Y *et al.* Novel combination of histone methylation modulators with therapeutic synergy against acute myeloid leukemia in vitro and in vivo. *Cancer Lett* 2018; 413: 35-45.
- West AC, Johnstone RW. New and emerging HDAC inhibitors for cancer treatment. *J Clin Invest* 2014; 124(1): 30-39.
- Whyte WA, Bilodeau S, Orlando DA, Hoke HA, Frampton GM, Foster CT *et al.* Enhancer decommissioning by LSD1 during embryonic stem cell differentiation. *Nature* 2012; 484: 221-225.
- Xiao YH, Li XH, Tan T, Liang T, Yi H, Li MY *et al.* Identification of GLIPR1 tumor suppressor as methylation-silenced gene in acute myeloid leukemia by microarray analysis. *J Cancer Res Clin Oncol* 2011; 137(12): 1831-1840.
- Yamamoto R, Kawahara M, Ito S, Satoh J, Tatsumi G, Hishizawa M *et al.* Selective dissociation between LSD1 and GFI1B by a LSD1 inhibitor NCD38 induces the activation of ERG super-enhancer in erythroleukemia cells. *Oncotarget* 2018; 9(30): 21007-21021.
- Yang JJ, Park TS, Wan TS. Recurrent cytogenetic abnormalities in acute myeloid leukemia. *Methods Mol Biol* 2017; 1541: 223-245.
- Yang M, Culhane JC, Szewczuk LM, Jalili P, Ball HL, Machius M *et al.* Structural basis for the inhibition of the LSD1 histone demethylase by the antidepressant trans-2-phenylcyclopropylamine. *Biochemistry* 2007; 46(27): 8058-8065.
- Yang M, Gocke CB, Luo X, Borek D, Tomchick DR, Machius M *et al.* Structural basis for CoREST-dependent demethylation of nucleosomes by the human LSD1 histone demethylase. *Mol Cell* 2006; 23(3): 377-387.
- Yoshida T, Hazan I, Zhang J, Ng SY, Naito T, Snippert HJ *et al.* The role of the chromatin remodeler Mi-2beta in hematopoietic stem cell self-renewal and multilineage differentiation. *Genes Dev* 2008; 22(9): 1174-1189.
- You A, Tong JK, Grozinger CM, Schreiber SL. CoREST is an integral component of the CoREST-human histone deacetylase complex. *Proc Natl Acad Sci USA* 2001; 98(4): 1454-1458.
- Yucel R, Kosan C, Heyd F, Moroy T. Gfi1:green fluorescent protein knock-in mutant reveals differential expression and autoregulation of the growth factor independence 1 (Gfi1) gene during lymphocyte development. *J Biol Chem* 2004; 279(39): 40906-40917.
- Zeng H, Yucel R, Kosan C, Klein-Hitpass L, Moroy T. Transcription factor Gfi1 regulates self-renewal and engraftment of hematopoietic stem cells. *EMBO J* 2004; 23(20): 4116-4125.
- Zhao Z, Shilatifard A. Epigenetic modifications of histones in cancer. *Genome Biol* 2019; 20: 245.

Zweidler-Mckay PA, Grimes HL, Flubacher MM, Tschlis PN. Gfi-1 encodes a nuclear zinc finger protein that binds DNA and functions as a transcriptional repressor. *Mol Cell Biol* 1996; 16(8): 4024-4034.